Energetics and Passive Dynamics of Quadruped Robot Planar Running Gaits

P. Murali Krishna

A Thesis Submitted to

Indian Institute of Technology Hyderabad

In Partial Fulfillment of the Requirements for

The Degree of Doctor of Philosophy

भारतीय प्रौद्योगिकी संस्थान हैदराबाद

Indian Institute of Technology Hyderabad

Department of Mechanical and Aerospace Engineering

November 2014

Declaration

I declare that this written submission represents my ideas in my own words, and where ideas or words of others have been included, I have adequately cited and referenced the original sources. I also declare that I have adhered to all principles of academic honesty and integrity and have not misrepresented or fabricated or falsified any idea/data/fact/source in my submission. I understand that any violation of the above will be a cause for disciplinary action by the Institute and can also evoke penal action from the sources that have thus not been properly cited, or from whom proper permission has not been taken when needed.
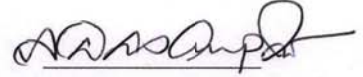
(Signature)

23-02-2015

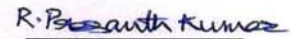(P. Murali Krishna)

ME10P004

(Roll No.)

Approval Sheet

This Thesis entitled Energetics and Passive Dynamics of Quadruped Robot Planar Running Gaits by P. Murali Krishna is approved for the degree of Doctor of Philosophy from IIT Hyderabad
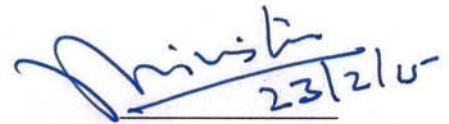
(Anirvan DasGupta) Examiner
Department of Mechanical Engineering
IIT Kharagpur

(M. Ramji) Examiner
Department of Mechanical and Aerospace Engineering
IIT Hyderabad

(R. Prasanth Kumar) Adviser
Department of Mechanical and Aerospace Engineering
IIT Hyderabad

(Suresh Srivastava) Co-Adviser
Director(TM), DG Aero Office
DRDO

(Ketan P Detroja) Chairman
Department of Electrical Engineering
IIT Hyderabad

Acknowledgements

To My Teachers

Abstract

Quadruped robots find application in military for load carrying over uneven terrain, humanitarian de-mining, and search and rescue missions. The energy required for quadruped robot locomotion needs to be supplied from on-board energy source which can be either electrical batteries or fuels such as gasolene/diesel. The range and duration of missions very much depend on the amount of energy carried, which is highly limited. Hence, energy efficiency is of paramount importance in building quadruped robots. Study of energy efficiency in quadruped robots not only helps in efficient design of quadruped robots, but also helps understand the biomechanics of quadrupedal animals. This thesis focuses on the energy efficiency of planar running gaits and presents: (a) derivation of cost of transport expressions for trot and bounding gaits, (b) advantages of articulated torso over rigid torso for quadruped robot, (c) symmetry based control laws for passive dynamic bounding and design for inherent stability, and (d) effect of asymmetry in zero-energy bounding gaits.

Trot and Bounding gaits are the most commonly used planar gaits in quadruped robots. Cost of transport or specific resistance expressions for both these gaits are derived based on the assumption that constant height of the body is maintained and the body does not pitch during locomotion, maintaining horizontal configuration. These assumptions, though seem to be restrictive, are necessary to arrive at analytical expressions of cost of transport that can be obtained in simplified form. Analytical expressions have advantage over numerical results of cost of transport in determining which parameters influence the energy consumption and how. The effect of asymmetric mass distribution is also considered when deriving the cost of transport expressions. It was found that constant height level trotting at constant speed is not possible and acceleration/deceleration are unavoidable. Again, in the case of bounding, only variable speed gaits are possible. Results indicate an energetic advantage of having center of mass away from geometric center of the body under the conditions considered.

Having an articulated torso is found to be advantages in aspects such as speed, stride length, and ground clearance. Such studies have been done on only flat terrain. This thesis presents a simulation study of quadruped robot with articulated torso on surfaces with height obstacles.

In recent years, passive dynamics has been used to obtain near zero-energy bounding gaits. Although theoretically such gaits consume no energy, in practice some additional energy is required to overcome losses. Existence and stability of such gaits have been thoroughly studied in literature for quadruped models with the assumption that the mass distribution and stiffness in the front and back legs are symmetric. Fixed points found using Poincare map indicate touchdown angle-liftoff angle symmetry between front and back legs. This property can be used to search for fixed points with ease. However, the range of initial conditions where the bounding gait is stable is highly limited. Control laws based on symmetry conditions observed are proposed in this thesis to improve the stability region. One such control law based on body-fixed touchdown angles theoretically allows redesign of quadruped robot with physical cross coupling between legs to achieve inherent stability without leg actuation.

Although methods reported in literature are sufficient to search for fixed points in quadruped robots with mass and stiffness asymmetry, no such method has been reported in literature for finding fixed points in the presence of asymmetry. In this thesis, a method to find fixed points in the presence of mass or stiffness asymmetry is proposed. Results indicate that the touchdown angle-liftoff angle symmetry no longer holds in the presence of either mass or stiffness asymmetry.

Further, the pitch angle at apex of flight phase is nonzero unlike in symmetric quadruped case. In general, as the asymmetry is increased the number of fixed points decreased which indicates that high asymmetry is undesirable for passive dynamic bounding. Control laws based on touchdown angle-liftoff angle symmetry condition cannot be directly applied in the presence of asymmetry. With mass asymmetry, stability is improved at low pitch angular velocities and high forward velocities. With stiffness asymmetry, stability is improved at low pitch angular velocities if the spring stiffness of backleg is greater than that of the front leg.

The results presented in this thesis provide guidelines for the design of energy efficient quadruped robots for a particular class of planar running gaits considering the presence of asymmetry which may be intentionally/unintentionally introduced in a field robot. Results are also useful to understand the biomechanics of similar gaits present in quadrupedal animals.

Contents

List of Figures

List of Tables

Chapter 1

Introduction and Literature Review

1.1   Introduction

Human beings invented robots to perform tasks that are repetitive and/or dangerous, and those that require high precision and speed. Robots have found their most successful application in manufacturing industries as robot manipulators with fixed base. A robot manipulator that has moving base is much more useful as it will not be limited to working in one place. Mobility or locomotion of robots can be in several modes such as wheeled, tracked, flying, and legged. Of all these modes, wheeled mobility gives highest efficiency on flat and even terrain. On the other hand, legged locomotion, which is inspired from nature, is more effective on uneven terrain [1, 2].

Legged robots are highly attractive for military purposes such as carrying heavy loads on uneven terrain for long durations because of the higher mobility and terrain adaptability they give on rough terrain compared to wheeled vehicles/robots. A legged robot can easily overcome obstacles by stepping on/over them if it is at a lower level than its maximum ground clearance, whereas a wheeled mobile robot cannot overcome obstacles of height greater than the radius of its wheels even if its ground clearance is large enough. Legged robots can isolate the payload by providing active suspension through leg actuators while traversing on rough terrain. They are also less prone to slipping and jamming when moving over soft terrain [1]. Further, they are capable of maintaining their average speed on rough terrain, whereas average speed of wheeled robots is quite low on a similar terrain. Climbing a steep slope by hooking its feet or jumping across a trench is also possible. However, moving speed of a legged robot is considerably lower than the speed of a wheeled vehicle on flat terrain. Based on the number of legs the robot has, there are bipeds like humans or birds, quadrupeds like mammals and reptiles, hexapods like insects, and octopods like spiders. Robots with one [3], three [4], five [5], nine [6] or more legs [7] are unusual, but not impossible.

Multi-legged robots are comparatively more stable than one and two-legged robots because of the larger stability margin they are capable of. However, robots with large number of legs require more complex mechanisms and higher number of actuators, adding weight and energy required for locomotion. Three legged robots cannot maintain static stability when one of the legs is in swing phase, whereas a four-legged robot can. This makes quadruped robot the right choice considering

1

simplicity and stability. For attaining a high moving speed with a legged robot, a dynamically stable gait, such as running for a trot gait or a bound gait for a quadruped robot, is a promising solution. Quadruped robots can be broadly classified into two types based on the kinematic structure of their legs. These are quadruped robots with insect-type 3-Degree-of-Freedom (DoF) legs and those with mammal-type 3- or 4-DoF legs. Numerous quadruped walking and running robots have been developed to date in both these types.

Quadrupedal animals are capable of moving with several gaits, of which, crawl, trot, pace and bounding are prominent [8]. Trot and bounding gaits are used when faster locomotion is desired. Trot is one of the most widely used gaits in quadruped robots [9, 8] in which the robot is supported on diagonally opposite legs during support phase. Trot gait is preferred where lower energy consumption is desirable [10]. Trot being a symmetric gait, there exist a similarity between biped walking and quadruped trotting where the quadruped can be viewed as two bipeds connected one behind the other [11].

The bounding gait is a form of fast running legged locomotion in which a quadruped animal uses front legs as a pair (LF-RF) and rear legs as a pair (LR-RR) [3]. In this gait, the quadruped lands with both of its front legs and moves the rear legs forward, lands, and swings the front leg pair further to the next step. It is reported that the energy efficiency of dynamically stable gait is usually lower than that of a statically stable gait because much power has to be supplied at each joint to support a body by few legs [12]. Hence, there is a need to know what parameters influence energy efficiency in dynamically stable gaits.

1.2 Motivation

Soldiers carry a variety of instruments, equipment and ammunition in their backpacks. Carrying heavy weights in this manner can make them tired and cause health issues. It is necessary to offload the non-essential weights to a vehicle that can travel on uneven terrain, wherever the soldiers need to go. This is where legged robots come to rescue. Legged robots not only need to carry such offloaded weights, but also their own power source. As the primary application of quadruped robots being load carrying over uneven terrain, it is important to understand what limits the performance of such robots in critical missions of long range and duration. Design parameters such as length of body/torso and legs, location of center of mass, and gait parameters such as stride length are important in deciding the energy expenditure. Study of energy efficiency in quadruped robots not only helps in efficient design of quadruped robots, but also helps to understand the biomechanics of quadrupedal animals.

1.3 Literature Review

The literature review looks at the state-of-the-art in four legged (quadruped) robots, energetics and passive dynamics of quadruped robotic research and how the current research provides a meaningful contribution. This topic is organized as follows: a history of relevant robots and topics that are pertinent to the development of the current research of energetics, articulated torso and passive dynamics.

1.3.1 History of Relevant Robots

Legged robots technology started with the development of simple walking methods that used in the development of toys for level terrain. Later biologists and researchers recorded the walking modes of animals and insects to understand the nature motion. Different gaits were mathematically formulated for better design of walking mechanisms. Gait generation schemes and stability analysis were carried out for the ideal cases, leading to the present condition of such technology.

The first walking machine was built around 1870 by Chebyshev [13]. A milestone in the history of the development of walking machines is the Mechanical Horse, in 1893 [1]. The first serious undertaking to build a legged vehicle with independently controlled legs and terrain adaptability was made in the UK in 1940, by A. C. Hutchinson [1]. In 1968, Mosher conducted a Testing of the GE Walking Truck. In 1972 at University of Rome, first walking robot was developed in Europe [1]. In 1977, McGhee conducted a Testing of the first computer controlled walking robot [5].

The actual development of quadruped robots and its dynamic locomotion performance studies was first started by Marc Raibert. He developed planar and three-dimensional one-legged hopping machines; biped and quadruped robots with prismatic legs which can run and jump [3]. This was a milestone of the motion control of dynamic gaits for quadruped robots. Leg mechanisms like four-bar linkages, pantograph, cam linkage were proposed by Shigley [14]. The double-rocker linkages mechanism for the legs was proposed sang [11]. The first quadruped robot "Phoney Pony" was developed by McGhee and Frank, this was first autonomous computer control robot [15]. Raibert developed a first quadruped to perform trotting, pacing, and bounding gaits under dynamic control in 1989 [3]. The trotting and pacing dynamic walking gaits and transition of between trotting and pacing gaits were observed in Collie-1 and Collie-2 robots [16]. The number of walking robots being developed around the world has increased in a very impressive manner. More than 200 different walking robots have already been cataloged [17]. About 50 of them are quadruped robots. This indicates that there have been a lot of developments with this kind of quadruped robots.

Hirose began developing a large family of quadruped robots since 1980. The first one was the Pre-ambulate Vehicle (PV-II); it is an important milestone in the development of quadruped robot. Hirose began development of the TITAN series quadruped robots[18]. TITAN-III was developed for higher terrain adaptability using attitude sensor and contact sensor. TITAN-IV was developed in 1986 [19]. This robot was climbing up and down three stairs for a total 40 km traveling. TITAN-V was developed and tested for dynamic walking. TITAN -VI was developed and tested for dynamic motion. TITAN-VII was developed for moving scaffold to assist at steep slope. TITAN-VIII was developed for general purpose application [20]. Subsequently TITAN IX, X, XI, XII [21], XIII also developed by Hirose. The development of the sprawling-type quadruped robot named "TITAN-XIII" and its dynamic walking algorithm "longitudinal acceleration trajectory" implemented in this robot [22]. With the further development of quadruped robots, a true walking robot called SIL04 a four legged robot and SILO6 a six-legged robotic system for humanitarian demining missions developed by P Gonzalez de Santos at the Centre for Automation and Robotics of the Spanish National Research Council [23, 24]. The four-legged walking machine named "BISAM" was developed by R. Dillmann and his team [25]. This robot uses Neural oscillators for periodic locomotion and adaptive control for its locomotion [26].

Hiroshi Kimura and his team used Central Pattern Generators (CPGs) for dynamic walking of "PATRUSH" a quadruped robot and also for their "TEKKEN" series robots. Tekken II was used

CPGs and reflexes for its dynamic walking [27]. Kimura's "KOTETSU" used phase modulations for adaptive dynamic walking [28]. In 2013, the author implemented parameter modulation of the CPG network on MINIMULE ROBOT [29], the gait transition for the robot and environment adaptability through limit cycle stability. Various parameters for locomotion like frequency, velocity, and gait can be obtained just by changing a single parameter, the duty factor. The CPG based controlled MINIMULE ROBOT can achieve both trot and walk gait and its transition by varying the phase relationship between the limbs and is stable due to the inherent property of CPG oscillator [29].

A dynamically stable running quadruped robot Scout II was designed and developed to explore the dynamic gaits of mammal animals by Martin Buehler [30]. To study the automatically walking in uneven terrain and to realize the static and dynamic walking locomotion a quadruped robot "WARP1" was developed by RIT [31]. The KOLT robot was designed by Kenneth Waldron [32]. Hydraulic actuated quadruped walking robot was developed by the Korea Institute of Industrial Technology. It carries heavy payloads and run fast on uneven terrain. This has achieved the basic trotting gait in even terrain at lab level [33, 34]. Combining hydraulic with electric actuators, researchers of the Italian Institute of Technology have developed a quadruped robot (called HyQ) for performing highly dynamic tasks like jumping, hopping and running [35, 36]. It combines on board perception with two locomotion strategies, a dynamic trot and a static crawl gait [37]. The mechanical design and control of a PNEUMATIC quadrupedal robot development reported in [38] and describes a method of joint control that combines stance/swing gain scheduling with open-loop damping, the combination of which provides stable joint level control, without the oscillatory behaviour associated with pneumatically actuated walking robots. FROG (Four-legged Robot for Optimal Gait), a quadruped research platform developed by Dr.Wei Wangs team at the Institute of Automation, Chinese Academy of Sciences, in Beijing [39].

Marc Raibert and his team established Boston Dynamics Inc. (BDI) in 1992. From BDI again they started the development of quadruped robots. BigDog was developed in 2008. The BigDog is 1m long, 0.7m height and weighed about 75 kg. BigDog is able to trot at speed up to 1.8m/s, carry over 153 kg of payload, trot through uneven surface, snow, recover balance after slide [10, 40]. The quadruped walking robot "JINPOONG" is developed to be able to walk in the field which is used to detection, surveillance, reconnaissance, security, and assistance [41]. The Legged Squad Support System (LS3) is a dynamic robot designed to go anywhere on foot was also developed by the BDI. LS3 carry up to 180 Kg of load and has sufficient fuel capacity for missions covering 20 miles and lasting 24 hours. LS3 will navigate automatically follow a leader with the help of on board sensors like vision and GPS [42]. Again DARPA funded BDI and MIT for the development of cheetah robot. The cheetah robot has four legs, a flexible spine, an articulated neck and tail [43]. The Cheetah robot is the fastest legged robot in the World, surpassing 29 mph, a new land speed record for legged robots. The previous record was 13.1 mph, set in 1989 at MIT. The next generation Cheetah robot, WildCat, is designed to operate untethered. WildCat recently entered initial testing. WildCat is a four-legged robot being developed to run fast on all types of terrain. So far WildCat has run at about 16 mph on flat terrain using bounding and galloping gaits reported on their website. WildCat is being developed by Boston Dynamics with funding from DARPA's M3 program.

Along with development of quadruped robots, other biped robots Honda's humanoid ASIMO, [44] and dancing humanoid QRIO/NAO [45, 46], robots have also taken on domestic duties.

1.3.2 Literature Review on Energetics

Energetics deals with the energy savings or the reduction of power and energy requirements for a system. Most robotic systems utilize some type of battery, although battery technology is still limiting. If it were possible to increase the range of a robot by decreasing its power and energy requirements, this may be the important point for an unmanned robotic system. Biological experiments have provided the information of energy storage capacity of elastic elements in the animal's mussels. Based on these experiments it may be possible to reduce the power and energy requirements in a robotic system through the use of energy saving methods. Experiments conducted by Hoyt and Taylor [47] reveals that the amount of oxygen consumption by horses trained at various gaits shows that itself optimises and adjust the gait to minimum consumption of oxygen. The theory was strengthen through experiments on horses changing from a walk to a trot, and a trot to a gallop, when oxygen consumption increased, revealing that each particular gait required approximately the same amount of energy at the animals' naturally selected gait for a particular speed range. For a certain critical speed, galloping is more economical than trotting.

R.M. Alexander has done fairly large research on the energetics of biological systems [48, 49, 50, 51, 52, 53, 54]. The biological optimization observed by Hoyt and Taylor details the energy saving mechanisms of elastic structures in the animals [55]. The internal and external energetics of animals particularly dog and deer's gallop motions was reported. Also presented, at high speeds the internal energy fluctuations are maximum. During these large internal fluctuations, the elastic elements are able to store energy, reducing the power necessary during high speed gallop gaits. Speed, locomotion, gait and power characteristics will work together in biological systems to create the optimal energy consumption. The field of biomimetic robots takes this assistance from animal's study to build systems that make use of the optimization [56, 57, 58, 59, 60]. In the process of building these robots, much about their biological counterparts has been studied. Legged vehicles has advantage of terrain negotiation, due to the use of isolated footholds and decoupling of the payload from the body allowing for smooth transportation of goods over unstructured terrain [3]. A bio-inspired architecture for a quadruped robot that is able to initiate/stop locomotion; generate different gaits, and to easily select and switch between the different gaits according to the speed and/or the behavioural context reported in [61].

The effects of linear and piecewise linear compliant spines on locomotion performance of quadruped robots in terms of energy efficiency and locomotion speed through a set of simulations and experiments presented in [62]. A gait adaptation method for a quadruped robot using a terrain classification and a gait optimization for an adaptation on various surfaces for energy efficiency presented in [63]. Bio-inspired structure of a quadruped is detailed in [64] a method of energy efficiency. An optimization process that determines the optimal gait patterns for a range of velocities were implemented and the author compared three optimization methods: the genetic algorithm, the radial basis function method and the Nelder-Mead simplex. Results presented in [65] that the preferred optimization method is genetic algorithm. The locomotion performances of a quadruped robot with compliant feet based on closed-chain six-bar linkage mechanism legs are presented [66]. The legs of this quadruped robot were made up of mechanism with one degree of freedom reducing the use of number of actuators leads to energy efficiency.

The energy used in transport forms a considerable part of the World's energy consumption. Therefore, it is necessary to see how increasing speed influences the energy consumption. Gabrielli

and Von Karman [67] were the earliest research who investigated this relationship. They reported the specific resistance of vehicles as a function of their speeds. Specific resistance was expressed as the power required propelling the vehicle divided by its weight time's speed. Gabrielli and Von Karman discovered a lower limit in the specific resistance. No vehicle was able to have a specific resistance/speed combination below this line. The performance of vehicles has improved over the years. Yong et al. [68] have shown that there is a trend in which vehicles that are able to show the same performance in terms of speed but with a lower specific resistance.

The minimization of energy consumption plays a major role in the locomotion of legged robots for reducing on-board battery weight or extending the range of a mission. Reduced energy consumption is possible using minimum number of actuators for specific cases such as motion on horizontal straight line [69]. Complaint elementof mechanical element and control element, can decrease the contact force and torque of both joints in a leg design [70]. Although minimizing the vertical motion of CoM increases the cost of transport [71], level bounding can be important where there are restrictions on the motion of load being carried by the robot.

1.3.3   Literature Review on Articulated Torso

There has been less work done in the area of articulated torso in robots. 32 DoF (Degree of Freedom) joints are found in the elephant trunk robot manipulator [72] and eel robots [73], the multi-segmented robots [74] and Omni-tread robots [75], and the single articulation models with single degree of freedom at torso are reported in [76]. The effect of the spinal passive joint on the dynamic performance of a quadrupedal model in galloping gait on sagittal planar is reported in [77]. Stumpy is a simple hopping robot [78, 79] with a pegged base and single articulation in the middle of the torso. The robot moves through an applied torque at this point and hops. The use of an articulated spine can be the primary motion generator in an animal or human. A spine-driven quadruped robot [80] called Kitty developed by using its flexible spine as a computational resource.

"Pneupard", a biomimetic platform, consists of musculoskeletal parameters (range of motion and moment arms) from the biological system with air muscles within a lightweight robotic structure reported in [81, 82]. Compliant spine of one-piece elastic material for the trunk of quadruped robot is reported to improve the stability of the robots in[83]. Biological research has concluded that the actuation of the spine contributes significantly to the performance of quadrupeds in terms of control. Three spine morphologies: rigid spine, passive spine, and actuated spine, are tested in Renny robot [84]. A solution for the steering problem of a quadruped robot such that it follows a desired path specified by a set of waypoints was presented in [85].

Four-segment legged robot with single joint articulation, BISAM, can rotate in the sagittal plane for mammalian gaits, and, in the transverse plane, for reptilian gaits. The articulation in the spine was investigated using a biologically inspired adaptive control concept in [86]. Learning gaits using advanced reinforcement learning techniques for posture control of robot was reported in [87]. ELIRO (Eating LIzard RObot) is an articulating robot that can bend passively in the transverse plane and actively in the dorsal plane, with a zig-zag gaiting methodology presented in [88, 89] uses the articulation in the spine for the negotiation of narrow spaces and direction changes, based on rotation around the articulating mode.

The implications of torso articulation on the dynamics of quadrupedal running are examined in a template setting in [90]. In this the authors presented the spring loaded inverted pendulum,

sagittal-plane model with a segmented articulated torso and with compliant legs was introduced for the dynamics of bounding. The energetics of quadrupedal running with a bounding gait in the context of two reductive sagittal plane models with and without torso compliance presented in [91]. Self-stable cyclic bounding gaits existence in the presence of articulated torso and hybrid controller implemented in [92, 93]. The presence of an actuated spinal joint improves the performance of the quadrupedal bounding compared with a rigid torso robot body [94, 95, 96, 97, 98].

Following in time, work focused on the autonomous mechanism of the robot [99]. Ikuo Mizuuchi created a line of articulated robots, starting with a quadrupedal known as SQ43 [100, 101]. More robots followed but all in the humanoid articulated spine form [102, 103, 104, 105]. In SQ43 the spine is a multi-segmented body integrated into the quadruped with a genetic algorithm as the motion generator [106]. The system incorporated finite element methods to model the spine. The use of the spine is also able to diffuse harsh forces by applying the load along its length rather than at a foot print.

Development of a three degree of freedom spine robot GEO was reported in [76]. Central pattern generators (CPG), postural reflexes, and forward models are used to control the robot [107]. The body was able to rotate in and out of the sagittal and transverse planes with a twist-slide mechanism. A planar quadruped robot with articulated spine developed at MIT's leg lab. The author presented the role of the spine and trunk as providing three functions: increasing the effective leg length, storing and transferring energy, and providing auxiliary power to legs in [108]. Passively compliant, actively controlled body joints can be found in the Whegs series of robots [87, 109]. Multi-segmented, articulated robot with passive legs moving between water and land using CPG's and reflex controllers to swim, crawl and walk were reported in [110, 111, 112].

Development of a biomimetic cheetah-inspired robot by BDI and MIT was featured with a lightweight, flexible spine and high-speed articulating quadruped robot. In general, the overall motivation for the articulation in the robots is to mimic nature. The majority of these robots focused on developing controllers like a CPG or reinforcement learning technique to enable a stable gait. The goal of high speed locomotion may not be obtained with a rigid torso. Understanding how articulation was incorporated in the past, lends insight to its integration in future systems [76].

1.3.4 Literature Review on Passive Dynamics

Passive dynamics means dynamical behavior of actuators, robots, or when there is no active supply of energy to achieve the motion. In legged robots design and more relaxed control of passive dynamics has become a complementary (or even alternative) approach to joint-positioning control methods. In terms of Ioannis Poulakakis, passive dynamics means the unforced response of a system under a set of initial conditions. In general, characterizing the properties and conditions of the passive behavior and identifying regions of the model parameters where the system can passively stabilize itself, can lead to designing controllers, which are not entirely based on continuous state-feedback like computed-torque controllers [113, 114].

Simulations and analysis suggest that suitably designed legged machines will be able to run passively i.e. without actuation and control. However, due to practical limitations, there are no legged robots which operate completely passively, except McGeer's passive dynamic walkers bipeds [115, 116]. Smith and Berkemeier extended McGeer's work from bipedal to quadrupedal locomotion [117]. While running, the leg acts as a spring compressing during contact with ground phase and

decompressing during the reactive phase. The Spring Loaded Inverted Pendulum (SLIP) system has been reported in [51, 118, 119, 120, 121, 122]. In the SLIP concept the authors explained, the kinetic and gravitational potential energies are stored as elastic energy in the spring at the contact phase and recovered in the reactive phase. Higher speeds can be achieved because of the compression of the spring, so that the leg remains in contact with the ground. Raibert used the SLIP model to develop controllers to stabilise the legged robots. An analytical study of the SLIP model can be found in [123].

Schmitt and Holmes, proposed a model similar with the SLIP to explain the motions of the body on the horizontal plane, called the Lateral Leg Spring (LLS), [124]. Two-dimensional dynamic model of a hexapedal runner was presented in [125]. The authors chose to model many-legged, sprawled posture animals because of their remarkable stability and self-stabilised to perturbations. The authors observed the recovery from rotational velocity perturbations occurred within one step, whereas for lateral perturbations took multiple strides. The self-stabilized behavior of the mechanical system without the need of any feedback mechanism was presented in the context of the Lateral Leg Spring (LLS) template [124]. LLS template can perform stable periodic motions with out any continuous or intermittent feedback to perturbations, Chigliazza [126] and Seyfarth [122]. The author presented asymptotically stable periodic gaits for the SLIP model existing over a range of parameter values. The authors derived analytically a Poincar map and performed detailed bifurcation and parameter studies. Stable periodic gaits for the SLIP have been reported in [127]. Mass between the hips in the body has a more effect on the behavior of a running system. The author included leg inertia in his model for the bounding and pronking gaits of a quadruped robot [128, 128]. He found that the attitude of the body can be passively stabilized in a bounding gait. Verification of Murphy's conclusions can be found in Berkemeier, [129]. A similar idea of passive cyclic motion can be found in [130].

The concept of templates and anchors is explained in [131]. A 'template' is a model with least number of variables and parameters that exhibits a targeted behavior and advances hypotheses concerning the high-level control strategy underlying the achievement of the task. An 'anchor' is a more elaborate dynamical system. Anchors can reveal the mechanisms by which legs, joints and actuators function to produce the behavior of the template. The SLIP models presented above are templates for studying walking and running in animals of various postures. To create a template, redundancies in locomotion can be explained by seeking synergies and symmetries [113].

Discrete dynamical system used for passive dynamics is available in the texts of [132, ?, 133]. A tool for understanding the stability of periodic orbits is the Poincare map, [134, 135]. It reduces an nth order continuous-time autonomous system by an $(n-1)^{th}$ order discrete-time system. The studying the stability properties of a periodic solution of a continuous-time system is thus reduced to the periodic points of the Poincar map [113, 136]. David Remy et al. [137, 138] presented a framework for the creation and analysis of efficient gaits for legged systems based on the exploitation of natural dynamics. In this they presented the stability of a passive dynamic walker that determines the ideal position of the leg's center of mass, a prismatic monopod hopper based on series elastic actuators for minimized cost of transportation, and a basic controller created for the model of a bounding robot. A design and the control concept of the Series Compliant Articulated Robotic Leg developed at ETH Zurich, [139] with combined application of a virtual model controller for ground contact and a modified Raibert style controller for flight phase was successfully tested in planar

running. A lightweight design of passive foot segment significantly reduces impact and damping losses to improve energetic efficiency in legged running [140, 141], while simultaneously allowing for a natural-looking stance configuration.

A complete model with the assumption of instantaneous thrust time of the one-dimensional hopping robot was presented in [142]. The design of feedback algorithms for controlling the periodic motions of the one-dimensional hopping monopod were reported in [143, 144], two-dimensional monopod model in [145]. The authors used Raibert's foot placement algorithm (FPA). An alternative approach for the analysis of a one-legged hopping robot, called the energy-balance method unexplained in [146]. A large variety of gaits created completely passively by a quadrupedal model with elastic legs were presented in [147]. The authors identified gaits in a single shooting implementation, varying the contact sequence to identify trotting, pacing, walking, toelting, bounding, and galloping within a single model. For each of these gaits the footfall pattern, ground contact forces, speed, and first order limit cycle stability were reported.

Fixed points are calculated by considering that the energy change along a limit cycle has to be zero. This is equivalent to the fixed points of the Poincar map. Berkemeier studied the bounding and pronking gaits of four-legged animals [148, 149, 129]. David Remy [150, 151] presented the principles of passive dynamic walking onto the three dimensional motion of a simplified quadrupedal model, the simulation framework of a planar system to include a rolling degree of freedom and searched for limit cycles that represent periodic gaits. Passive dynamic oscillation [152] enables energy-efficient locomotion for bounding robot driven by series elastic actuators, in which a highly compliant spring decouples the joint motion from the actual motor.

Passive dynamic bounding gait in quadruped robots was first reported in [153, 154]. Passive dynamic bounding gaits are periodic gaits and can begin at stable or unstable fixed points. Stable gaits do not require any control input and can tolerate disturbances (i.e., self-stabilizing). Unstable gaits can be stabilized by the application of appropriate control inputs. Whether a periodic gait is stable or unstable is determined by the eigenvalues of Poincare map. While self-stabilizing gaits are quite attractive to implement, the region of initial conditions (fixed points) where they exist is limited. Controller for stabilizing gaits starting from unstable fixed points is an active area of research.

1.4 Objectives

- To investigate the energetics of quadruped robots in trot and bounding gait

- To analyze of the effect of Articulated Torso for negotiating obstacle

- To propose a control law for passive dynamic bounding gait

- To anlyze the effect of mass and stiffness asymmetry in passive dynamic bounding gait

1.5 Scope

- Energetics through cost of transport under the assumption of constant height level trot gait and bounding gait

- Modeling and simulations of rigid torso and articulated torso of quadruped robot

- Control law for quadruped passive dynamic bounding with symmetric mass and stiffness

1.6   Outline of the dissertation

This thesis describes research where the goal has been to investigate ways to improve energy efficiency of quadruped robots, such as the energetics of quadruped robot while in trot and bound gaits, use of passive dynamics to achieve almost zero cost of transport, and the advantages of articulated torso. The basis for the energetics is calculate the work done by the individual actuators then estimate the cost of transport/specific resistance of the quadruped robot. Study of passive dynamics as applied to bounding gait includes control laws for symmetry quadruped robots and stability properties of quadruped robots with mass and stiffness asymmetry.

The dissertation is organised as follows:

Chapter 1: *Introduction.* The introductory chapter describes the meaning of locomotion for the legged mobile robot in trot and bound gaits. It also presents the research problem of how to utilize most efficient locomotion system with optimal design and gait parameters in an efficient and clever way. A through survey of literature is included to bring out state-of-the-art.

Chapter 2: *Energetics of Trot Gait.* The energetics of trot gait in quadruped robots in 2D with asymmetric body mass distribution for two cases of level trotting one at constant speed and other deceleration-acceleration with constant average speed are discussed. Quasi-passive trotting also presented for reduced energetic costs for these two cases. This analysis is repeated in 3D to account for roll moment.

Chapter 3: *Energetics of Bounding Gait.* The energetics of constant height level bounding gait in quadruped robots with asymmetric body-mass distribution along the longitudinal axis are discussed. Analytical expressions for mechanical specific resistance for two cases of bounding are derived: bounding with equal front and rear leg step lengths, and bounding with unequal front and rear leg step lengths were also presented.

Chapter 4: *Quadruped Robot with Articulated Torso.* The effect of articulated torso on stability and energy efficiency in walking mode, trot mode and running (bounding) mode are presented. How the articulation of the torso improves higher speed and enhanced mobility in quadruped robot is also discussed.

Chaper 5: *Passive Dynamic Bounding with Symmetry Condition Control Laws.* Passive dynamic bounding of quadruped robot control using symmetry condition observed in periodic gaits is introduced.

Chapter 6: *Passive Dynamic Bounding with Asymmetry.* Passive dynamic bounding of quadruped robot with mass and stiffness asymmetry presented. A new method of searching for fixed points is

also introduced.

Chapter 7: *Conclusions and Recommendations for Future Work* Conclusions of the work done in this thesis and recommendations for future work are presented.

Chapter 2

Energetics of Trot Gait

2.1 Introduction

Trot is one of most widely used gaits in quadruped robots in which the robot is supported on diagonally opposite legs during support phase [10, 155]. Trot gait is preferred where lower energy consumption is desirable [16]. Trot being a symmetric gait, there exists a similarity between biped walking and quadruped trotting where the quadruped can be viewed as two bipeds connected one behind the other. Although minimizing the vertical motion of center of mass (CoM) increases the cost of transport [71], level walking can be important when there are restrictions on the motion of load being carried by the robot, for instance, when a patient is being carried on the battle front.

In load carrying quadruped robots, especially where loads are changed often, it is a time consuming exercise to make the body mass distribution even. Whether such an exercise is desired from energy efficiency point of view is also not clear. Studies on the effect of body mass distribution show that asymmetric loading alters the vertical and horizontal forces generated by fore and hind limbs in level trotting gait of dogs [156]. While this holds true for quadruped robots, the effect of asymmetric body mass distribution on cost of transport has not been investigated yet.

In this chapter, level walking trot gaits with duty factor of 0.5 with no double support and flight phases are considered. The first part of the chapter analyzes trot as a purely planar gait without considering the possibility of the roll moment about the longitudinal axis. Asymmetry of mass is also considered. Two cases of level walking are considered: one with constant speed throughout the gait cycle, and another with varying speed but constant average speed. In order to investigate the effect of mass distribution, the quadruped robots are assumed to have asymmetric body-mass distribution both along the horizontal and vertical axes. Quasi-passive level trotting is also discussed where the cost of transport is significantly lowered by using springs to store energy during negative work and release it during positive work.

The second part of the chapter analyzes trot as a spatial gait considering the possibility of roll moment about the longitudinal axis. In order to simplify the analysis in 3D, symmetric mass distribution in the quadruped robot body is assumed. More accurate analysis in 3D indicates the impossibility of constant speed gait at constant height and zero pitch (level). For the gait with deceleration and acceleration, the cost of transport expression is identical to that derived in planar case.

2.2   Model of the Quadruped Robot

The legs of the quadruped robot studied in this chapter consists of two joints each: hip and knee. The upper and lower leg lengths are assumed to be equal. Center of mass (CoM) is at a distance of (a_x, a_y) from the body center.

The forces produced by the knee actuators act along the line joining the point of contact of the leg with the ground and the hip joint. The forces produced by hip actuators act perpendicular to the forces produced by knee actuators. The net force produced by knee and hip actuator of a leg is such that the vertical component of the ground reaction force is always upward.

For determining specific resistance, we use mechanical cost of transport obtained from

$$c_m = \frac{\frac{1}{T} \int_0^T |P| dt}{mgv}, \tag{2.1}$$

where P is instantaneous power, m is the mass of the quadruped robot, g is the acceleration due to gravity, v is the average speed and T is the cycle time. Mechanical cost of transport can also be obtained from

$$c_m = \frac{\sum_i |W_i|}{mgd}, \tag{2.2}$$

where W_i is the absolute sum of work done by i^{th} actuator for all the phases of one gait cycle, and d is the corresponding distance travelled.

For low speeds and high torques, Joule-thermal losses dominate the energy consumed by actuators [16]. Here we assume that, actuators operate at sufficiently high speed where mechanical cost of transport reasonably approximates the actual cost of transport. Although the motors run at high speed and low torque where Joule-thermal losses are very low, the torque required at the joints is obtained after speed reduction using gear head. If efficient gear heads such as harmonic gear drives are used then gear friction loss can be neglected.

Two quadruped robot leg configurations are possible as shown in Fig. 2.1. In this chapter we consider quadruped robot leg with prismatic joint as shown on Fig. 2.1 right.
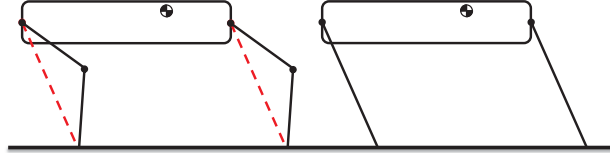
Figure 2.1: Model of quadruped robot

2.3   Level Walking at Constant Speed

Let L_s be the distance traveled by the center of mass for one complete cycle (all the four leg swings). For trot gait, one cycle can be divided into four phases, where phases 3 and 4 are performed with diagonally opposite legs and are identical to phases 1 and 2 shown in Fig. 2.2.

Let $\boldsymbol{F_F}$ and $\boldsymbol{F_R}$ be the forces applied by the front and rear legs respectively on the quadruped body. These are same as the reaction forces at the points of contact of the front and rear legs with
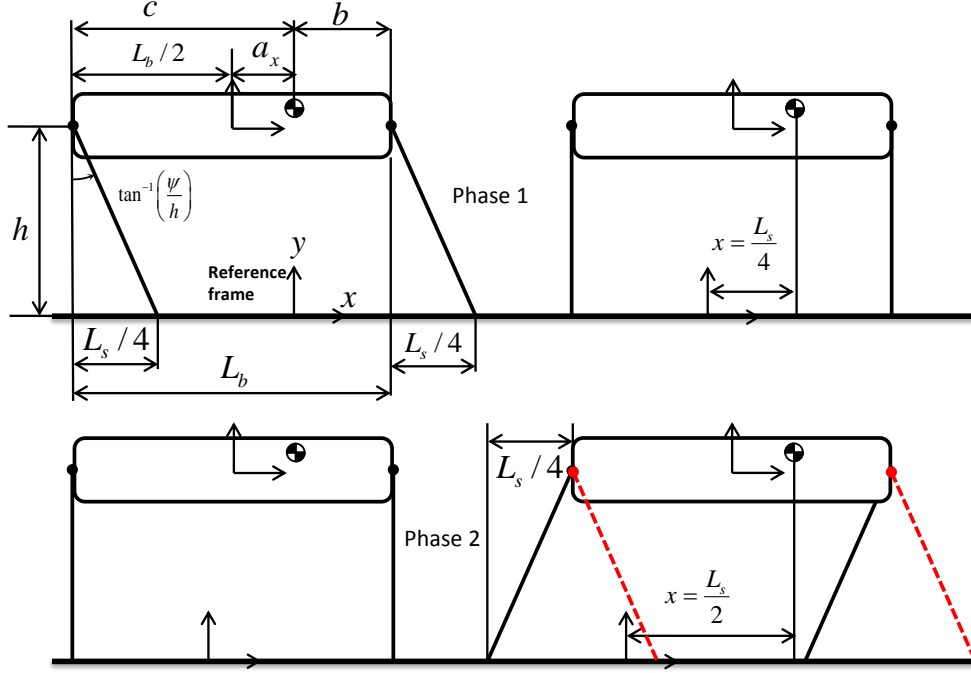
Figure 2.2: Phases 1 and 2 in trot gait (Legs shown in black are Right Front and Left Back legs, legs shown in red are Left Front and Right Back

the ground. For the quadruped robot to continue to move at the same horizontal speed, sum of all horizontal forces should be zero.

$$F_{Rx} + F_{Fx} = 0. \tag{2.3}$$

Here, we make a simplifying assumption that

$$F_{Rx} = F_{Fx} = 0. \tag{2.4}$$

The advantage of having zero horizontal reaction forces is that the quadruped robot can trot on low friction surfaces without slipping. However, in practice, nonzero net horizontal force is required for starting or stopping.

For level walking at constant height, weight of the robot should be balanced by total vertical force:

$$F_{Ry} + F_{Fy} = mg, \qquad F_{Ry} > 0, \quad F_{Fy} > 0. \tag{2.5}$$

Body of the quadruped should always remain horizontal. Therefore, net moment about the center of mass should be equal to zero. Reaction forces at the point of contact with the ground is as shown in Fig. 2.3. Let r_R and r_F be the positions of ground contact points of rear and front feet with respect to the center of mass. Then,
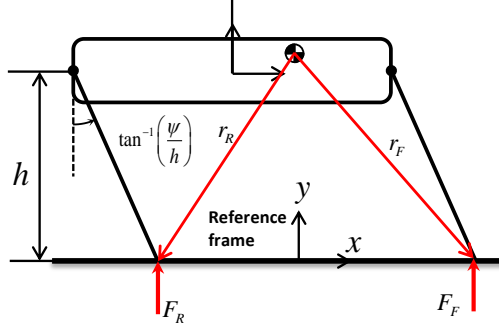
Figure 2.3: Reaction forces at the point of contact with the ground

$$\boldsymbol{r_R} \times \boldsymbol{F_R} = -\boldsymbol{r_F} \times \boldsymbol{F_F}, \tag{2.6}$$

$$r_{Rx}F_{Ry} - r_{Ry}F_{Rx} = -r_{Fx}F_{Fy} + r_{Fy}F_{Fx}, \tag{2.7}$$

$$F_{Ry} = -\frac{r_{Fx}}{r_{Rx}}F_{Fy}. \tag{2.8}$$

Substituting (2.8) in (2.5), we get:

$$F_{Ry} = \frac{r_{Fx}mg}{r_{Fx} - r_{Rx}}, \qquad F_{Fy} = -\frac{r_{Rx}mg}{r_{Fx} - r_{Rx}}. \tag{2.9}$$

Here,

$$r_{Fx} = b - \psi, \quad r_{Rx} = -c - \psi, \tag{2.10}$$

where

$$b = \left(\frac{L_b}{2} - a_x\right), \quad c = \left(\frac{L_b}{2} + a_x\right),$$

$$\psi = \left(x - \frac{L_s}{4}\right).$$

Forces exerted by one leg on the quadruped robot body is related to the hip and knee joint torques of the leg as:

$$\begin{Bmatrix} F_x \\ F_y \end{Bmatrix} = \begin{bmatrix} a_{11} & a_{12} \\ a_{21} & a_{22} \end{bmatrix} \begin{Bmatrix} \tau_h \\ \tau_k \end{Bmatrix}, \tag{2.11}$$

where the matrix A is Jacobian inverse transpose of the leg with base at hip joint. Considering the rear leg, each of the joint torques τ_h and τ_k individually produce $\boldsymbol{F_{Rh}}$ and $\boldsymbol{F_{Rk}}$ respectively whose resultant is $\boldsymbol{F_R}$.

Since $F_{Rx} = 0$, $F_{Rkx} = -F_{Rhx}$. During phase 1, F_{Rkx} does negative work, whereas F_{Rhx} does equal amount of positive work. During phase 2, this is reversed. Work done by vertical components of forces is zero because there is no vertical movement.

15
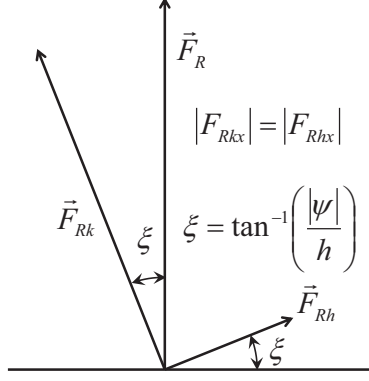
Figure 2.4: Forces at the point of contact

From Fig. 2.4, we can write

$$\frac{F_{Rkx}}{F_{Rky}} = \frac{\psi}{h}, \qquad \frac{F_{Rhx}}{F_{Rhy}} = -\frac{h}{\psi}, \tag{2.12}$$

and therefore

$$F_{Rkx} = \frac{h\psi}{\psi^2 + h^2} F_{Ry}. \tag{2.13}$$

Let W_{Rk1} and W_{Rk2} be the work done by knee joint during phases 1 and 2 respectively.

$$W_{Rk1} = \int_0^{\frac{L_s}{4}} F_{Rkx} dx = -W_{Rh1}, \tag{2.14}$$

$$W_{Rk2} = \int_{\frac{L_s}{4}}^{\frac{L_s}{2}} F_{Rkx} dx = -W_{Rh2}. \tag{2.15}$$

Here,

$$F_{Rkx} = \left(\frac{h\psi}{\psi^2 + h^2}\right) \left(\frac{b - \psi}{L_b}\right) mg. \tag{2.16}$$

Therefore,

$$W_{Rk1} = \int_{-\frac{L_s}{4}}^{0} \left(\frac{h\psi}{\psi^2 + h^2}\right) \left(\frac{b - \psi}{L_b}\right) mg\, d\psi, \tag{2.17}$$

$$= -\frac{mghb}{2L_b} \ln\left[1 + \left(\frac{L_s}{4h}\right)^2\right] + \frac{mgh^2}{L_b}\left[\tan^{-1}\left(\frac{L_s}{4h}\right) - \frac{L_s}{4h}\right]. \tag{2.18}$$

Similarly,

$$W_{Rk2} = \int_0^{\frac{L_s}{4}} \left(\frac{h\psi}{\psi^2 + h^2}\right) \left(\frac{b - \psi}{L_b}\right) mg\, d\psi, \tag{2.19}$$

$$= \frac{mghb}{2L_b} \ln\left[1 + \left(\frac{L_s}{4h}\right)^2\right] + \frac{mgh^2}{L_b}\left[\tan^{-1}\left(\frac{L_s}{4h}\right) - \frac{L_s}{4h}\right]. \tag{2.20}$$

16

Energy consumed by rear leg for phases 1 and 2 is

$$E_R = |W_{Rk1}| + |W_{Rh1}| + |W_{Rk2}| + |W_{Rh2}|, \tag{2.21}$$

$$E_R = 2|W_{Rk1}| + 2|W_{Rk2}|. \tag{2.22}$$

Consider the front leg now. Let W_{Fk1} and W_{Fk2} be the work done by knee joint during phases 1 and 2 respectively.

$$W_{Fk1} = \int_0^{\frac{L_s}{4}} F_{Fkx} dx = -W_{Fh1}, \tag{2.23}$$

$$W_{Fk2} = \int_{\frac{L_s}{4}}^{\frac{L_s}{2}} F_{Fkx} dx = -W_{Fh2}. \tag{2.24}$$

Here,

$$F_{Fkx} = \frac{h\psi}{\psi^2 + h^2} F_{Fy}, \tag{2.25}$$

$$= \left(\frac{h\psi}{\psi^2 + h^2} \right) \left(\frac{c + \psi}{L_b} \right) mg. \tag{2.26}$$

Therefore,

$$W_{Fk1} = \int_{-\frac{L_s}{4}}^{0} \left(\frac{h\psi}{\psi^2 + h^2} \right) \left(\frac{c + \psi}{L_b} \right) mg\, d\psi, \tag{2.27}$$

$$= -\frac{mghc}{2L_b} \ln\left[1 + \left(\frac{L_s}{4h} \right)^2 \right] + \frac{mgh^2}{L_b} \left[\frac{L_s}{4h} - \tan^{-1}\left(\frac{L_s}{4h} \right) \right]. \tag{2.28}$$

Similarly,

$$W_{Fk2} = \int_0^{\frac{L_s}{4}} \left(\frac{h\psi}{\psi^2 + h^2} \right) \left(\frac{c + \psi}{L_b} \right) mg\, d\psi \tag{2.29}$$

$$= \frac{mghc}{2L_b} \ln\left[1 + \left(\frac{L_s}{4h} \right)^2 \right] + \frac{mgh^2}{L_b} \left[\frac{L_s}{4h} - \tan^{-1}\left(\frac{L_s}{4h} \right) \right]. \tag{2.30}$$

Energy consumed by front leg for phases 1 and 2 is

$$E_F = |W_{Fk1}| + |W_{Fh1}| + |W_{Fk2}| + |W_{Fh2}|, \tag{2.31}$$

$$E_F = 2|W_{Fk1}| + 2|W_{Fk2}|. \tag{2.32}$$

The mechanical cost of transport (c_m) of the quadruped robot is given by

$$c_m = 2 \frac{|W_{Rk1}| + |W_{Rk2}| + |W_{Fk1}| + |W_{Fk2}|}{mg \frac{L_s}{2}}, \tag{2.33}$$

$$= 2 \frac{mgh \ln \left[1 + \left(\frac{L_s}{4h}\right)^2\right]}{mg \frac{L_s}{2}}, \tag{2.34}$$

$$c_m = \frac{4h}{L_s} \ln \left[1 + \left(\frac{L_s}{4h}\right)^2\right]. \tag{2.35}$$

The mechanical cost of transport for a point mass planar biped in level walking at constant speed is $L_s/6h$ [157].

2.4 Level Walking with Deceleration and Acceleration

We make a simplifying assumption that only knee forces are used for walking. Hence, the forces generated by knee actuators will be along the line joining the hip joint and the point of contact of the foot with the ground. In order to maintain constant height and zero orientation, the following conditions have to be satisfied:

$$\boldsymbol{r_R} \times \boldsymbol{F_R} = -\boldsymbol{r_F} \times \boldsymbol{F_F}, \tag{2.36}$$

$$F_{Ry} + F_{Fy} = mg, \qquad F_{Ry} > 0, \quad F_{Fy} > 0. \tag{2.37}$$

Let $\psi = \left(x - \frac{L_s}{2}\right)$. Horizontal forces due to front and rear legs are related to respective vertical forces as:

$$F_{Rx} = \frac{\psi}{h} F_{Ry}, \qquad F_{Fx} = \frac{\psi}{h} F_{Fy}. \tag{2.38}$$

Equation (2.36) can be expanded as follows:

$$r_{Rx} F_{Ry} - r_{Ry} F_{Rx} = -r_{Fx} F_{Fy} + r_{Fy} F_{Fx} \tag{2.39}$$

where $r_{Ry} = r_{Fy} = -(h + a_y)$, $r_{Fx} = b - \psi$, $r_{Rx} = -c - \psi$, $b = \left(\frac{L_b}{2} - a_x\right)$, and $c = \left(\frac{L_b}{2} + a_x\right)$. Substituting (2.38) in the above equation, we get

$$F_{Ry} = \frac{bh + a_y \psi}{ch - a_y \psi} F_{Fy}. \tag{2.40}$$

From (2.37) and (2.40), we can write:

$$F_{Ry} = (bh + a_y \psi) \frac{mg}{hL_b}, \qquad F_{Fy} = (ch - a_y \psi) \frac{mg}{hL_b}. \tag{2.41}$$

Let W_{R1} and W_{F1} be the work done by the rear and front legs for motion in phase 1, which are determined as follows:

$$W_{R1} = \int_0^{\frac{L_s}{4}} F_{Rx} dx = -\frac{mgL_s^2}{32hL_b} \left[b - a_y \frac{L_s}{6h} \right], \tag{2.42}$$

$$W_{F1} = \int_0^{\frac{L_s}{4}} F_{Fx} dx = -\frac{mgL_s^2}{32hL_b} \left[c + a_y \frac{L_s}{6h} \right]. \tag{2.43}$$

Similarly, the work done by rear and front legs for the second phase can be determined as

$$W_{R2} = \int_{\frac{L_s}{4}}^{\frac{L_s}{2}} F_{Rx} dx = \frac{mgL_s^2}{32hL_b} \left[b + a_y \frac{L_s}{6h} \right], \tag{2.44}$$

$$W_{F2} = \int_{\frac{L_s}{4}}^{\frac{L_s}{2}} F_{Fx} dx = \frac{mgL_s^2}{32hL_b} \left[c - a_y \frac{L_s}{6h} \right]. \tag{2.45}$$

Therefore, the total energy consumed for phases 1 and 2 is given by

$$E = \frac{mgL_s^2}{16hL_b}(b + c) = \frac{mgL_s^2}{16h}. \tag{2.46}$$

The mechanical cost of transport can be calculated as

$$c_m = \frac{\frac{mgL_s^2}{16h}}{mg\frac{L_s}{2}}, \tag{2.47}$$

$$c_m = \frac{L_s}{8h}. \tag{2.48}$$

This is identical to the mechanical cost of transport of a point mass biped robot undergoing level walking with acceleration and deceleration [157]. In fact, quadruped robot in this mode of locomotion is equivalent to two point mass biped robots of half of the mass of quadruped, each connected by a mass less rod as in [8].

2.5   Quasi-Passive Level Trot

Legged robots usually have repetitive leg motions where large negative work is done by joint actuators [158]. Energetic performance can be improved by minimizing the negative work dissipated in the actuators by proper trajectory design, or dynamic walking or by storing energy in compliant elements. Parallel elastic actuators can be used in such cases to improve energy efficiency [159, 160]. In this chapter, we consider springs operating parallel to the actuators at the knee joints only. If we draw the force profile of knee actuator for one gait cycle, we can see that it is always pushing the robot upwards as the actuators have to work against gravity. In order to save energy used by the actuator, a parallel spring can be provided which can take part of the vertical load while the actuator can provide the remaining force to achieve the given conditions of constant height and zero pitch. The Knee actuator is a parallel elastic actuator (or hybrid) as shown in the Fig. 2.5 consisting of spring in parallel to linear actuator.

Let Δl be the maximum compression of the spring due to knee joint motion for the entire
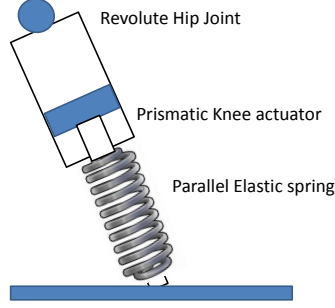
Figure 2.5: Quasi-Passive leg with spring in parallel to linear actuator

duration of a step. Assume that the spring starts compression from the beginning of step. Maximum compression occurs when the line joining ground contact point and the hip joint is vertical. At the end of the step the compression is again zero, since the step length is symmetric about vertical. The energy stored in the spring during phase 1 in each leg is given by

$$E_{s1} = \frac{1}{2}k_l \Delta l^2. \tag{2.49}$$

During phase 1, negative work being done by the knee joint is partly stored in the spring and partly dissipated by the motor in parallel. Equation (2.49) also gives the energy released by the spring during phase 2. Positive work done by the knee joint during phase 2 is also shared by the spring and the knee actuator in parallel. Therefore, considering the energy stored and released by springs in the front and rear legs for phases 1 and 2, the effective mechanical cost of transport is given by

$$c_{me} = c_m - \frac{\frac{1}{2}k_{lf}\Delta l^2 + \frac{1}{2}k_{lf}\Delta l^2 + \frac{1}{2}k_{lr}\Delta l^2 + \frac{1}{2}k_{lr}\Delta l^2}{mg\frac{L_s}{2}}, \tag{2.50}$$

where k_{lf} and k_{lr} are the effective linear spring stiffnesses for the front and rear knee joints respectively. If the maximum spring forces at the front and rear leg knee joints together balance the weight of the quadruped, then

$$k_{lf}\Delta l + k_{lr}\Delta l = mg, \tag{2.51}$$

$$k_{lf}\Delta l^2 + k_{lr}\Delta l^2 = mg\Delta l. \tag{2.52}$$

where

$$\Delta l = \sqrt{h^2 + \left(\frac{L_s}{4}\right)^2} - h. \tag{2.53}$$

Therefore, the effective mechanical cost of transport for level trotting is given by

$$c_{me} = c_m - \frac{2h}{L_s}\left(\sqrt{1 + \left(\frac{L_s}{4h}\right)^2} - 1\right). \tag{2.54}$$

Further reduction in cost may be possible with nonzero initial compression of knee springs at the beginning of each step.

Here we have assumed that the knee springs are free at the beginning and the end of each step. However, in order to prevent the leg from scuffing the ground during the swing phase, knee should undergo almost the same angular motion as in stance phase or more when crossing obstacles. If knee springs are compressed during swing phase through knee actuators, significant energy is lost when it is released for the beginning of the step. We assume that by suitable mechanism design, knee springs can be engaged only during stance phase.

2.6   Results and Discussion for Trot in 2D

Figure 2.6 shows the specific resistance plotted as a function of maximum angle ($\alpha = \arctan(L_s/(4h))$) made by legs with respect to vertical at the beginning of phase 1 or end of phase 2. Comparison of specific resistances of the level trot gaits shows that, for the same step length, constant speed gaits have relatively higher energy consumption for larger heights or smaller α. This trend is reversed for higher α. Lower specific resistance at higher step length to height ratios is an advantage when the quadruped robot is required to traverse in restricted spaces where limited height is available.
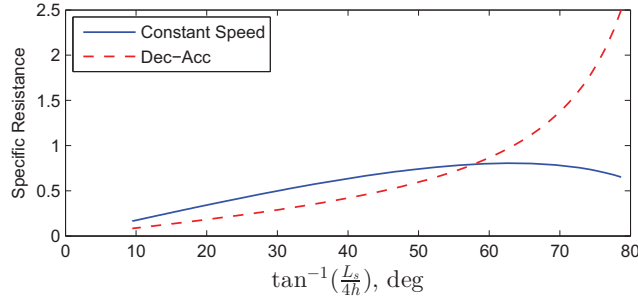
Figure 2.6: Specific resistance Vs maximum leg angle

Significant energetic cost reduction can be achieved using a passive compliant energy storage element in parallel with the knee joint actuators. Figure 2.7 shows the reduced specific resistances obtained with quasi-passive trotting.
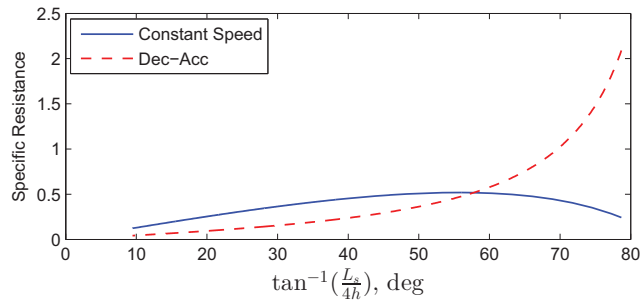
Figure 2.7: Specific resistance Vs maximum leg angle for quasi-passive trotting

Comparison of energetics of quadruped and biped robots in constant speed level walking in Fig. 2.8 shows an interesting difference. In deceleration-acceleration case, specific resistances are identical for quadruped and biped robots. In constant speed case, while specific resistance for biped robot increases monotonously, for quadruped robot it increases initially and then decreases below

that of biped robot. In fact, constant speed level walking is technically not possible for biped robots because of the requirement of double support phase through out the gait cycle. It is possible in quadruped robots in level trot since at any point of time two legs (front and rear) are in support phase.
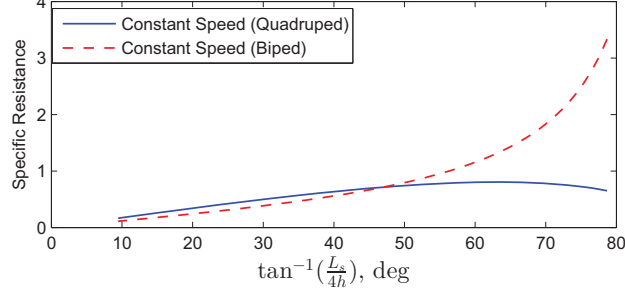
Figure 2.8: Comparison of specific resistances of quadruped robot in constant speed level trotting and biped robot in constant speed level walking

Asymmetric body mass distribution has no effect on specific resistance in level trotting with constant speed and with deceleration-acceleration. Though constant speed level trotting is energetically more costly than level trotting with deceleration-acceleration at lower step length to height ratios, specific resistance tends to decrease significantly at higher step length to height ratios. Energetic costs in both the cases can be further reduced by storing negative work using compliant storage elements such as springs or by electrical regeneration.

2.7   Reconsidering Constant Height Level Trot Gait in 3D

Assuming the quadruped robot starts moving from a level posture, the net moment on the body about the center of mass should be zero in order to maintain the same level posture. Mathematically,

$$\boldsymbol{r}_F \times \boldsymbol{f}_F + \boldsymbol{r}_R \times \boldsymbol{f}_R = 0, \tag{2.55}$$

where $\boldsymbol{r}_F$ and $\boldsymbol{r}_R$ are the position vectors of the front and rear foot contact point with respect to center of mass of the body, $\boldsymbol{f}_F$ and $\boldsymbol{f}_R$ are the reaction forces from the ground at the front and rear foot contact points. In expanded form,

$$(r_{Fy}f_{Fz} - r_{Fz}f_{Fy}) + (r_{Ry}f_{Rz} - r_{Rz}f_{Ry}) = 0 \tag{2.56}$$

$$(r_{Fz}f_{Fx} - r_{Fx}f_{Fz}) + (r_{Rz}f_{Rx} - r_{Rx}f_{Rz}) = 0 \tag{2.57}$$

$$(r_{Fx}f_{Fy} - r_{Fy}f_{Fx}) + (r_{Rx}f_{Ry} - r_{Ry}f_{Rx}) = 0 \tag{2.58}$$

where the position vectors $\boldsymbol{r}_F$ and $\boldsymbol{r}_R$ can be written as:

$$\boldsymbol{r}_F = \left\{ \begin{array}{c} \left(\frac{L_b}{2} - a_x - \psi\right) \\ -(a_y + h) \\ -w \end{array} \right\} \quad \boldsymbol{r}_R = \left\{ \begin{array}{c} -\left(\frac{L_b}{2} + a_x + \psi\right) \\ -(a_y + h) \\ w \end{array} \right\}$$

where $\psi = x - \frac{L_s}{4}$.

22

Further, forces along y-axis and z-axis should be balanced:

$$f_{Fy} + f_{Ry} = mg \tag{2.59}$$

$$f_{Fz} + f_{Rz} = 0 \tag{2.60}$$

Equations (2.56-2.60) are five equations in six unknowns and hence the solution is non-unique. These set of five equations can be written in matrix form as follows:

$$\boldsymbol{A}\boldsymbol{f} = \boldsymbol{b} \tag{2.61}$$

where $\boldsymbol{A}$ is a rectangular matrix of size 5×6, $\boldsymbol{f} = [f_{Fx}\ f_{Fy}\ f_{Fz}\ f_{Rx}\ f_{Ry}\ f_{Rz}]^T$, and $\boldsymbol{b} = [0\ 0\ 0\ mg\ 0]^T$.

Determinant of the left-most 5×5 matrix of $\boldsymbol{A}$ is $4w^2(a_y + h)$. Since this is independent of x, this holds for the entire (half) cycle from $x = 0$ to $x = L_s/2$ for phases 1 and 2. Assuming nonzero values for width of the quadruped w, and the term $(a_y + h)$, the rank of matrix $\boldsymbol{A}$ is 5. According to Rouché-Capelli theorem, if the augmented matrix $[\boldsymbol{A}|\boldsymbol{b}]$ has same rank as $\boldsymbol{A}$, then (2.61) is a consistent set of equations. Since this is satisfied, solution to (2.61) exists.

The general solution for $\boldsymbol{f}$ is given by

$$\boldsymbol{f} = \boldsymbol{A}^+\boldsymbol{b} + (I - \boldsymbol{A}^+\boldsymbol{A})\boldsymbol{u} \tag{2.62}$$

where $\boldsymbol{A}^+$ is the Moore-Penrose psuedo inverse of $\boldsymbol{A}$, $\boldsymbol{u}$ is an arbitrary vector. Minimum norm solution is obtained for $\boldsymbol{u} = 0$. A minimum norm solution is one that minimizes sum of squares of elements of $\boldsymbol{f}$.

2.7.1 Gait with Deceleration and Acceleration

Since $\boldsymbol{A}$ has a rank of 5, the rows of $\boldsymbol{A}$ are linearly independent. Psuedo-inverse of $\boldsymbol{A}$ can be determined as

$$\boldsymbol{A}^+ = \boldsymbol{A}^T(\boldsymbol{A}\boldsymbol{A}^T)^{-1}. \tag{2.63}$$

Minimum norm solution of (2.61) that satisfies all the five equations exactly has nonzero, but equal, force components along x-axis, and zero force components along z-axis as shown below.

$$\boldsymbol{f} = \left\{ \begin{array}{c} \frac{mg}{2}\left(\frac{a_x+\psi}{a_y+h}\right) \\ \frac{mg}{2} \\ 0 \\ \frac{mg}{2}\left(\frac{a_x+\psi}{a_y+h}\right) \\ \frac{mg}{2} \\ 0 \end{array} \right\} \tag{2.64}$$

Each of the vertical force components is equal to half the weight of the robot. If the mass distribution is uniform ($a_x = a_y = 0$), the reaction force generated at each foot contact point due to the leg actuator forces/torques is along the line joining the contact point and the hip joint. This indicates that, since knee actuator generates such a force/torque, only knee actuator is sufficient for propulsion in constant height level trot gait if there is no mass asymmetry.

The resultant force of the reaction forces at front and rear foot contact points at any point of time during the gait cycle is in the direction of the center of mass and occurs on the line joining the front and rear foot contact points. This satisfies the zero moment point condition for stable walking.

Augmenting the system of equations (2.61) to include a condition $f_{Fy} = 0$ or $f_{Ry} = 0$ increases the rank of the matrix to 6, and yields a unique solution $\boldsymbol{f}$ which is identical to the minimum norm solution obtained with the original system.

2.7.2 Gait with Constant Speed

For constant speed gait, the net reaction force along x-axis should be zero:

$$f_{Fx} + f_{Rx} = 0. \tag{2.65}$$

Adding this equation to the set (2.56-2.60), we have six equations in six unknowns, which can be written in matrix form as

$$\boldsymbol{A}_1 \boldsymbol{f} = \boldsymbol{b}_1. \tag{2.66}$$

Matrix $\boldsymbol{A}_1$ has a rank 5, and hence unique solution cannot be determined. For this set of equations to be consistent, rank of the augmented matrix $[\boldsymbol{A}_1 | \boldsymbol{b}_1]$ should be 5. However, the rank of the augmented matrix is found to be 6, which means, there is no solution to (2.66). Nonzero horizontal force is unavoidable which leads to a gait with acceleration and deceleration.

This result can also be obtained by reasoning as follows: Any point on the line joining the front and rear foot leg contact points is where the resultant of gravitational and inertia forces should pass. For constant speed gait where inertia force is zero, this resultant passes through a point on the ground directly below the center of mass as shown in Fig. 2.9. Since this does not lie on the support pattern, the robot tends to tipover. Stable gait does not seem to be possible.
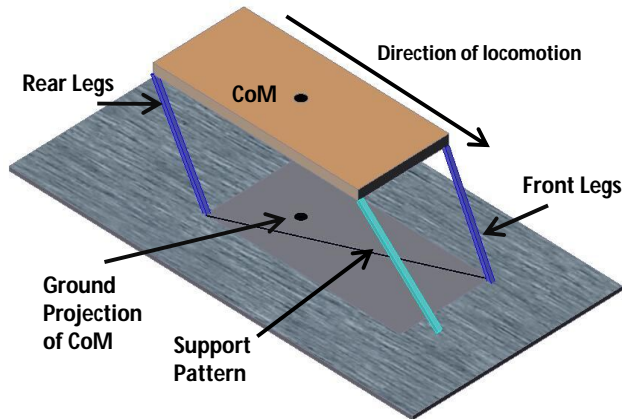
Figure 2.9: Constant speed gait is unstable

If point foot assumption is relaxed and sufficient foot width is provided, the projection of center of mass on the ground can be maintained within the support pattern, and constant speed gait can be made possible.

2.8　Specific Resistance

During phase 1, f_{R1} and f_{F1} do equal amount of negative work. During phase 2, both do positive work. Work done by vertical components of forces is zero because there is no vertical movement.

From (2.64), reaction forces at the front and rear leg contact points can be written as

$$f_{Fx} = \frac{mg}{2}\left(\frac{a_x + \psi}{a_y + h}\right) \quad f_{Fy} = \frac{mg}{2} \quad f_{Fz} = 0 \tag{2.67}$$

$$f_{Rx} = \frac{mg}{2}\left(\frac{a_x + \psi}{a_y + h}\right) \quad f_{Ry} = \frac{mg}{2} \quad f_{Rz} = 0 \tag{2.68}$$

where

$$\psi = \left(x - \frac{L_s}{4}\right).$$

Since the centre of mass is at geometric centre, and both the front and back legs are making same angle with the verticle, the vertical components of the front and back legs reaction forces are equal to half the weight.

Assuming symmetry mass distribution $a_x = a_y = 0$, work done by horizontal force f_{Fx} is given by

$$\left|\int_0^{\frac{L_s}{4}} \frac{mg}{2}\left(\frac{\psi}{h}\right) dx\right| = \frac{mgL_s^2}{64h} \tag{2.69}$$

Total work done by front and rear legs in phase 1 is

$$\frac{mgL_s^2}{32h}. \tag{2.70}$$

Work done for phase 2 is positive and is equal to the work done in phase 1 due to symmetry of phases 1 and 2. The total work done by front and rear legs for phases 1 and 2 is

$$\frac{mgL_s^2}{16h}. \tag{2.71}$$

Therefore, the specific resistance is

$$c_m = \frac{\frac{mgL_s^2}{16h}}{\frac{mgL_s}{2}} = \frac{L_s}{8h} \tag{2.72}$$

This is identical to the cost of transport expression derived earlier under planar assumption of trot gait.

2.9　Conclusions

Although the cost of transport expression was derived for trot gait under planar assumption, it has been shown with more accurate 3D analysis that constant speed locomotion is not possible in constant height level trotting gait. Minimum norm solution gives deceleration and acceleration with

requirement of only the knee actuator force or torque. The cost of transport expressions derived for deceleration and acceleration case are identical in 3D and 2D analysis. However, an assumption of symmetric mass distribution is used in 3D analysis. In the presence of asymmetry, the cost could differ from the expression derived.

Chapter 3

Energetics of Bounding Gait

3.1 Introduction

Quadrupedal animals choose a gait based on speed required [161]. Of various possible quadruped gaits, bounding gait is a form of fast running legged locomotion in which a quadruped animal uses front legs as a pair and rear legs as a pair [8]. In this gait, the quadruped lands with both of its front legs and moves the rear legs forward, lands, and swings the front leg pair further to the next step. Unlike other quadrupedal gaits, bounding is a highly dynamic gait which requires proper planning and control based on dynamic considerations [162, 163]. In addition to being fast, bounding gait is also energetically more expensive gait for locomotion [164]. Hence, there is a need to study bounding gait in order to choose optimal design and gait parameters.

The minimization of energy consumption plays a major role in the locomotion of legged robots for reducing on-board battery weight or extending the range of a mission. Reduced energy consumption is possible using minimum number of actuators for specific cases such as motion on horizontal straight line [69]. Legged robots usually have repetitive leg motions where large negative work is done by joint actuators [158]. Energetic performance can be improved by minimizing the negative work dissipated in the actuators by proper trajectory design, or dynamic walking or by storing energy in compliant elements. Parallel elastic actuators can be used in such cases to improve energy efficiency [159, 160]. Our approach to minimize energy expenditure for bounding gaits in this chapter is to determine analytical expressions for mechanical cost of transport or specific resistance and then choose the design and gait parameters that reduce energy expenditure.

Constant height level bounding gait, which is the focus of this chapter, is a type of bounding gait in which the body of the quadruped robot is horizontal (no pitching motion) and at constant height from the ground throughout the gait cycle. Assuming the body weight is significant (say, at least 60 to 80 times in quadruped robots) compared to leg weights, the center of mass (CoM) remains essentially at the same height. Although minimizing the vertical motion of CoM increases the cost of transport [71], level bounding can be important where there are restrictions on the motion of load being carried by the robot. Specific resistance or cost of transport for quadruped robots reported in literature are based on experiments and/or numerical simulations for bounding gaits with flight phase [165, 166, 30]. However, there is a need to determine analytical expressions for cost of transport as a function of design and gait parameters in order to evaluate their influence

on energy efficiency. This helps in an energy efficient design of quadruped robots. Some recent works on deriving analytical expressions for constant level trot gaits in quadruped robots in 2D and 3D are reported in [9] and [167] respectively.

Studies on the effect of body mass distribution show that asymmetric loading alters the vertical and horizontal forces generated by fore and hind limbs in level trotting gait of dogs [156]. While this holds true to quadruped robots, the effect of asymmetric body mass distribution on cost of transport has not been investigated yet in biomechanics and robotics literature. It is important to study the effect of mass asymmetry on energy efficiency in quadruped robots because symmetric distribution of payload on a quadruped robot and the robot mass itself cannot be guaranteed in general. In fact, trying to place the center of mass at the geometric center of the robot body places severe restrictions the design of quadruped robot. A recent work reports the effect of asymmetrical body mass distribution on stability and dynamics in bounding gaits [168]. However, no such work has been reported for energetics.

The objective of this chapter is to derive analytical expressions for cost of transport of a specific bounding gait of a quadruped robot with general mass distribution. The constant height level bounding gaits studied in this work will have a duty factor of 0.5 with no double support and flight phases. Two cases of bounding are considered: with equal front and rear leg step length, and with unequal front and rear leg step length. In order to investigate the effect of mass distribution, the quadruped robot being studied is assumed to have asymmetric body-mass distribution along the longitudinal axis. Analytical expressions for specific resistance are derived based on the assumption that total energy expenditure for each gait cycle is equal to the sum of energies consumed by each actuator for the gait cycle when no correcting control is applied and there is no regeneration. In real world applications, control is required to achieve the prescribed gait due to uncertainty in robot parameters or working conditions, in which case the energy consumed will be higher due to the additional correcting joint torques or forces that try to enforce the given gait trajectory. Therefore, the specific resistance expressions derived in this chapter indicate highest possible energetic efficiency (or lowest specific resistance) that is ideally achievable.

3.2   Model of the Quadruped Robot

The legs of the quadruped robot studied in this chapter consist of two joints each: hip and knee. Hip and knee joints are assumed to be revolute and prismatic respectively. The center of mass (CoM) is at a distance of a from the body center in the longitudinal direction. Body center is half-way between the front and rear hip joints. Further, the leg masses are assumed to be negligible compared to the body mass. Therefore, energetic cost of swinging the legs will be negligible compared to the energetic cost of moving the body mass.

The net force produced by knee and hip actuators of a leg is such that the ground reaction force is always upward in order to maintain contact with the ground as shown in the Fig. 3.1.

Linear velocities of the tip and the joint velocities of the leg are related through Jacobian matrix as

$$\begin{Bmatrix} \dot{x} \\ \dot{y} \end{Bmatrix} = \begin{bmatrix} l\cos\theta & \sin\theta \\ l\sin\theta & -\cos\theta \end{bmatrix} \begin{Bmatrix} \dot{\theta} \\ \dot{l} \end{Bmatrix} = J \begin{Bmatrix} \dot{\theta} \\ \dot{l} \end{Bmatrix}, \tag{3.1}$$
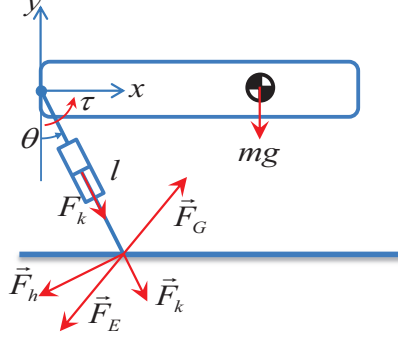
Figure 3.1: Tip of the rear leg (which is the end effector) produces reaction force $\boldsymbol{F}_G$ from the ground whose vertical component is upward; the hip joint is revolute with counter clock-wise rotation positive; the knee joint is prismatic with outward motion positive

where J is the Jacobian matrix relating the tip velocity and joint velocities. Equating the power input to the leg through the hip and knee joints, to the power output at the tip of the leg, one can obtain the relationship between joint forces or torques $\boldsymbol{\tau}$ and end effector forces $\boldsymbol{F}_E$ as

$$\boldsymbol{\tau} = J^T \boldsymbol{F}_E \text{ or } \begin{Bmatrix} \tau_h \\ F_k \end{Bmatrix} = J^T \begin{Bmatrix} F_x \\ F_y \end{Bmatrix} \tag{3.2}$$

The actuator forces or torques in $\boldsymbol{\tau}$ can be used as nominal control input to a controller that controls the torques produced by the actuators. Forces produced by hip and knee actuators can be independently determined by taking $F_k = 0$ and $\tau_h = 0$ respectively, the sum of which will be equal to $\boldsymbol{F}_E$. The force produced by hip actuator alone is given by

$$\boldsymbol{F}_h = \begin{Bmatrix} \frac{1}{l}\tau_h \cos\theta \\ \frac{1}{l}\tau_h \sin\theta \end{Bmatrix}. \tag{3.3}$$

Similarly, the force produced by knee actuator alone is given by

$$\boldsymbol{F}_k = \begin{Bmatrix} F_k \sin\theta \\ -F_k \cos\theta \end{Bmatrix}. \tag{3.4}$$

The following observations can be made on the nature of these forces:

1. The forces produced by hip actuators act perpendicular to the forces produced by knee actuators.

2. The force produced by the knee actuator acts along the line joining the point of contact of the leg with the ground and the hip joint, whereas the force produced by hip actuator acts perpendicular to the leg.

We will use these two observations in the next section where the expressions for specific resistance are derived.

The ground reaction force $\boldsymbol{F}_G$ is equal and opposite to the force developed by the leg at the tip

of the leg.

$$\boldsymbol{F}_G = -\boldsymbol{F}_E. \tag{3.5}$$

For any given ground reaction force $\boldsymbol{F}_G$, the hip and knee actuator forces can be uniquely determined using (3.2). The work done by leg actuator forces on the ground is equal to the work done by reaction force on the quadruped robot body. During a gait cycle, work done by actuators can be negative. This will reduce the total work done on the quadruped robot body and hence is not a proper indication of the energetic cost. In order to avoid this, we consider absolute value of work done by each actuator in determining total energetic cost.

For determining specific resistance [169], we use mechanical cost of transport obtained from

$$c_m = \frac{\frac{1}{T}\int_0^T |P|\, dt}{mgv}, \tag{3.6}$$

where P is instantaneous power, m is the mass of the quadruped robot, g is the acceleration due to gravity, and v is the average speed. Mechanical cost of transport can also be obtained from

$$c_m = \frac{\sum_i |W_i|}{mgd}, \tag{3.7}$$

where $|W_i|$ is the absolute value of work done by i^{th} actuator for one gait cycle, and d is the distance traveled during that gait cycle.

For low speeds and high torques, Joule-thermal losses dominate the energy consumed by actuators [16]. Here we assume that, actuators operate in a region where Joule-thermal losses are low and the mechanical cost of transport reasonably approximates actual cost of transport.

3.3 Energetics of Level Bounding with Equal Front and Rear Leg Step Lengths

Following are the assumptions used in the derivation of specific resistance:

1. Gait cycle consists of only two phases: rear-leg support phase and front-leg support phase. Hence, there is no double support phase where both front and rear legs are in contact with the ground. Similarly, there is no flight phase where neither of the legs are in contact with the ground. The complete gait cycle of bounding is as shown in Fig. 3.2

2. Acceleration and deceleration of the body are unavoidable during gait cycle. Front legs decelerate the body while rear legs accelerate the body during their respective support phases. This is a consequence of ground contact being in front of and behind the center of mass during these phases [170]. Initial nonzero forward velocity is assumed at the beginning of the gait cycle. The gait cycle starts with rear leg support phase (accelerating phase) first.

3. Rear foot or front foot does not cross the projection of center of mass in rear leg support phase or front leg support phase. This ensures that the assumption of sign for knee or hip work is valid for the given phase.

4. Friction is sufficiently large to prevent sliding between foot and ground surface.
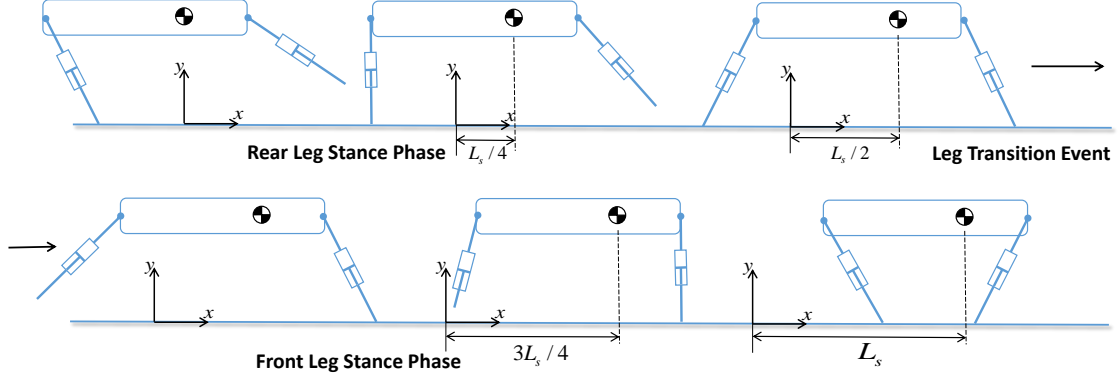
Figure 3.2: Complete gait cycle of bounding gait

Let L_s be the distance traveled by the center of mass for one complete cycle (front and rear leg pair swings). For bound gait, one cycle can be divided into four phases, where phases 1 and 2 are performed with rear legs, and phases 3 and 4 are performed with front legs. Table 3.1 shows various phases with respect to the displacement x of the center of mass. During each of these phases, the center of mass moves a distance of $L_s/4$. The variable ψ is the horizontal component of the position of hip joint with respect to the point of contact the leg with the ground. Various phases of the gait cycle are pictorially shown in Fig. 3.3.

Let L_b be the length of the quadruped robot body and a be the distance of the center of mass of the body from the geometric center. The asymmetry of mass distribution is assumed to be only along the longitudinal axis. In order respect assumption 3, the following condition on stride length L_s should be satisfied:

$$\frac{L_s}{4} \leq \left(\frac{L_b}{2} - a \right). \tag{3.8}$$

During each of these phases, we determine the energy consumed by each actuator by considering

Table 3.1: Displacement of center of mass for various phases

Phase	x	ψ
Phase 1	0 to $L_s/4$	$-L_s/4$ to 0
Phase 2	$L_s/4$ to $L_s/2$	0 to $L_s/4$
Phase 3	$L_s/2$ to $3L_s/4$	$-L_s/4$ to 0
Phase 4	$3L_s/4$ to L_s	0 to $L_s/4$

the work done by each actuator separately. Energy consumed by an actuator for a particular phase is taken as the absolute value of the work done by the actuator during that phase.

Rear leg support phase

Line of action of the reaction force $\boldsymbol{F_R}$ generated by the rear leg should pass through the center of mass so that there is no unbalanced moment on the body that causes pitching motion. Vertical
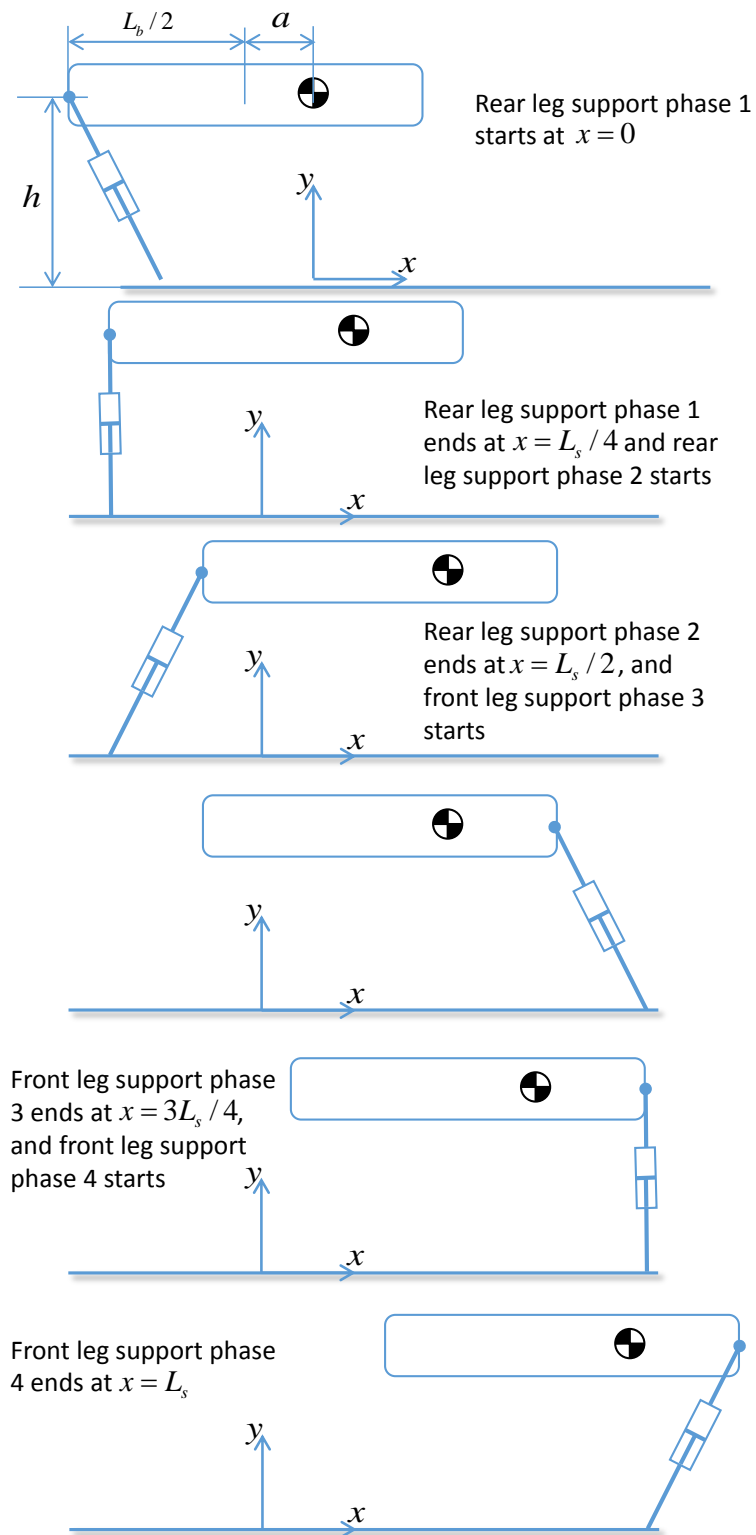
Figure 3.3: Locomotion of constant height level bounding gait for one gait cycle for equal and symmetric front and rear leg step lengths. Front and rear legs are not shown in rear and front leg support phases respectively.
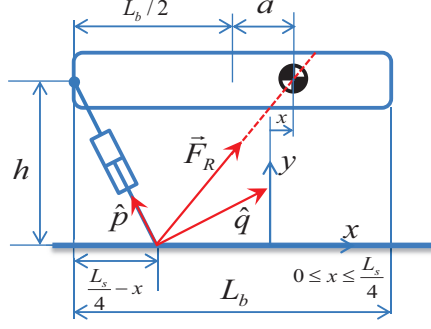
Figure 3.4: Rear-leg support phase 1

component of this reaction force should balance the weight, and the horizontal component accelerates the body. Therefore,

$$\text{if } \boldsymbol{F_R} = F_{Rx}\hat{\boldsymbol{i}} + F_{Ry}\hat{\boldsymbol{j}}, \tag{3.9}$$

$$\text{then } F_{Ry} = mg, \qquad F_{Rx} = \frac{F_{Ry}}{h}(x - x_R), \tag{3.10}$$

$$\text{where } x_R = -\left(\frac{L_b}{2} + a\right) + \frac{L_s}{4}. \tag{3.11}$$

Let $\psi = x - \frac{L_s}{4}$, and $c = \left(\frac{L_b}{2} + a\right)$. Therefore,

$$\boldsymbol{F_R} = \frac{mg}{h}(\psi + c)\hat{\boldsymbol{i}} + mg\hat{\boldsymbol{j}}. \tag{3.12}$$

Reaction force generated by the rear leg can be written as the resultant of the reaction forces generated by the knee and hip actuators:

$$\boldsymbol{F_R} = \boldsymbol{F_{Rk}} + \boldsymbol{F_{Rh}}. \tag{3.13}$$

Let $\hat{\boldsymbol{p}}$ be the unit vector at the point of contact of the leg with the ground pointing towards the hip joint. Let $\hat{\boldsymbol{q}}$ be the unit vector at the point of contact, perpendicular to $\hat{\boldsymbol{p}}$ and whose horizontal component is forward (in the direction of center of mass) as shown in the Fig. 3.4. These unit vectors can be written as:

$$\hat{\boldsymbol{p}} = \frac{\psi\hat{\boldsymbol{i}} + h\hat{\boldsymbol{j}}}{\sqrt{\psi^2 + h^2}}, \qquad \hat{\boldsymbol{q}} = \frac{h\hat{\boldsymbol{i}} - \psi\hat{\boldsymbol{j}}}{\sqrt{\psi^2 + h^2}}. \tag{3.14}$$

The force vector $\boldsymbol{F_R}$ can be resolved into two components along $\hat{\boldsymbol{p}}$ and $\hat{\boldsymbol{q}}$. The component along $\hat{\boldsymbol{p}}$ is $\boldsymbol{F_{Rk}}$ since the force generated by knee actuator always acts along the line joining hip and point of contact of the foot with the ground. Similarly, the force generated by hip actuator always acts perpendicular to this line along $\hat{\boldsymbol{q}}$. Therefore,

$$\boldsymbol{F_{Rk}} = (\boldsymbol{F_R} \cdot \hat{\boldsymbol{p}})\hat{\boldsymbol{p}}, \qquad \boldsymbol{F_{Rh}} = (\boldsymbol{F_R} \cdot \hat{\boldsymbol{q}})\hat{\boldsymbol{q}}. \tag{3.15}$$

The resolved forces $\boldsymbol{F_{Rk}}$ and $\boldsymbol{F_{Rh}}$ are

$$\boldsymbol{F_{Rk}} = \frac{\frac{mg}{h}(\psi + c)\psi + mgh}{\psi^2 + h^2}(\psi\hat{\boldsymbol{i}} + h\hat{\boldsymbol{j}}), \tag{3.16}$$

$$\boldsymbol{F_{Rh}} = \frac{mgc}{\psi^2 + h^2}(h\hat{\boldsymbol{i}} - \psi\hat{\boldsymbol{j}}). \tag{3.17}$$

Work done by $\boldsymbol{F_R}$ is equal to the sum of works done by $\boldsymbol{F_{Rk}}$ and $\boldsymbol{F_{Rh}}$.

$$W_R = W_{Rk} + W_{Rh}. \tag{3.18}$$

If work done by knee and hip actuators are of opposite sign, the magnitude of total work done will not be equal to the energy consumed because of the cancellation of negative and positive work. Actual energy consumed would be the absolute sum of work done by the actuators. In order to determine energy consumed from the work done by the actuators at individual joints, rear leg support phase is divided into two phases, phase 1 and phase 2, during which the signs of work done by knee and hip actuators are known and remain unchanged during these phases. Note that the ground reaction force has both vertical and horizontal components. The vertical component does no mechanical work because of zero vertical displacement. This holds true for the vertical components of forces produced by hip and knee actuators.

Phase 1

During this phase, work done by ground reaction forces generated by knee and hip actuators are negative and positive respectively which can be inferred from the directions of $\hat{\boldsymbol{p}}$ and $\hat{\boldsymbol{q}}$ as shown in Fig. 3.4. From now on, we will simply use the phrase "work done by actuator" to actually mean "work done by the ground reaction force component generated by the actuator." Work done by hip actuator alone is given by

$$W_{Rh1} = \int_0^{\frac{L_s}{4}} F_{Rhx}dx = \int_{-\frac{L_s}{4}}^0 \frac{mgch}{\psi^2 + h^2}d\psi, \tag{3.19}$$

$$W_{Rh1} = mgc\arctan\left(\frac{L_s}{4h}\right), \tag{3.20}$$

where $W_{Rh1} > 0$.

Work done by knee actuator alone is given by

$$W_{Rk1} = \int_0^{\frac{L_s}{4}} F_{Rkx}dx = \int_{-\frac{L_s}{4}}^0 \frac{\frac{mg}{h}(\psi + c)\psi + mgh}{\psi^2 + h^2}\psi d\psi. \tag{3.21}$$

Since this integral is difficult to evaluate symbolically, we will indirectly determine it as follows:

Since $W_{R1} = W_{Rk1} + W_{Rh1}$, $W_{Rk1} = W_{R1} - W_{Rh1}$, where W_{R1} is the net work done by hip and

knee actuators together given by

$$W_{R1} = \int_0^{\frac{L_s}{4}} F_{Rx} dx = \int_{-\frac{L_s}{4}}^0 \frac{mg}{h}(\psi + c)d\psi, \tag{3.22}$$

$$W_{R1} = \frac{mgL_s}{4h}\left[\frac{L_b}{2} + a - \frac{L_s}{8}\right]. \tag{3.23}$$

Therefore,

$$W_{Rk1} = \frac{mgL_s}{4h}\left[\frac{L_b}{2} + a - \frac{L_s}{8}\right] - mgc\arctan\left(\frac{L_s}{4h}\right), \tag{3.24}$$

where $W_{Rk1} < 0$.

Since W_{Rh1} is positive and W_{Rk1} is negative throughout the phase, energy consumed during the rear leg support phase 1 is

$$E_{R1} = 2mgc\arctan\left(\frac{L_s}{4h}\right) - \frac{mgL_s}{4h}\left[\frac{L_b}{2} + a - \frac{L_s}{8}\right]. \tag{3.25}$$

Phase 2

During this phase, work done by knee and hip actuators are both positive as shown in Fig. 3.5. Work done by hip actuator alone is given by

$$W_{Rh2} = \int_{\frac{L_s}{4}}^{\frac{L_s}{2}} F_{Rhx} dx = \int_0^{\frac{L_s}{4}} \frac{mgch}{\psi^2 + h^2}d\psi, \tag{3.26}$$

$$W_{Rh2} = mgc\arctan\left(\frac{L_s}{4h}\right) \tag{3.27}$$

Work done by hip and knee actuators together is given by

$$W_{R2} = \int_{\frac{L_s}{4}}^{\frac{L_s}{2}} F_{Rx} dx = \int_0^{\frac{L_s}{4}} \frac{mg}{h}(\psi + c)d\psi \tag{3.28}$$

$$W_{R2} = \frac{mgL_s}{4h}\left[\frac{L_b}{2} + a + \frac{L_s}{8}\right] \tag{3.29}$$

Work done by knee actuator alone is given by

$$W_{Rk2} = W_{R2} - W_{Rh2} \tag{3.30}$$

$$W_{Rk2} = \frac{mgL_s}{4h}\left[\frac{L_b}{2} + a + \frac{L_s}{8}\right] - mgc\arctan\left(\frac{L_s}{4h}\right) \tag{3.31}$$

Therefore, energy consumed during the rear leg support Phase 2 is

$$E_{R2} = \frac{mgL_s}{4h}\left[\frac{L_b}{2} + a + \frac{L_s}{8}\right]. \tag{3.32}$$
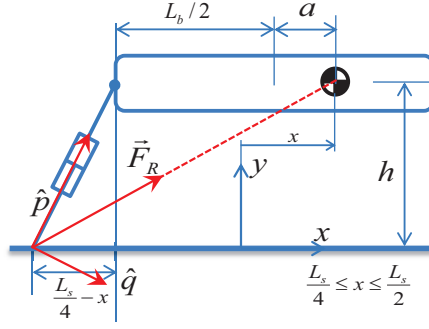
Figure 3.5: Rear-leg support phase 2

Front leg support phase
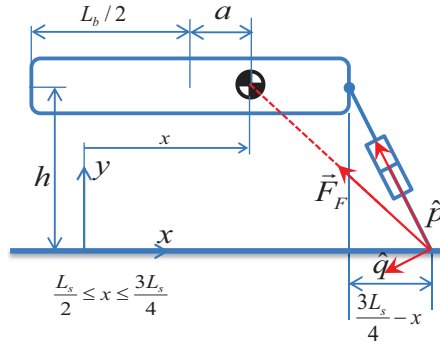
Figure 3.6: Front-leg support phase 3

Line of action of the force generated by the front leg should pass through the center of mass so that there is no unbalanced moment on the body as shown in Fig. 3.6. Hence,

$$\boldsymbol{F_F} = F_{Fx}\hat{\boldsymbol{i}} + F_{Fy}\hat{\boldsymbol{j}}, \tag{3.33}$$

$$F_{Fy} = mg, \qquad F_{Fx} = \frac{F_{Ry}}{h}(x - x_F), \tag{3.34}$$

$$x_F = \left(\frac{L_b}{2} - a\right) + \frac{3L_s}{4}. \tag{3.35}$$

Let $\psi = x - \frac{3L_s}{4}$, and $b = \left(\frac{L_b}{2} - a\right)$. Therefore,

$$\boldsymbol{F_F} = \frac{mg}{h}(\psi - b)\hat{\boldsymbol{i}} + mg\hat{\boldsymbol{j}}. \tag{3.36}$$

Force generated by the front leg shown in Fig. 3.6 can be written as the resultant of the forces generated by the knee and hip torques:

$$\boldsymbol{F_F} = \boldsymbol{F_{Fk}} + \boldsymbol{F_{Fh}}. \tag{3.37}$$

The unit vectors $\hat{p}$ and $\hat{q}$ during this phase can be written as:

$$\hat{p} = \frac{\psi\hat{i} + h\hat{j}}{\sqrt{\psi^2 + h^2}}, \qquad \hat{q} = \frac{-h\hat{i} + \psi\hat{j}}{\sqrt{\psi^2 + h^2}}. \tag{3.38}$$

The force vector $\boldsymbol{F_F}$ can be resolved into two components along $\hat{p}$ and $\hat{q}$. Therefore,

$$\boldsymbol{F_{Fk}} = (\boldsymbol{F_F} \cdot \hat{p})\hat{p}, \qquad \boldsymbol{F_{Fh}} = (\boldsymbol{F_F} \cdot \hat{q})\hat{q}. \tag{3.39}$$

The resolved forces $\boldsymbol{F_{Fk}}$ and $\boldsymbol{F_{Fh}}$ are

$$\boldsymbol{F_{Fk}} = \frac{\frac{mg}{h}(\psi - b)\psi + mgh}{\psi^2 + h^2}(\psi\hat{i} + h\hat{j}), \tag{3.40}$$

$$\boldsymbol{F_{Fh}} = \frac{mgb}{\psi^2 + h^2}(-h\hat{i} + \psi\hat{j}). \tag{3.41}$$

Work done by $\boldsymbol{F_F}$ is equal to the sum of works done by $\boldsymbol{F_{Fk}}$ and $\boldsymbol{F_{Fh}}$.

$$W_F = W_{Fk} + W_{Fh}. \tag{3.42}$$

The front leg support phase is divided into two phases, phase 3 and phase 4, during which the signs of work done by knee and hip actuators do not change.

Phase 3

During this phase, work done by knee and hip actuators are both negative as shown in Fig. 3.6. Work done by hip actuator alone is given by

$$W_{Fh1} = \int_{\frac{L_s}{2}}^{\frac{3L_s}{4}} F_{Fhx}dx = -\int_{-\frac{L_s}{4}}^{0} \frac{mgbh}{\psi^2 + h^2}d\psi, \tag{3.43}$$

$$W_{Fh1} = -mgb\arctan\left(\frac{L_s}{4h}\right). \tag{3.44}$$

Work done by knee and hip actuators together is given by

$$W_{F1} = \int_{\frac{L_s}{2}}^{\frac{3L_s}{4}} F_{Fx}dx = -\int_{-\frac{L_s}{4}}^{0} \frac{mg}{h}(\psi - b)d\psi, \tag{3.45}$$

$$W_{F1} = -\frac{mgL_s}{4h}\left[\frac{L_b}{2} - a + \frac{L_s}{8}\right]. \tag{3.46}$$

Work done by knee actuator alone is given by

$$W_{Fk1} = W_{F1} - W_{Fh1} \tag{3.47}$$

$$W_{Fk1} = mgb\arctan\left(\frac{L_s}{4h}\right) - \frac{mgL_s}{4h}\left[\frac{L_b}{2} - a + \frac{L_s}{8}\right] \tag{3.48}$$

Therefore, after considering the signs of works done, energy consumed during the front leg support

phase 3 can be determined as

$$E_{F1} = \frac{mgL_s}{4h}\left[\frac{L_b}{2} - a + \frac{L_s}{8}\right]. \tag{3.49}$$

Phase 4

During this phase, work done by knee and hip actuators are positive and negative respectively as shown in Fig. 3.7. Work done by hip actuator alone is given by

$$W_{Fh2} = \int_{\frac{3L_s}{4}}^{L_s} F_{Fhx}dx = -\int_0^{\frac{L_s}{4}} \frac{mgbh}{\psi^2 + h^2}d\psi, \tag{3.50}$$

$$W_{Fh2} = -mgb\arctan\left(\frac{L_s}{4h}\right) \tag{3.51}$$

Work done by knee and hip actuators together is given by

$$W_{F2} = \int_{\frac{3L_s}{4}}^{L_s} F_{Fx}dx = \int_0^{\frac{L_s}{4}} \frac{mg}{h}(\psi - b)d\psi, \tag{3.52}$$

$$W_{F2} = \frac{mgL_s}{4h}\left[\frac{L_s}{8} - \frac{L_b}{2} + a\right]. \tag{3.53}$$

Work done by knee actuator alone is

$$W_{Fk2} = W_{F2} - W_{Fh2}, \tag{3.54}$$

$$W_{Fk2} = \frac{mgL_s}{4h}\left[\frac{L_s}{8} - \frac{L_b}{2} + a\right] + mgb\arctan\left(\frac{L_s}{4h}\right) \tag{3.55}$$

Therefore, after considering the signs of works done, energy consumed during the front leg support Phase 4 can be determined as

$$E_{F2} = \frac{mgL_s}{4h}\left[\frac{L_s}{8} - \frac{L_b}{2} + a\right] + 2mgb\arctan\left(\frac{L_s}{4h}\right). \tag{3.56}$$
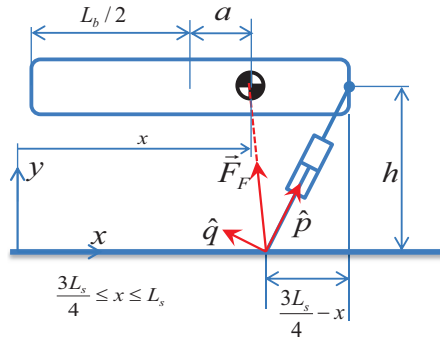
Figure 3.7: Front-leg support phase 4

Mechanical Cost of Transport or Specific Resistance

Total energy consumed is

$$E_{Total} = E_{R1} + E_{R2} + E_{F1} + E_{F2} \tag{3.57}$$

$$E_{Total} = \frac{mgL_s^2}{8h} + 2mgL_b \arctan\left(\frac{L_s}{4h}\right). \tag{3.58}$$

The mechanical Cost of Transport (CoT) is given by

$$\text{CoT} = \frac{E_{Total}}{mgL_s} \tag{3.59}$$

$$\text{CoT} = \frac{L_s}{8h} + \frac{2L_b}{L_s} \arctan\left(\frac{L_s}{4h}\right). \tag{3.60}$$

For small stride lengths, we can write

$$\arctan\left(\frac{L_s}{4h}\right) \approx \frac{L_s}{4h}. \tag{3.61}$$

Therefore, the approximate cost of transport is

$$\text{CoT} = \frac{L_s}{8h} + \frac{L_b}{2h}. \tag{3.62}$$

Following observations can be made:

- Specific resistance depends on both the stride length and the body length. Lower body lengths and lower stride lengths give lower specific resistance.

- Specific resistance does not depend on unsymmetric distribution of mass when equal front and rear step lengths are used.

- The total work done on the robot body for one gait cycle consisting of rear and front leg support phases is nonzero and depends on mass distribution or location of the center of mass.

$$W = W_{R1} + W_{R2} + W_{F1} + W_{F2} = \frac{mgL_s a}{h} \neq 0. \tag{3.63}$$

Kinetic energy of the quadruped robot at the end of a gait cycle is not the same as that at the beginning of that gait cycle because of the net nonzero work done on it. This means, if $a > 0$, the quadruped robot has average positive acceleration because of the unsymmetric distribution of mass, with equal front and rear leg step lengths. Similarly, if $a < 0$, the robot would lose its initial kinetic energy and decelerate for every gait cycle. The front and rear leg step lengths can be made unequal to compensate the effect of unsymmetric mass distribution so as to preserve initial forward velocity of the quadruped robot after each gait cycle.

3.4   Energetics of Level Bounding with Unequal Front and Rear Step Lengths

In this section, we assume that the front and rear leg step lengths are different. However, we keep the front and rear leg step lengths symmetrical about the vertical lines passing through the front and rear hip joints respectively. Let $L_{sr}/2$ and $L_{sf}/2$ be the rear and front leg step lengths. L_{sr} is the stride length if front leg step length were the same as the rear leg step length $L_{sr}/2$. Similarly, L_{sf} is the stride length if rear leg step length were same as the front leg step length $L_{sf}/2$. Since the front and rear leg step lengths are different, the stride length is

$$L_s = \frac{L_{sr}}{2} + \frac{L_{sf}}{2}. \tag{3.64}$$

Let us define the rear leg step length in terms of stride length as

$$\frac{L_{sr}}{2} + k = \frac{L_s}{2}. \tag{3.65}$$

Therefore, the front leg step length becomes

$$\frac{L_{sf}}{2} - k = \frac{L_s}{2}, \tag{3.66}$$

so that (3.64) is satisfied. For positive values of a, condition (3.8) now becomes

$$\frac{L_{sf}}{4} \leq \frac{L_b}{2} - a. \tag{3.67}$$

Now the task is to determine the value of k such that the net work done for one gait cycle is zero. Our derivation of mechanical cost of transport for unequal front and rear leg step lengths relies on results derived for equal front and rear leg step lengths in the previous section.

Rear leg support phase

In this phase, rear leg step length is $L_{sr}/2$ which is distributed as $L_{sr}/4$ each for rear leg support phases 1 and 2. The work done and energy expressions for phase 1 and phase 2 can be derived similar to section 3 with L_s replaced by L_{sr}.

Phase 1

Work done by knee actuator is

$$W_{Rk1} = \frac{mgL_{sr}}{4h}\left[\frac{L_b}{2} + a - \frac{L_{sr}}{8}\right] - mgc\arctan\left(\frac{L_{sr}}{4h}\right). \tag{3.68}$$

Similarly, work done by hip actuator is given by

$$W_{Rh1} = mgc\arctan\left(\frac{L_{sr}}{4h}\right). \tag{3.69}$$

Therefore, energy consumed during the rear leg support phase 1 is

$$E_{R1} = 2mgc\arctan\left(\frac{L_{sr}}{4h}\right) - \frac{mgL_{sr}}{4h}\left[\frac{L_b}{2} + a - \frac{L_{sr}}{8}\right]. \tag{3.70}$$

Phase 2

Work done by knee actuator is

$$W_{Rk2} = \frac{mgL_{sr}}{4h}\left[\frac{L_b}{2} + a + \frac{L_{sr}}{8}\right] - mgc\arctan\left(\frac{L_{sr}}{4h}\right). \tag{3.71}$$

Similarly, work done by hip actuator is given by

$$W_{Rh2} = mgc\arctan\left(\frac{L_{sr}}{4h}\right). \tag{3.72}$$

Therefore, energy consumed during the rear leg support phase 2 is

$$E_{R2} = \frac{mgL_{sr}}{4h}\left[\frac{L_b}{2} + a + \frac{L_{sr}}{8}\right]. \tag{3.73}$$

Total energy consumed for rear leg support phase is given by

$$E_R = E_{R1} + E_{R2} \tag{3.74}$$

$$= 2mgc\arctan\left(\frac{L_{sr}}{4h}\right) + \frac{mgL_{sr}}{4h}\left[\frac{L_{sr}}{4}\right]. \tag{3.75}$$

Front leg support phase

In this phase, front leg step length is $L_{sf}/2$ which is distributed as $L_{sf}/4$ each for front leg support phases 3 and 4. The work done and energy expressions for phase 3 and phase 4 can be derived similar to section 3 with L_s replaced by L_{sf}.

Phase 3

Work done by knee actuator is

$$W_{Fk1} = mgb\arctan\left(\frac{L_{sf}}{4h}\right) - \frac{mgL_{sf}}{4h}\left[\frac{L_b}{2} - a + \frac{L_{sf}}{8}\right]. \tag{3.76}$$

Similarly, work done by hip actuator is given by

$$W_{Fh1} = -mgb\arctan\left(\frac{L_{sf}}{4h}\right) \tag{3.77}$$

Therefore, energy consumed during the front leg support phase 3 is

$$E_{F1} = \frac{mgL_{sf}}{4h}\left[\frac{L_b}{2} - a + \frac{L_{sf}}{8}\right]. \tag{3.78}$$

Phase 4

Work done by knee actuator is

$$W_{Fk2} = \frac{mgL_{sf}}{4h}\left[\frac{L_{sf}}{8} - \frac{L_b}{2} + a\right] + mgb\arctan\left(\frac{L_{sf}}{4h}\right). \tag{3.79}$$

Similarly, work done by hip actuator is given by

$$W_{Fh2} = -mgb\arctan\left(\frac{L_{sf}}{4h}\right). \tag{3.80}$$

Therefore, energy consumed during the rear leg support phase 4 is

$$E_{F2} = \frac{mgL_{sf}}{4h}\left[\frac{L_{sf}}{8} - \frac{L_b}{2} + a\right] + 2mgb\arctan\left(\frac{L_{sf}}{4h}\right). \tag{3.81}$$

Total energy consumed during the front leg support phase is given by

$$E_F = E_{F1} + E_{F2} \tag{3.82}$$

$$= 2mgb\arctan\left(\frac{L_{sf}}{4h}\right) + \frac{mgL_{sf}}{4h}\left[\frac{L_{sf}}{4}\right] \tag{3.83}$$

Now, W_R and W_F can be calculated in terms of stride length L_s and the unknown k by substituting

$$L_{sr} = L_s - 2k, \qquad L_{sf} = L_s + 2k. \tag{3.84}$$

The value of k which makes the net work done per gait cycle can be determined by taking

$$W_R + W_F = 0, \tag{3.85}$$

which gives,

$$k = \frac{aL_s}{L_b}. \tag{3.86}$$

This means, if the center of mass is in front of geometric center ($a > 0$), the rear step length has to be smaller than the front step length in order to achieve constant average forward velocity.

Substituting L_{sr}, L_{sf} and k in energy expressions, and calculating total energy consumed for complete gait cycle is given by

$$E = E_R + E_F. \tag{3.87}$$

Mechanical Cost of Transport for Steady Gait with Unequal Rear and Front Leg Step Lengths

Total energy consumed is

$$E = \frac{mg}{h} \left(\frac{L_s{}^2}{8} + \frac{a^2 L_s^2}{2L_b^2} \right)$$
$$+ 2mg \left[c \arctan \left(\frac{L_{sr}}{4h} \right) + b \arctan \left(\frac{L_{sf}}{4h} \right) \right] \tag{3.88}$$

from which the specific resistance or Cost of Transport (CoT) is determined as

$$\text{CoT} = \frac{L_s}{h} \left(\frac{1}{8} + \frac{a^2}{2L_b^2} \right)$$
$$+ \frac{2}{L_s} \left[c \arctan \left(\frac{L_{sr}}{4h} \right) + b \arctan \left(\frac{L_{sf}}{4h} \right) \right]. \tag{3.89}$$

Substituting $a = 0$ in the above equation, one can obtain the specific resistance for uniform mass distribution as in (3.60).

3.5 Results and Discussion

3.5.1 For Accelerating or Decelerating Gaits

From (3.63), it can be seen that equal front and rear leg step lengths lead to accelerating gait if the body center of mass is in the front of the body center ($a > 0$). If the robot needs to be accelerated to a different average forward velocity, equal front and rear leg step lengths can be chosen. Generally, the center of mass position is fixed by adjusting the payload either in front of or behind the body center before the robot is started on a mission. If the robot is designed such that the center of mass can be changed during the gait, one can move the center of mass behind the body center in order to decelerate the robot using equal front and rear leg step lengths.

There is an easier way of achieving acceleration or deceleration than by changing the position of center of mass. For level bounding gait studied in this chapter, rear leg support phase is accelerating and front leg support phase is decelerating. Hence, when acceleration is desired, front leg step length can be made smaller or rear leg step length can be made larger. Similarly, when deceleration is desired, front leg step length can be made larger or rear leg step length can be made smaller.

3.5.2 Energetics for Uniform or Symmetric Mass Distribution

Figure 3.8 shows the variation of energetic cost with respect to height for stride length $L_s = 0.5$, with body length $L_b = 1$ m. Energetic cost decreases monotonously with increase in body height h.

For smaller stride lengths L_s, energetic cost is directly proportional to L_s as is evident from (3.62). This is true for $L_s/(4h) < 0.5$ within 10% deviation. For a height of $h = 1$ m, L_s can be as large as 2 m for the linearity assumption to hold (See Fig. 3.9). As the step length is decreased, energetic cost converges to a limiting value of $L_b/(2h)$ as shown in Fig. 3.9. Note that, from (3.8), one fourth of the maximum stride length cannot exceed half the body length in order to maintain the assumptions made for various phases, namely, the foot does not cross the line of projection of center of mass on the ground. Hence, in Fig. 3.9, the maximum stride length is shown to be different for different body lengths.
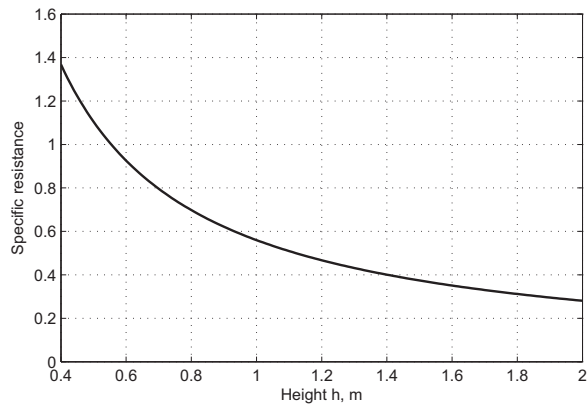
Figure 3.8: Variation of energetic cost with height ($L_b = 1$ m, $L_s = 0.5$, $a = 0$ m)
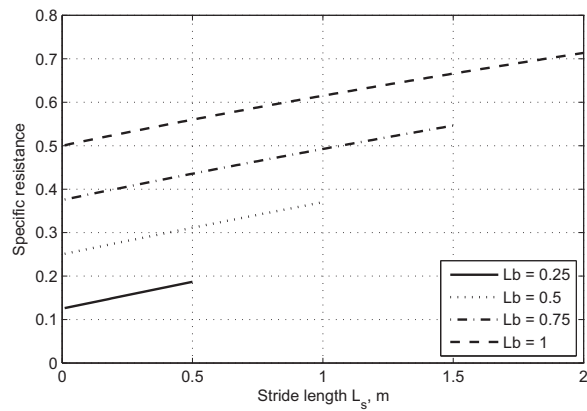

Figure 3.9: Variation of energetic cost with stride length for various values of body length ($h = 1$ m, $a = 0$ m)

The mechanical Cost of Transport of a point mass biped robot undergoing level walking with acceleration and deceleration is $L_s/8h$ [157]. This can be obtained from (3.60) by taking $L_b = 0$, which indicates that quadruped robot in constant height level walking gait with zero body length is a biped robot in constant height walking.

3.5.3   Energetics for Unsymmetric Mass Distribution

With body mass asymmetry and equal front and rear leg step lengths, the expression for energetic cost remains same as without body mass asymmetry. The effect of asymmetry comes in terms of accelerated gait for the same energetic cost. This indicates that there is a natural tendency to accelerate in quadruped robots with center of mass in front of the body center. It is well known fact in quadrupedal animals that the rear legs (hind limbs) tend to accelerate the body whereas the front legs (fore limbs) tend to decelerate the body [170, 171, 172]. With the center of mass shifted forward, larger step lengths are possible with rear legs and smaller with the front legs without violating the condition that the front or rear foot does not cross the projection of center of mass on the ground. This will further increase the acceleration due to increased duration of propulsive effect from the rear legs and with the decreased duration of braking effect from the front legs.

The center of mass can be either in front of the body center ($a > 0$) or behind the body center ($a < 0$). Since the specific resistance is an even function of a for steady gait with equal front and rear leg step lengths as described by (3.89), the energetic cost depends only on the distance from the body center and not on whether a is positive or negative as shown in Fig. 3.10. For steady forward speed, the energetic cost function is almost quadratic with rapid decrease in energetic cost with increase in the distance of the center of mass from the body center.
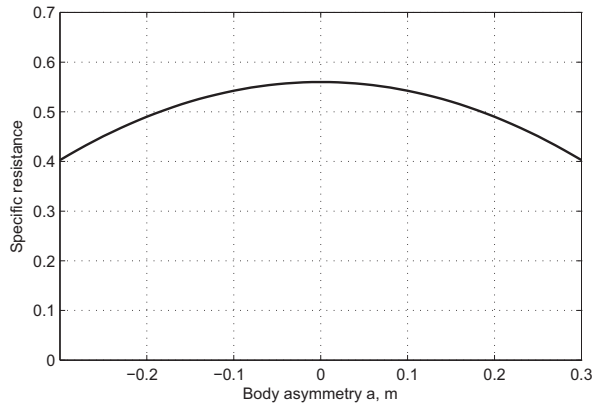
Figure 3.10: Energetic cost versus position of center of mass with respect to body center ($h = 1$ m, $L_b = 1$ m, $L_s = 0.5$ m)

In most of the quadrupedal mammals, evolution has shifted the body center forward, thereby increasing their ability to accelerate [173]. Our model indicates that forward shifted center of mass is both energy efficient as well as acceleration biased (higher ability to accelerate). A rearward shifted center of mass is deceleration biased. Fast running quadrupedal animals like cheetahs and greyhounds, though have their center of mass forward of their body center, have less asymmetry [173, 174, 175], indicating a trade-off between ability to accelerate as well as decelerate. Note that our model's prediction is only indicative because of the massless legs assumption we make.

In Fig. 3.10, the energetic cost is plotted with a varying up to 60% of half the body length on either side of the body center. Though further reduction in energetic cost is possible by increasing $|a|$, it may not be practical to achieve a steady gait (constant average speed) by making front and rear leg step lengths unequal. For steady gait, as a increases, the front and rear leg step lengths for the same stride length of $L_s = 0.5$ m vary as shown in Fig. 3.11. For this stride length of 0.5 m, $|a|$ cannot be increased further due to violation of condition under which the energetic cost is derived, i.e., foot would cross the projection of center of mass on the ground. For the given body length and the distance of center of mass from the body center, the maximum stride length that is possible can be determined from (3.67), (3.84), and (3.86) as

$$L_{smax} = 2L_b \frac{(L_b - 2a)}{(L_b + 2a)}. \tag{3.90}$$
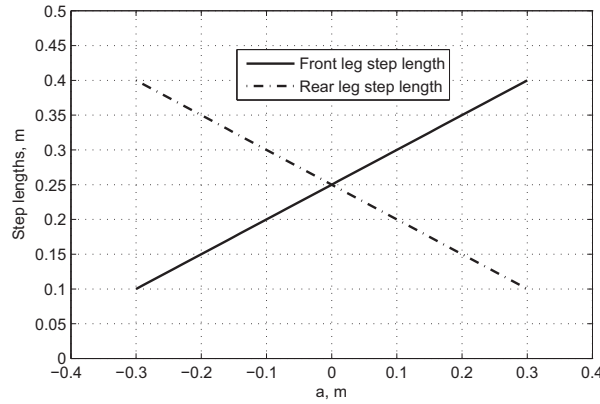
Figure 3.11: Front and rear leg step lengths as a function of a for the same stride length of $L_s = 0.5$ m with $L_b = 1$ m

The consequence of allowing lower step lengths for either front leg or rear leg is rise in the energetic cost of swinging the leg forward. When the rear leg step length is lower, the front leg (pair) has to swing forward in preparation of the next step. If sufficient time is not available, the forward legs have to swing forward rapidly and then brought to rest. This increases the energetic cost of swinging which has not been considered in our analysis.

With the variation of bounding height, the effect of increased body mass asymmetry is reduced specific resistance. This effect can be observed even with lower body heights for the same stride length and body length as shown in Fig. 3.12. With the increase of the distance of center of mass from body center, the decrease in energetic cost and also the maximum possible stride lengths for three different values of body length L_b and height h are shown in Fig. 3.13, Fig. 3.14, and Fig. 3.15 respectively. With the increase in the value of a, rapid decrease in energetic cost can be observed. At the same time, the maximum stride length possible also decreases. For higher values of body length, there is an increase in the maximum stride length and at the same time, the energetic cost also increases with the increase in L_b/h ratio.
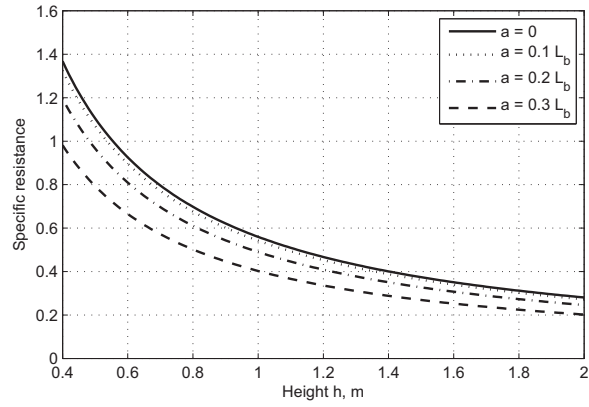
Figure 3.12: Variation of energetic cost with height ($L_b = 1$ m, $L_s = 0.5$)
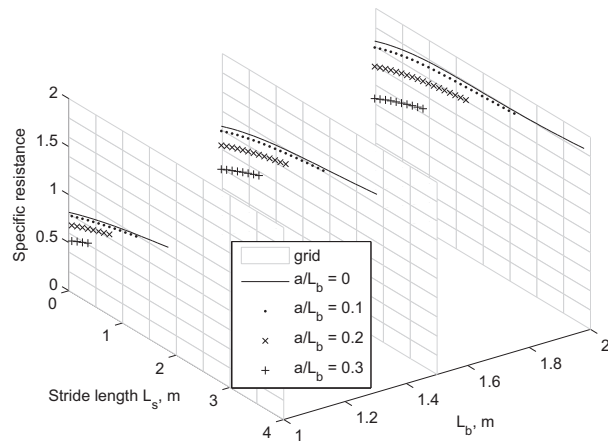
Figure 3.13: Variation of energetic cost with stride length for various values of a and L_b with $h = 0.6m$
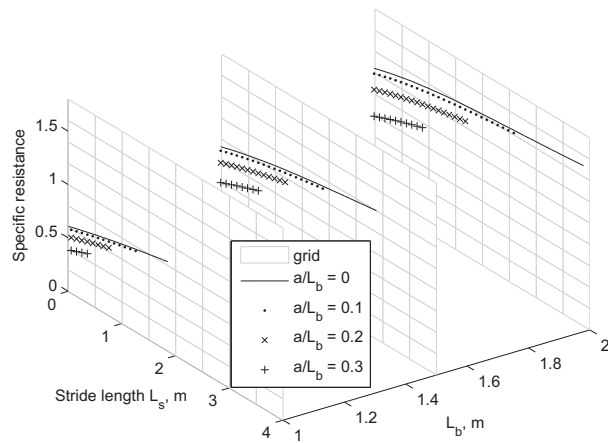
Figure 3.14: Variation of energetic cost with stride length for various values of a and L_b with $h = 0.8m$
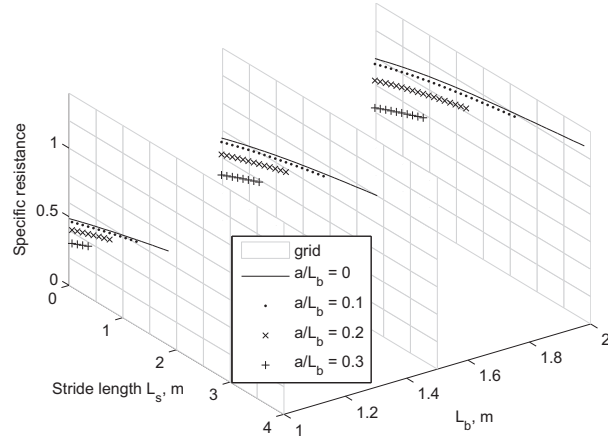
Figure 3.15: Variation of energetic cost with stride length for various values of a and L_b with $h = 1m$

3.5.4 Actual Energetic Cost

The energetic cost expressions derived in this chapter are based on mechanical work considerations of individual actuators rather than purely mechanical work done on the body by the net actuator forces. This is closer to the actual energetic cost determined considering electrical energy expenditure in the joint actuators. The actual cost is bound to be higher than the one derived from the expressions given in this chapter due to various factors that have not been considered. The actuators produce forces which have vertical components that balance the weight of the robot. Though no mechanical work is done to keep the body at constant height, energy is consumed by the actuators to generate these forces. This means, if more time is taken to traverse the same distance, higher energy would be consumed, making the cost of transport a function of stride frequency too as observed in quadrupedal animals [176]. There are other factors such as motor efficiency, gear head efficiency etc. that contribute to increased actual cost. Since the energetic cost obtained by considering the absolute values of mechanical work done by individual actuators are also a significant contributing factor to the actual energetic cost, the results presented in this work are useful in choosing the optimal design and gait parameters that would reduce the actual energetic cost.

3.6 Conclusions

In this chapter, we investigated the energetics of level bounding gaits in quadruped robots with asymmetric body-mass distribution in longitudinal axis. Main results of the chapter are the analytical expressions for mechanical specific resistance in constant height level bounding with equal front and rear leg step lengths, and with unequal front and rear leg step lengths for steady gait with body mass asymmetry. The specific resistance is found to be independent of mass distribution in the first case where the gait is found to be accelerating if mass asymmetry is present. The front and rear leg step lengths are made unequal in the second case in order to obtain a steady gait with constant average speed. The effect of design parameters such as body length and distance of center of mass from the body center, and gait parameters such as gait height and step lengths have been discussed in detail.

Chapter 4

Quadruped Robot with Articulated Torso

4.1 Introduction

Existing state-of-the-art quadruped robots developed by Boston Dynamics such as little Dog [177] and Big Dog [10] do not have Articulated Torso. In case of four legged animals like dogs, cats, deer etc. mobility depends to a large extent on the flexing of their torso. Kwon and Yoo [178] report a simulation study on energy efficiency of a quadruped robot in sagittal plane. A fuzzy control strategy for 3D quadruped trot to execute high-speed turns over a range of speeds and turning rates were presented in [179]. A quasi-static step climbing behavior for a minimal sensing wheel-legged quadruped robot PAW [180] uses wheel traction and its legs to reconfigure itself with respect to the step during the climb. MHT [181] makes use of velocity model for inverse kinematics of the vehicle and incorporates optimization technique to minimize joint torques. The Static Stability Margin used in this chapter, is as defined by Papadopoulos and Rey in [182].

However, simulation study on height obstacle crossing in 3D quadruped robot locomotion with active articulating torso has not been reported in literature till date. This chapter aims to study the effect of articulated torso on stability and energy efficiency in walking mode, trot mode and running mode on height obstacle crossing. This chapter includes mathematical modelling, creating solid model, importing to simulation software (ADAMS) where the physics engine based simulation is carried out. Finally interfacing with Simulink based on MATLAB programmes will completely execute the quadruped robot gaits mechanism with articulated torso. Validity of the algorithm has been extensively tested via simulations using MSC ADAMS and MATLAB/SIMULINK interface.

4.2 System Description

The Articulated Torso Quadruped Robot (ATQR) has a total of 14 DoF (Degree of Freedom) with 3 DoF per leg and 2 DoF for the Torso. The legs will have mammal type configuration with two DoF hip joint, and one DoF knee joint. The schematic diagram of the proposed kinematic structure is shown in Fig. 4.1. The first leg is lifted for the walking to be initialized. At this point of time the other three legs will form the polygon pattern of three sides and the projection of the Centre

of Mass (CoM) lies within this pattern forming stable walking. Articulating of the Torso in pitch and roll is effected by Torso joints 1 and 2 respectively. The length of the obstacle that can be overcome depends on the distance between the knee joints of the front and rear legs. The knee bending direction of the legs will be outward in order to overcome obstacles of larger length. The knee bending direction of legs will be inward in order to get better stability at faster speed.
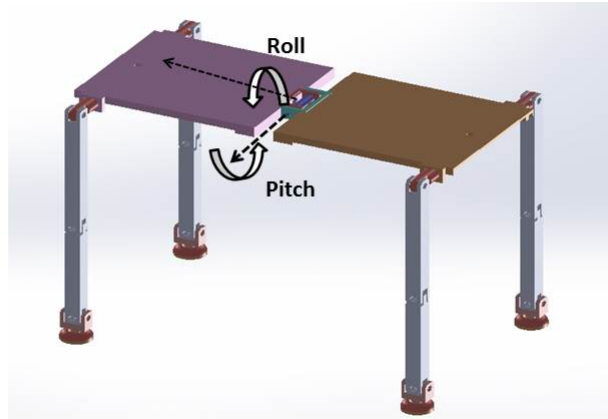
Figure 4.1: Schematic diagram of ATQR

Fig. 4.2 shows the mechanical structure of the proposed model of the vehicle (ATQR). The system has been designed as a legged robot. It consists of four legs connected to the Torso. Each leg has three degrees of freedom . The leg tip has a semi-circular foot to provide proper traction for the leg placement. Next, we derive the forward kinematics of each leg. The leg is considered to be from the hip joint to the semicircular foot attached to last link.
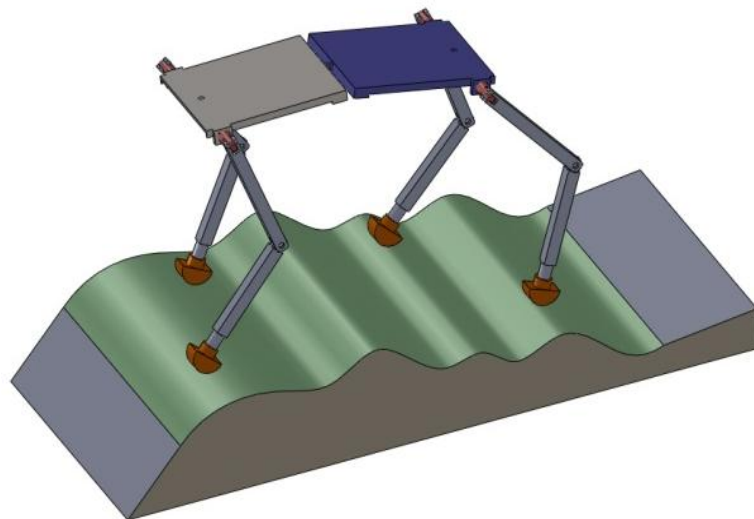
Figure 4.2: Mechanical Structure of ATQR

4.3 Kinematic Analysis of Quadruped Robot

Analysis of quadruped robot requires first geometrical analysis leg frame assignment and D-H parameter.

Frame Assignment of Robot

This section describes the frame assignment of the leg and Torso of the quadruped robot. With the help of frame assignment of the robot one can get the idea of the position and orientation because this is the arbitrary reference and totally depends on the observer reference frame. Three types of frames are used in quadruped first global reference frame $\{T\}$ for the Torso of quadruped followed by Roll frame $\{R\}$, and Pitch frame $\{P\}$ next local reference frame $\{0\}$ for legs and followed by 3 frames $\{1\}$,$\{2\}$and$\{3\}$ for each joint. Frame assignment is given in the Fig. 4.3. We always considers the Z axis is in vertical direction (outward to Torso)and aligned to gravity. For leg frame assignment we always follow Denavit and Hartenberg (DH) rule. For Frame assignment of the leg, the color
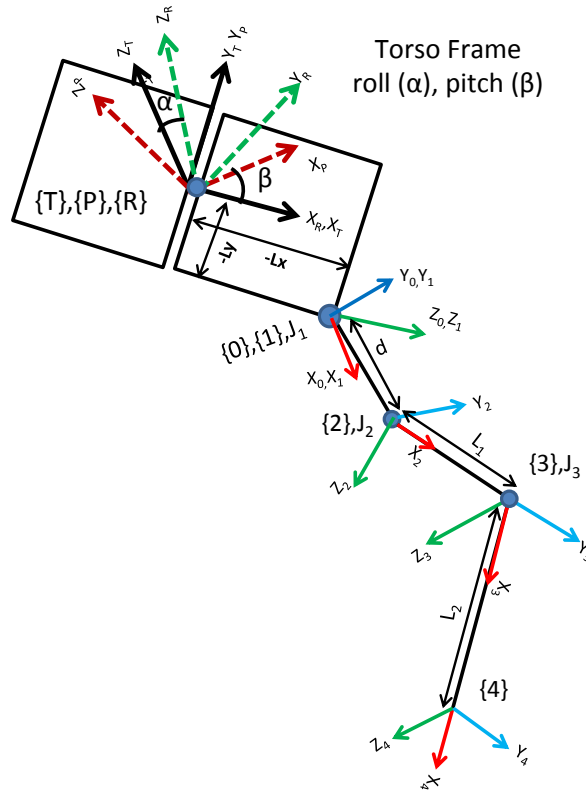
Figure 4.3: Frame assignment of the quadruped

code is used for clear understanding. Red is used for X axis, green is for Z axis and blue is for the Y axis.

D-H Parameters of Quadruped Robot

DH parameters of quadruped robot is defined on the basis of Fig. 4.4. The DH parameters of the

$$^{i-1}_iT = R_X(\alpha_{i-1})D_X(a_{i-1})R_Z(\theta_i)D_Z(d_i)$$
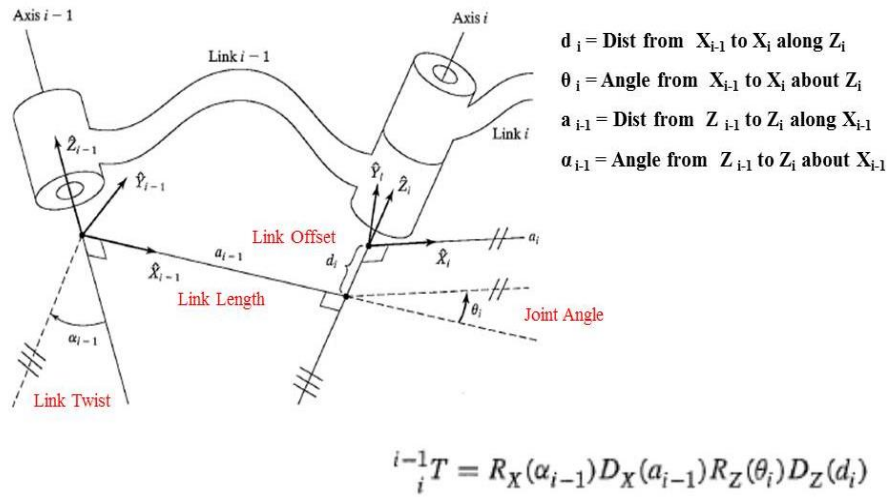
Figure 4.4: DH Parameters of Joints
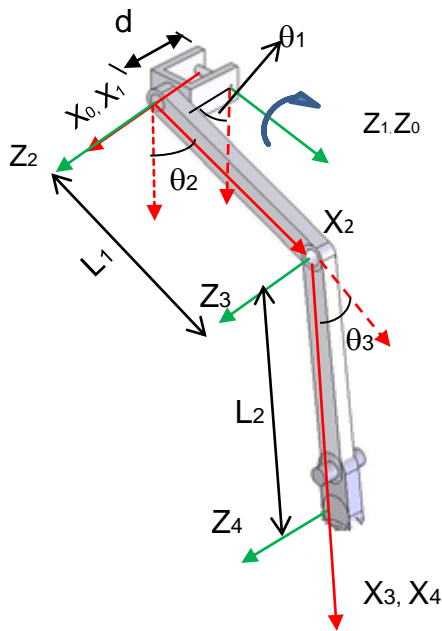
Figure 4.5: Leg Kinematic Configuration

Table 4.1: DH Parameters of Leg

i	α_{i-1}	a_{i-1}	d_i	θ_i
1	0	0	0	θ_1
2	+90	d	0	θ_2
3	0	L_1	0	θ_3
4	0	L_2	0	0

leg are shown in Table 4.1 θ_1, θ_2, θ_3 are joint angles and d, L_1, L_2 are link lengths of the quadruped robot leg as shown in Fig. 4.5. With the help of D-H parameters, calculated forward kinematics for both leg and Torso.

Forward transformation of Leg from Local Reference Frame {0}

Here we do the transformation of leg from local frame {0} to frame {4} as mentioned in Fig. 4.3. Using DH parameters the transformation of the first link from frame {0} to frame {1} for joint 1 is given (4.1)

$$
{}^0_1T = \begin{bmatrix} cos\theta_1 & -sin\theta_1 & 0 & 0 \\ sin\theta_1 & cos\theta_1 & 0 & 0 \\ 0 & 0 & 1 & 0 \\ 0 & 0 & 0 & 1 \end{bmatrix} \tag{4.1}
$$

Similarly, transformations from frame {1} to frame {2} for joint 2.

$$
{}^1_2T = \begin{bmatrix} cos\theta_2 & -sin\theta_2 & 0 & d \\ 0 & 0 & -1 & 0 \\ sin\theta_2 & cos\theta_2 & 0 & 0 \\ 0 & 0 & 0 & 1 \end{bmatrix} \tag{4.2}
$$

Similarly, transformations from frame {2} to frame {3} for joint 3.

$$
{}^2_3T = \begin{bmatrix} cos\theta_3 & -sin\theta_3 & 0 & L_1 \\ sin\theta_3 & cos\theta_3 & 0 & 0 \\ 0 & 0 & 1 & 0 \\ 0 & 0 & 0 & 1 \end{bmatrix} \tag{4.3}
$$

Transformations from frame {3} to frame {4}, the contact point with the ground for the leg.

$$
{}^3_4T = \begin{bmatrix} cos\theta_3 & -sin\theta_3 & 0 & L_2 \\ sin\theta_3 & cos\theta_3 & 0 & 0 \\ 0 & 0 & 1 & 0 \\ 0 & 0 & 0 & 1 \end{bmatrix} \tag{4.4}
$$

Final transformation from frame {0} to frame {4} for quadruped leg

$$
{}^0_4T = {}^0_1T\,{}^1_2T\,{}^2_3T\,{}^3_4T \tag{4.5}
$$

$$
{}^0_4T = \begin{bmatrix} cos\theta_1 cos\theta_{23} & -cos\theta_1 sin\theta_{23} & sin\theta_1 & cos\theta_1(L_2cos\theta_{23} + L_1cos\theta_2 + d) \\ sin\theta_1 cos\theta_{23} & -cos\theta_1 sin\theta_{23} & -cos\theta_1 & sin\theta_1(L_2cos_{23} + L_1cos\theta_2 + d) \\ sin\theta_{23} & cos\theta_{23} & 1 & (L_2sin\theta_{23} + L_1cos\theta_2 + d) \\ 0 & 0 & 0 & 1 \end{bmatrix} \tag{4.6}
$$

Similarly the transformations for remaining three legs will be same because of the assumption that frame assignment is same for all the legs.

$$
k = L_1cos\theta_2 + d + L_2cos(\theta_2 + \theta_3)
$$

$$
x = cos\theta_1 * (k)
$$

$$
y = sin\theta_1 * (k)
$$

$$
z = L_2sin(\theta_2 + \theta_3) + L_1sin\theta_2
$$

Generalized Transformation from Torso Frame to Leg Frame

From the Fig. 4.3, it is clear that, one rotational joint (Roll,α) about X- axis for the torso and another rotational joint (Pitch, β) about Y axis for the torso forms two DoF articulation torso. Respective orientation matrix of the Torso about these joints and translation matrix of P_x, P_y and P_z towards each leg forms Transformation matrix. Rotations from X, Y axis will be taken for the torso and the translation for all legs also considered as shown in Fig. 4.3. Magnitude of the translation will be same for all the legs and only direction will be different. R_x, R_y are rotations about X and Y axis and generalized transformation from Torso to leg frame {i} calculated using homogenous transformation matrix.

$$
R_X = \begin{bmatrix} 1 & 0 & 0 \\ 0 & cos\alpha & -sin\alpha \\ -1 & sin\alpha & cos\alpha \end{bmatrix}, R_y = \begin{bmatrix} cos\beta & 0 & -sin\beta \\ 0 & 1 & 0 \\ -sin\beta & 0 & cos\beta \end{bmatrix} \tag{4.7}
$$

$$
{}^R_T R = \begin{bmatrix} 1 & 0 & 0 \\ 0 & cos\alpha & -sin\alpha \\ -1 & sin\alpha & cos\alpha \end{bmatrix} \begin{bmatrix} cos\beta & 0 & -sin\beta \\ 0 & 1 & 0 \\ -sin\beta & 0 & cos\beta \end{bmatrix}
$$

$$
{}_T^R R = \begin{bmatrix} cos\beta & 0 & sin\beta \\ sin\alpha sin\beta & cos\alpha & -sin\alpha sin\beta \\ -cos\beta - cos\alpha sin\beta & sin\alpha & -sin\beta + cos\alpha cos\beta \end{bmatrix} \tag{4.8}
$$

$$
{}_0^T T = \begin{bmatrix} cos\beta & 0 & sin\beta & P_x \\ sin\alpha sin\beta & cos\alpha & -sin\alpha sin\beta & P_y \\ -cos\beta - cos\alpha sin\beta & sin\alpha & -sin\beta + cos\alpha cos\beta & P_z \\ 0 & 0 & 0 & 1 \end{bmatrix} \tag{4.9}
$$

Where

α is an angle of rotation about X axis of the Torso Roll.

β is an angle of rotation about Y axis of the Torso Pitch.

P_x=distance from the center of the Torso to leg frame in X direction

P_y=distance from the center of the Torso to leg frame in Y direction

P_z=distance from the center of the Torso to leg frame in Z direction

P_x, P_y, P_z is different for each leg then transformation of Torso frame to leg frame for each leg of quadruped is given as following

For LEG 1

From Fig. 4.3 we obtain the value of P_x, P_y, P_z and $P_x = -L_x$, $P_y = L_y$, $P_z = 0$, α, β

Put these value in (4.9) we can find the transformation from frame {T} to frame {0} is ${}_T^0 T$ total transformation from Torso frame {T} to frame {4} is

$$
{}_4^T T = {}_0^T T {}_4^0 T \tag{4.10}
$$

${}_0^4 T$ is be same for all legs.

For LEG 3

From Fig. 4.3 we obtain the value of P_x, P_y, P_z and $P_x = -L_x$, $P_y = -L_y$, $P_z = 0$, α, β

Put these value in (4.9) we can find the transformation from frame {T} to frame {0} is ${}_T^0 T$ total transformation from Torso frame {T} to frame {4} is

$$
{}_4^T T = {}_0^T T {}_4^0 T \tag{4.11}
$$

For LEG 2

From Fig. 4.3 we obtain the value of P_x, P_y, P_z and $P_x = L_x$, $P_y = L_y$, $P_z = 0$, α, β

Put these value in (4.9) we can find the transformation from frame {T} to frame {0} is ${}_T^0 T$ total transformation from Torso frame {T} to frame {4} is

$$
{}_4^T T = {}_0^T T {}_4^0 T \tag{4.12}
$$

For LEG 4

From Fig. 4.3 we obtain the value of P_x, P_y, P_z and $P_x = L_x$, $P_y = -L_y$, $P_z = 0$, α, β

Put these value in (4.9) we can find the transformation from frame {T} to frame {0} is ${}_T^0 T$ total

transformation from Torso frame {T} to frame {4} is

$$_4^T T = {}_0^T T {}_4^0 T$$

(4.13)

4.4 Jacobian Analysis of Quadruped Robot for Velocities

Derived the equation of Jacobian for all joints of legs starting from frame {0} to frame {4} and also for Torso frames.

Linear Velocity and Angular Velocity from Leg Frame of the Quadruped Robot

Linear velocity describes an attribute of a point and angular velocity describes an attribute of link. Jacobian is always associated with the angular velocity and describes the linear velocity. Here derived the velocity propagation of 3 DoF leg of quadruped robot.

A. Velocity Propagation of Leg Links

In considering the motion of legs as robot manipulator links, use link frame {0} as our reference base frame. Hence, v_i is the linear velocity of the origin of link frame {i} and ω_i is the angular velocity of link frame {i}. A manipulator is a chain of bodies, each one capable of motion relative to its neighbors. Based on this concept, computed the velocity of each link in order, starting from the base. The velocities of link $i+1$ will be that of link i, plus new velocity components were added by joint $i+1$ [183].

$$_{i+1}^{i+1}\omega = {}_i^{i+1}R \, {}_i^i\omega + \dot{\theta}_{i+1} \, {}_{i+1}^{i+1}Z$$

(4.14)

$$_{i+1}^{i+1}V = {}_i^{i+1}R({}_i^iV + {}_i^i\omega \, {}_{i+1}^iP)$$

(4.15)

Velocity propagation of each link of Quadruped Robot leg from leg frame {0} to {4}
For Link0

$$_0^0\omega = [0]$$

(4.16)

$$_0^0V = [0]$$

(4.17)

For Link1

From above equaions angular velocity and linear velocity calculated, here i= 0;

$$_1^1\omega = {}_0^1R \, {}_0^0\omega + \dot{\theta}_1 \, {}_1^1Z$$

(4.18)
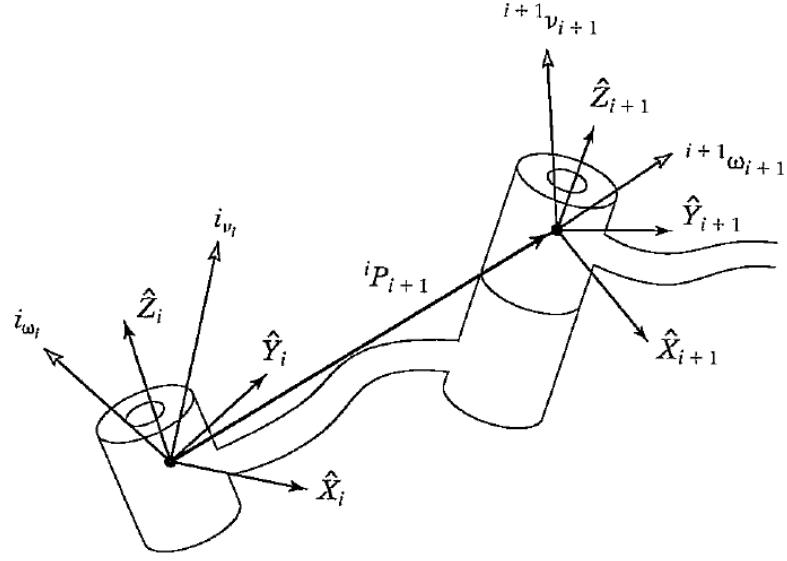
Figure 4.6: Velocity vector of neighboring link

$$
{}_0^1R = {}_1^0R' = \begin{bmatrix} \cos\theta_1 & \sin\theta_1 & 0 \\ -\sin\theta_1 & \cos\theta_1 & 0 \\ 0 & 0 & 1 \end{bmatrix} \tag{4.19}
$$

$$
{}_1^1\omega = \begin{bmatrix} \cos\theta_1 & \sin\theta_1 & 0 \\ -\sin\theta_1 & \cos\theta_1 & 0 \\ 0 & 0 & 1 \end{bmatrix} \begin{bmatrix} 0 \\ 0 \\ 0 \end{bmatrix} + \dot{\theta}_1 \begin{bmatrix} 0 \\ 0 \\ 1 \end{bmatrix} = \begin{bmatrix} 0 \\ 0 \\ \dot{\theta}_1 \end{bmatrix} \tag{4.20}
$$

Similarly for linear velocity of first frame

$$
{}_1^1V = {}_0^1R({}_0^0V + {}_1^1\omega \times {}_1^0P) \tag{4.21}
$$

$$
= \begin{bmatrix} \cos\theta_1 & \sin\theta_1 & 0 \\ -\sin\theta_1 & \cos\theta_1 & 0 \\ 0 & 0 & 1 \end{bmatrix} \left(\begin{bmatrix} 0 \\ 0 \\ 0 \end{bmatrix} + \begin{bmatrix} 0 \\ 0 \\ \dot{\theta}_1 \end{bmatrix} \times \begin{bmatrix} 0 \\ 0 \\ 0 \end{bmatrix} \right) = \begin{bmatrix} 0 \\ 0 \\ 0 \end{bmatrix} \tag{4.22}
$$

For Link2

$$
{}_2^2\omega = {}_1^2R\,{}_1^1\omega = \dot{\theta}_2\,{}_2^2Z \tag{4.23}
$$

$$\,^2_1R = \,^1_2R' = \begin{bmatrix} \cos\theta_2 & 0 & \sin\theta_2 \\ -\sin\theta_2 & 0 & \cos\theta_2 \\ 0 & -1 & 0 \end{bmatrix} \tag{4.24}$$

$$\,^2_2\omega = \begin{bmatrix} \cos\theta_2 & 0 & \sin\theta_2 \\ -\sin\theta_2 & 0 & \cos\theta_2 \\ 0 & -1 & 0 \end{bmatrix} \begin{bmatrix} 0 \\ 0 \\ \dot\theta_1 \end{bmatrix} + \dot\theta_2 \begin{bmatrix} 0 \\ 0 \\ 1 \end{bmatrix} = \begin{bmatrix} \dot\theta_1\sin\theta_2 \\ \dot\theta_1\cos\theta_2 \\ \dot\theta_2 \end{bmatrix} \tag{4.25}$$

Similarly for linear velocity of 2nd frame

$$\,^2_2V = \,^2_1R(\,^1_1V + \,^2_2\omega \times \,^1_2P) \tag{4.26}$$

$$= \begin{bmatrix} \cos\theta_2 & 0 & \sin\theta_2 \\ -\sin\theta_2 & 0 & \cos\theta_2 \\ 0 & -1 & 0 \end{bmatrix} \left(\begin{bmatrix} 0 \\ 0 \\ 0 \end{bmatrix} + \begin{bmatrix} \dot\theta_1\sin\theta_2 \\ \dot\theta_1\cos\theta_2 \\ \dot\theta_2 \end{bmatrix} \times \begin{bmatrix} d \\ 0 \\ 0 \end{bmatrix} \right) = \begin{bmatrix} 0 \\ 0 \\ -d\dot\theta_1 \end{bmatrix} \tag{4.27}$$

For Link3

Angular velocity and linear velocity is

$$\,^{i+1}_{i+1}\omega = \,^{i+1}_{i}R \,^i_i\omega + \dot\theta_{i+1} \,^{i+1}_{i+1}Z \tag{4.28}$$

Here, i=2;

$$\,^3_3\omega = \,^3_2R \,^2_2\omega + \dot\theta_2 \,^2_2Z \tag{4.29}$$

$$\,^3_2R = \,^2_3R' = \begin{bmatrix} \cos\theta_3 & -\sin\theta_3 & 0 \\ \sin\theta_3 & \cos\theta_3 & 0 \\ 0 & 0 & 1 \end{bmatrix} \tag{4.30}$$

$$\,^3_3\omega = \begin{bmatrix} \cos\theta_3 & -\sin\theta_3 & 0 \\ \sin\theta_3 & \cos\theta_3 & 0 \\ 0 & 0 & 1 \end{bmatrix} \begin{bmatrix} \dot\theta_1\sin\theta_2 \\ \dot\theta_1\cos\theta_2 \\ \dot\theta_2 \end{bmatrix} + \dot\theta_3 \begin{bmatrix} 0 \\ 0 \\ 1 \end{bmatrix} \tag{4.31}$$

$$\,^3_3\omega = \begin{bmatrix} \sin(\theta_2+\theta_3)\dot\theta_1 \\ \cos(\theta_2+\theta_3)\dot\theta_1 \\ \dot\theta_2 + \dot\theta_3 \end{bmatrix} \tag{4.32}$$

Similarly for velocity of third frame

$$\ _{3}^{3}V = \ _{2}^{3}R(\ _{2}^{2}V + \ _{2}^{2}\omega \times \ _{3}^{2}P) \tag{4.33}$$

$$= \begin{bmatrix} \cos\theta_3 & -\sin\theta_3 & 0 \\ \sin\theta_3 & \cos\theta_3 & 0 \\ 0 & 0 & 1 \end{bmatrix} \left(\begin{bmatrix} 0 \\ 0 \\ -d\dot{\theta}_1 \end{bmatrix} + \begin{bmatrix} \dot{\theta}_1\sin\theta_2 \\ \dot{\theta}_1\cos\theta_2 \\ \dot{\theta}_2 \end{bmatrix} \times \begin{bmatrix} L_1 \\ 0 \\ 0 \end{bmatrix} \right) \tag{4.34}$$

$$= \begin{bmatrix} L_1\dot{\theta}_2\sin\theta_3 \\ L_1\dot{\theta}_2\cos\theta_3 \\ -L_1\dot{\theta}_1\cos\theta_2 - d\dot{\theta}_1 \end{bmatrix} \tag{4.35}$$

For End Point of Link3 and Frame {4}

There is no revolute joint at the frame 4 then

$$\ _{4}^{4}\omega = \ _{3}^{3}\omega \tag{4.36}$$

But linear velocity will be different due to the angular velocity of joint 3 at 4 frame is

$$\ _{4}^{4}V = \ _{3}^{4}R(\ _{3}^{3}V + \ _{3}^{3}\omega \times \ _{4}^{3}P) \tag{4.37}$$

$$= \begin{bmatrix} 1 & 0 & 0 \\ 0 & 1 & 0 \\ 0 & 0 & 1 \end{bmatrix} \left(\begin{bmatrix} L_1\dot{\theta}_2\sin\theta_3 \\ L_1\dot{\theta}_2\cos\theta_3 \\ -L_1\dot{\theta}_1\cos\theta_2 - d\dot{\theta}_1 \end{bmatrix} + \begin{bmatrix} \sin(\theta_2+\theta_3)\dot{\theta}_1 \\ \cos(\theta_2+\theta_3)\dot{\theta}_1 \\ \dot{\theta}_2 + \dot{\theta}_3 \end{bmatrix} \times \begin{bmatrix} L_2 \\ 0 \\ 0 \end{bmatrix} \right) \tag{4.38}$$

$$= \begin{bmatrix} L_1\dot{\theta}_2\sin\theta_3 \\ L_1\dot{\theta}_2\cos\theta_3 + L_2(\dot{\theta}_2 + \dot{\theta}_3) \\ -L_1\dot{\theta}_1\cos\theta_2 - d\dot{\theta}_1 + L_2\cos(\theta_2+\theta_3)\dot{\theta}_1 \end{bmatrix} \tag{4.39}$$

B. Jacobian for Quadruped Leg from Frame {0} to Frame {4}

we have velocity for frame {4} w.r.t same frame is

$$\ _{4}^{4}V = \begin{bmatrix} L_1\dot{\theta}_2\sin\theta_3 \\ L_1\dot{\theta}_2\cos\theta_3 + L_2(\dot{\theta}_2 + \dot{\theta}_3) \\ -L_1\dot{\theta}_1\cos\theta_2 - d\dot{\theta}_1 + L_2\cos(\theta_2+\theta_3)\dot{\theta}_1 \end{bmatrix} \tag{4.40}$$

Velocity of frame {4} w.r.t to {0} frame is

$$\ _{4}^{0}V = \ _{4}^{0}R\ _{4}^{4}V \tag{4.41}$$

$$\ _{4}^{0}V = \ _{4}^{0}J_v \begin{bmatrix} \dot{\theta}_1 \\ \dot{\theta}_2 \\ \dot{\theta}_3 \end{bmatrix} \tag{4.42}$$

From the transformation matrix we know x, y, z after differentiating it we can get the velocity along

x, y, z. From (4.6) and (4.10) we will get the transformation matrix. After doing comparison of transformation matrix we can have x, y, z.

$$k = L_1 \cos\theta_2 + d + L_2 \cos(\theta_2 + \theta_3) \tag{4.43}$$

$$x = \cos\theta_1(L_2 \cos(\theta_2 + \theta_3) + L_1 \cos\theta_2 + d) \tag{4.44}$$

$$y = \sin\theta_1(L_2 \cos(\theta_2 + \theta_3) + L_1 \cos\theta_2 + d) \tag{4.45}$$

$$z = L_2 \sin(\theta_2 + \theta_3) + L_1 \sin\theta_2 \tag{4.46}$$

After differentiation of above equations we get the Jacobian matrix from frame {4} w.r.t to frame {0}.

$$
{}^0_4 V = \begin{bmatrix}
-k\sin\theta_1 & -\cos\theta_1(L_2\sin\theta_{23} + L_1\sin\theta_2) & -\cos\theta_1 L_2\sin\theta_{23} \\
-k\cos\theta_1 & -\sin\theta_1(L_2\sin\theta_{23} + L_1\sin\theta_2) & -\sin\theta_1 L_2\sin\theta_{23} \\
0 & L_2\cos\theta_{23} + L_1\cos\theta_2 & L_2\cos\theta_{23}
\end{bmatrix}
\begin{bmatrix}
\dot\theta_1 \\
\dot\theta_2 \\
\dot\theta_3
\end{bmatrix}
\tag{4.47}
$$

$$
{}^0_4 J_v = \begin{bmatrix}
-k\sin\theta_1 & -\cos\theta_1(L_2\sin\theta_{23} + L_1\sin\theta_2) & -\cos\theta_1 L_2\sin\theta_{23} \\
-k\cos\theta_1 & -\sin\theta_1(L_2\sin\theta_{23} + L_1\sin\theta_2) & -\sin\theta_1 L_2\sin\theta_{23} \\
0 & L_2\cos\theta_{23} + L_1\cos\theta_2 & L_2\cos\theta_{23}
\end{bmatrix}
\tag{4.48}
$$

Jacobian for Torso Frame of the Quadruped

All the joint velocities are independent with the frame so all the joint velocity will be same from the Torso frame and leg frame. Only difference will come quadruped when we will take the joint velocity from Torso frame ${}^T_4 V$ one rotation matrix will come to multiply with transformation matrix.

$$
{}^T_4 R = {}^T_0 R \, {}^0_1 R \, {}^1_2 R \, {}^2_3 R \, {}^3_4 R \tag{4.49}
$$

We know the joint velocity of frame {4} w.r.t to its own frame, then velocity from Torso frame is

$$
{}^T_4 V = \begin{bmatrix}
0 & L_2\cos\theta_{23} + L_1\cos\theta_2 & L_2\cos\theta_{23} \\
-k\cos\theta_1 & -\sin\theta_1(L_2\sin\theta_{23} + L_1\sin\theta_2) & -\sin\theta_2 L_2\sin\theta_{23} \\
-k\sin\theta_1 & -\cos\theta_1(L_2\sin\theta_{23} + L_1\sin\theta_2) & -\cos\theta_2 L_2\sin\theta_{23}
\end{bmatrix}
\begin{bmatrix}
\dot\theta_1 \\
\dot\theta_2 \\
\dot\theta_3
\end{bmatrix}
\tag{4.50}
$$

$$
{}^T_4 J_v = \begin{bmatrix}
0 & L_2\cos\theta_{23} + L_1\cos\theta_2 & L_2\cos\theta_{23} \\
-k\cos\theta_1 & -\sin\theta_1(L_2\sin\theta_{23} + L_1\sin\theta_2) & -\sin\theta_2 L_2\sin\theta_{23} \\
-k\sin\theta_1 & -\cos\theta_1(L_2\sin\theta_{23} + L_1\sin\theta_2) & -\cos\theta_2 L_2\sin\theta_{23}
\end{bmatrix}
\tag{4.51}
$$

4.5   Trajectory Planning for Quadruped Leg

A trajectory describes the desired motion of a manipulator (here leg) in multidimensional space. Here, trajectory refers to a time history of position, velocity and acceleration for each leg. When we simulate legs of quadruped without their trajectory planning, one can found leg is moving randomly in the Cartesian space. If leg moves randomly in the space, then control of leg will be difficult for motion and balancing aspects of robot. Similarly on physical robot if we want leg should move

from one point to another point in Cartesian space. It should follow a particular trajectory then balancing of robot will be easier. Trajectory planning of leg is important parameter for kinematics of robots. Here the trajectory planning for legged quadruped robot considered with and without via point. For Stance phase the trajectory used is without via point and whereas for the swing phase the trajectory plan is through via point. Quadruped robot has three DoF leg so robot is moving in the Cartesian space in all the directions.

4.5.1 Trajectory planning with via point

The trajectory of leg with via point that mean we consider the more points between starting and goal point of trajectory of the leg for making smooth motion. For formulation of trajectory equation with via points we divide the whole trajectory into small segments shown in Fig. 4.7 [183]. Each segment contains two point starting and end point and for making the continuous trajectory we assume the value velocity, displacement, acceleration of initial point of second segment and final point of first segment will be same and time will start from zero for each segment of trajectory.
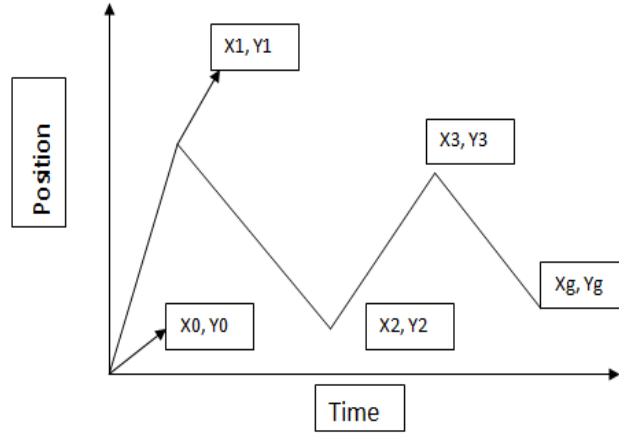
Figure 4.7: Trajectory planning with via point

Assumptions for Formulation of Equations

$$t = 0; \ x(0) = x_0; \ y(0) = y_0; \ z(0) = z_0 \tag{4.52}$$

$$\dot{x}(0) = x_0; \ \dot{y}(0) = y_0; \ \dot{z}(0) = z_0$$

$$t = t_{f1}; \ x(t_{f1}) = x_v; \ y(t_{f1}) = y_v; \ z(t_{f1}) = z_v \tag{4.53}$$

$$\dot{x}(t_{f1}) = \dot{x_2}(0); \ \dot{y}(t_{f1}) = \dot{y_2}(0); \ \dot{z}(t_{f1}) = \dot{z_2}(0)$$

$$\ddot{x}(t_{f1}) = \ddot{x}_2(0); \ddot{y}(t_{f1}) = \ddot{y}_2(0); \ \ddot{z}(t_{f1}) = \ddot{z}_2(0)$$

$$t = t_{f2}; \; x(t_{f2}) = x_f; \; y(t_{f2}) = y_f; \; z(t_{f2}) = z_f \tag{4.54}$$

$$\dot{x}(t_{f2}) = 0; \; \dot{y}(t_{f2}) = 0; \; \dot{z}(t_{f2}) = 0$$

A. Straight Line Trajectory of Quadruped Leg with Via Point

$$\begin{cases} x_1(t) = a_{10} + a_{11}t \\ y_1(t) = a'_{10} + a'_{11}t \\ z_1(t) = a''_{10} + a''_{11}t \end{cases} \; ..... \; \text{segment 1 } t = 0 \text{ to } t_{f1} \tag{4.55}$$

$$\begin{cases} x_2(t) = a_{20} + a_{21}t \\ y_2(t) = a'_{20} + a'_{21}t \\ z_2(t) = a''_{20} + a''_{21}t \end{cases} \; ..... \; \text{segment 1 } t = 0 \text{ to } t_{f2} \tag{4.56}$$
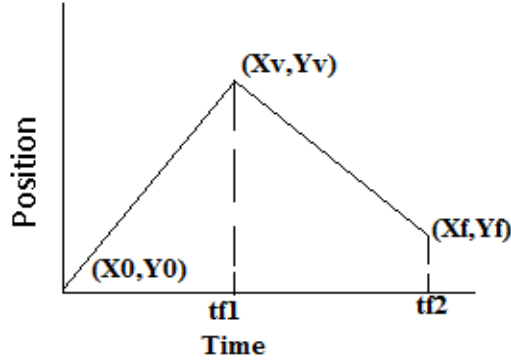
Figure 4.8: Straight line trajectory

$$x_1(t) = x_0 + \left(\frac{x_v - x_0}{t_{f1}}\right)t \tag{4.57}$$

$$y_1(t) = y_0 + \left(\frac{y_v - y_0}{t_{f1}}\right)t \tag{4.58}$$

$$z_1(t) = z_0 + \left(\frac{z_v - z_0}{t_{f1}}\right)t \tag{4.59}$$

$$x_2(t) = x_v + \left(\frac{x_f - x_v}{t_{f2}}\right)(t - t_{f1}) \tag{4.60}$$

$$y_2(t) = y_v + \left(\frac{y_f - y_v}{t_{f2}}\right)(t - t_{f1}) \tag{4.61}$$

$$z_2(t) = z_v + \left(\frac{z_f - z_v}{t_{f2}}\right)(t - t_{f1}) \tag{4.62}$$

$$x_1(t) = x_0 + \frac{12x_v - 3x_f - 9x_0}{4t_{f1}^2}t^2 + \frac{-8x_v + 3x_f + 5x_0}{4t_{f1}^3}t^3 \tag{4.63}$$

$$x_2(t) = x_v + \frac{3x_g - 3x_0}{4t_{f2}^2}(t - t_{f1}) + \frac{-12x_v + 6x_f + 6x_0}{4t_{f2}^2}(t - t_{f1})3 \tag{4.64}$$

$$y_1(t) = y_0 + \frac{12y_v - 3y_f - 9y_0}{4t_{f1}^2}t^2 + \frac{-8y_v + 3y_f + 5y_0}{4t_{f1}^3}t^3 \tag{4.65}$$

$$y_2(t) = y_v + \frac{3y_g - 3y_0}{4t_{f2}^2}(t - t_{f1}) + \frac{-12y_v + 6y_f + 6y_0}{4t_{f2}^2}(t - t_{f1})3 \tag{4.66}$$

$$z_1(t) = z_0 + \frac{12z_v - 3z_f - 9z_0}{4t_{f1}^2}t^2 + \frac{-8z_v + 3z_f + 5z_0}{4t_{f1}^3}t^3 \tag{4.67}$$

$$z_2(t) = z_v + \frac{3z_g - 3z_0}{4t_{f2}^2}(t - t_{f1}) + \frac{-12z_v + 6z_f + 6z_0}{4t_{f2}^2}(t - t_{f1})3 \tag{4.68}$$

B. Cubic Trajectory of Quadruped Leg with Via Point

$$\begin{cases} x_1(t) = a_{10} + a_{11}t + a_{12}t^2 + a_{13}t^3 \\ y_1(t) = a'_{10} + a'_{11}t + a'_{12}t^2 + a'_{13}t^3 \\ z_1(t) = a''_{10} + a''_{11}t + a''_{12}t^2 + a''_{13}t^3 \end{cases} \text{..... segment 1 } t = 0 \text{ to } t_{f1} \tag{4.69}$$

$$\begin{cases} x_2(t) = a_{20} + a_{21}t + a_{22}t^2 + a_{23}t^3 \\ y_2(t) = a'_{20} + a'_{21}t + a'_{22}t^2 + a'_{23}t^3 \\ z_2(t) = a''_{20} + a''_{21}t + a''_{22}t^2 + a''_{23}t^3 \end{cases} \text{..... segment 1 } t = 0 \text{ to } t_{f2} \tag{4.70}$$

Each cubic will be evaluated over an interval starting at t=0 and end $t = t_{fi}$ and i=1, 2.

$$\begin{cases} x_1(0) = x_0 = a_{10} \\ x_1(t_{f1}) = x_v = a_{10} + a_{11}t_{f1} + a_{12}t_{f1}^2 + a_{13}t_{f1}^3 \\ x_2(0) = x_v = a_{20} \\ x_2(t_{f2}) = x_f = a_{20} + a_{21}t_{f2} + a_{22}t_{f2}^2 + a_{23}t_{f2}^3 \\ \dot{x}_1(0) = 0 = a_{11} \\ \dot{x}_2(t_{f2}) = 0 = a_{21} + 2a_{22}t_{f2} + 3a_{23}t_{f2}^3 \\ \dot{x}_1(t_{f1}) = \dot{x}_2(0) \\ \ddot{x}_1(t_{f1}) = \ddot{x}_2(0) \\ a_{11} + a_{12}t_{f1} + 3a_{13}t_{f1}^2 = a_{21} \\ 2a_{12} + 3a_{13}t_{f1} = 2a_{22} \end{cases} \tag{4.71}$$

$$\begin{cases} a_{10} = x_0 \\ a_{11} = 0 \\ a_{12} = \frac{12x_v - 3x_f - 9x_0}{4t_{f1}^2} \\ a_{13} = \frac{-8x_v + 3x_f + 5x_0}{4t_{f1}^3} \\ a_{20} = x_v \\ a_{21} = \frac{3x_g - 3x_0}{4t_{f2}} \\ a_{22} = \frac{-12x_v + 6x_f + 6x_0}{4t_{f2}^2} \\ a_{22} = \frac{8x_v - 5x_f - 3x_0}{4t_{f2}^2} \end{cases} \qquad (4.72)$$

After solving the equation above we get

$$x_1(t) = x_0 + \frac{12x_v - 3x_f - 9x_0}{4t_f 1^2} t^2 + \frac{-8x_v + 3x_f + 5x_0}{4t_f 1^3} t^3$$

$$x_2(t) = x_v + \frac{3x_g - 3x_0}{4t_f 2}(t - t_{f1}) + \frac{-12x_v + 6x_f + 6x_0}{4t_{f2}^2}(t - t_{f1}^2 + \frac{8x_v - 5x_f - 3x_0}{4t_{f2}^2}(t - t_{f1})^3$$

Similarly for y and z

$$y_1(t) = y_0 + \frac{12y_v - 3y_f - 9y_0}{4t_{f1}^2} t^2 + \frac{-8y_v + 3y_f + 5y_0}{4t_{f1}^3} t^3 \qquad (4.73)$$

$$y_2(t) = y_v + \frac{3y_g - 3y_0}{4t_{f2}}(t - t_{f1}) + \frac{-12y_v + 6y_f + 6y_0}{4t_{f2}^2}(t - t_{f1})^2 + \frac{8y_v - 5y_f - 3y_0}{4t_{f2}^2} t - t_{f1?}^3$$

$$z_1(t) = x_0 + \frac{12z_v - 3z_f - 9z_0}{4t_{f1}^2} t^2 + \frac{-8z_v + 3z_f + 5z_0}{4t_{f1}^3} t^3$$

$$z_2(t) = z_v + \frac{3z_g - 3z_0}{4t_f 2}(t - t_{f1}) + \frac{-12z_v + 6z_f + 6z_0}{4t_{f2}^2}(t - t_{f1})^2 + \frac{8z_v - 5z_f - 3z_0}{4t_{f2}^2}$$

C. Trajectory Planning Results for Quadruped Leg

The simulation results of quadruped leg with different trajectories in Cartesian space were shown. Imported CAD model of single leg with 3 DoF as shown in the Fig. 4.9 and define input and output variable for leg into ADAMS. This model has 3 input variables as joint velocity and 3 output variable as joint angle. A Matlab program is written using kinematics, Jacobian and trajectory equations. The results are as shown in Fig. 4.9 and Fig. 4.10

4.5.2 Simulation model of ATQR

3D design software (Solidworks) is used to design ATQR. The simulation model is a mammalian type ATQR with 3 DoF each leg and 2DoF (Roll and Pitch) Articulated Torso. The solidworks model file was imported to ADAMS software and then the input/output variables of the plant were assigned to the joints, motors and constraints. The material was assumed to be Aluminum alloy for all the components for simulation. A dummy mass was attached to the body of the quadruped to
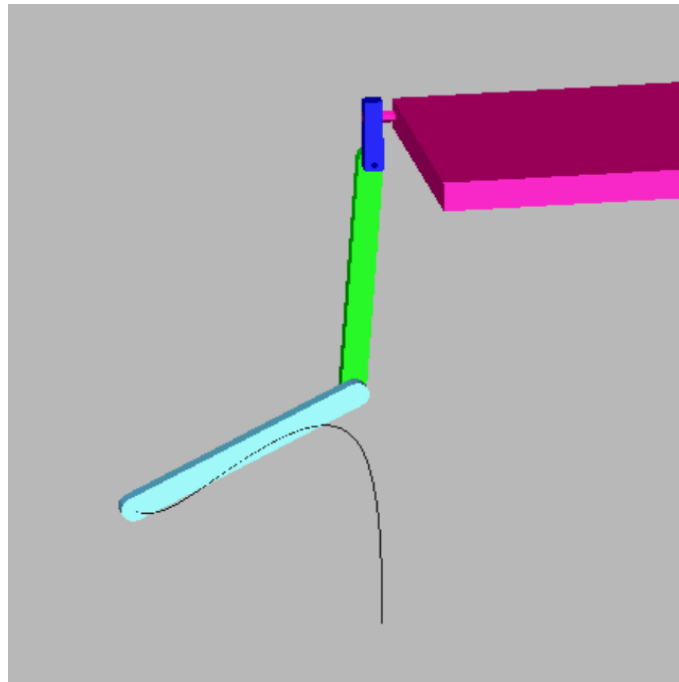
Figure 4.9: Trajectory of leg tip of quadruped robot
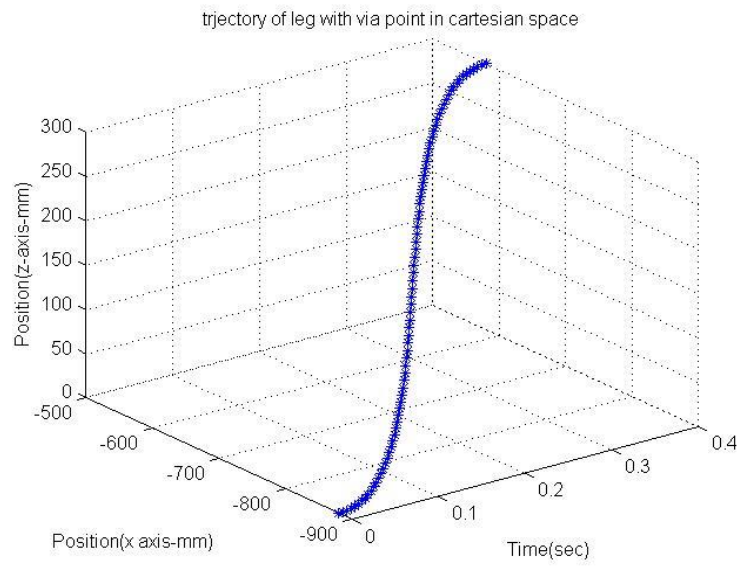
Figure 4.10: Cubic spline trajectory of Leg Tip

65

Table 4.2: Quadruped Robot Parameters

Mass, m	40 Kg
Body length, L_b	1.0 m
Body width, w	0.5 m
Height of Trotting, h	0.9m
Stride length (Max), Ls	0.6m

imitate the payload carrying capability. The quadruped robot parameters are as shown in Table 4.2, have been used for the simulation of the robot. The frictional coefficient between the ground and the leg foot was considered to be 0.7. Link lengths are $d = 80mm$, L_1=400mm L_2=400mm
Simulation model of articulated torso quadruped robot is as shown in Fig. 4.11. Using this model,
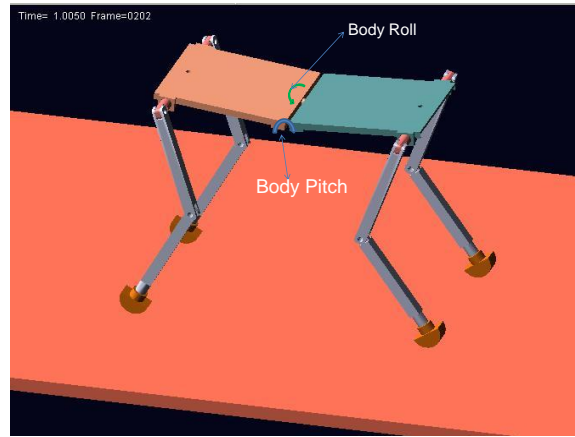
Figure 4.11: Simulation model of ATQR

physical simulations were carried out for walking (crawling) gait, trot gait and bounding gait with articulated torso.

4.6 Control System

The MATLAB Simulink was used along with the physics engine based MSC ADAMS plant. The complete quadruped robot with articulated torso can be controlled using this tool. Fig. 4.12 shows the simulation control plant. The ADAMS_PLANT provides the angular positions of each joint. The MATLAB function programme consists of various control algorithms depending on the requirement for the leg placement. This function program supplies the angular velocity control commands to the plant.

The overall control is hierarchical in nature. The highest is the torso level control followed by leg control and finally joint control. Based on the velocity of the torso, the trajectory of the legs in the stance phase is defined which is in the negative direction of the torso. This would be straight line trajectory of the feet equal to step length. The total trajectory is calculated as a cubic spline
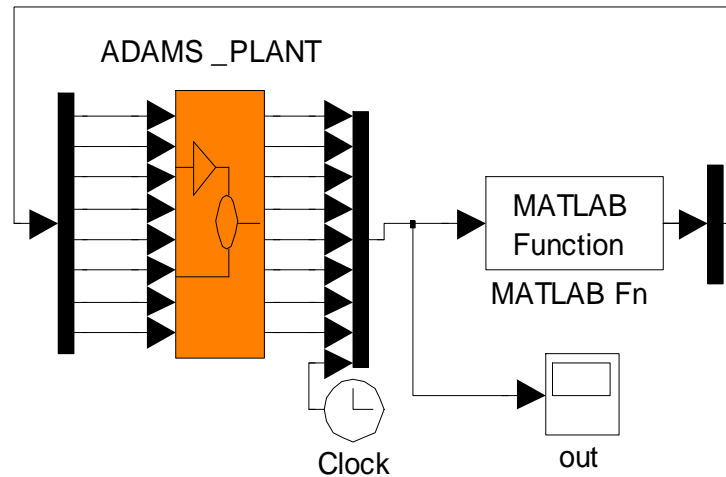
Figure 4.12: Simulation of Control Plant

interpolation from start to end point in the Cartesian space with a total time of 0.2 sec. At every time step, 10 millisec, the error in the present position and desired position is used to determine the leg velocities. These are used to calculate joint velocities using inverse Jacobian. This value is integrated to give the desired angle and used as an error for the position control of joint. The joint position controller uses PD control. In simulation output of the PD control is directly the velocity for the joint. However in real system this is the PWM input for the drive with appropriately chosen gains. In both cases close loop is on position. In simulation the position is directly obtained from the ADAMS Software while in practical system it is obtained from the incremental encoder available on the motor. For the legs in the swing phase the trajectory is calculated with step length in the direction of torso motion with the via point in the Z-direction. The control is similar to the legs in the stance phase. The total time for completion of the trajectory in the stance phase and swing phase are kept same. The leg position controller, leg velocity controller and joint position controller are as shown in Fig. 4.13.

The trajectory function is responsible for coordinating the simultaneous motion of all four legs to perform straight line or circular motions. This trajectory plan is used for normal walking and trot gaits, where as circular motion is used for individual legs for the gallop and bounding gaits. The gallop gait can be achieved by providing small phase difference between pair of front legs and pair of back legs.

The force control processes the terrain adaptation with attitude control. The static stability controller determines whether a given foot placement configuration is stable or not. The gait generator scheme generates the sequence of leg lifting and foot placement to move the robot in stable manner and foot placements are based on the particular gait sequence for walking, trot and bounding or galloping.

Leg tip velocity controller uses the leg Jacobian to determine the joint angular velocities which are controlled by joint velocity controller as shown in Fig. 4.13. Leg tip position control is achieved by driving the leg velocities based on the error in leg tip position. The actuator controls are analysed
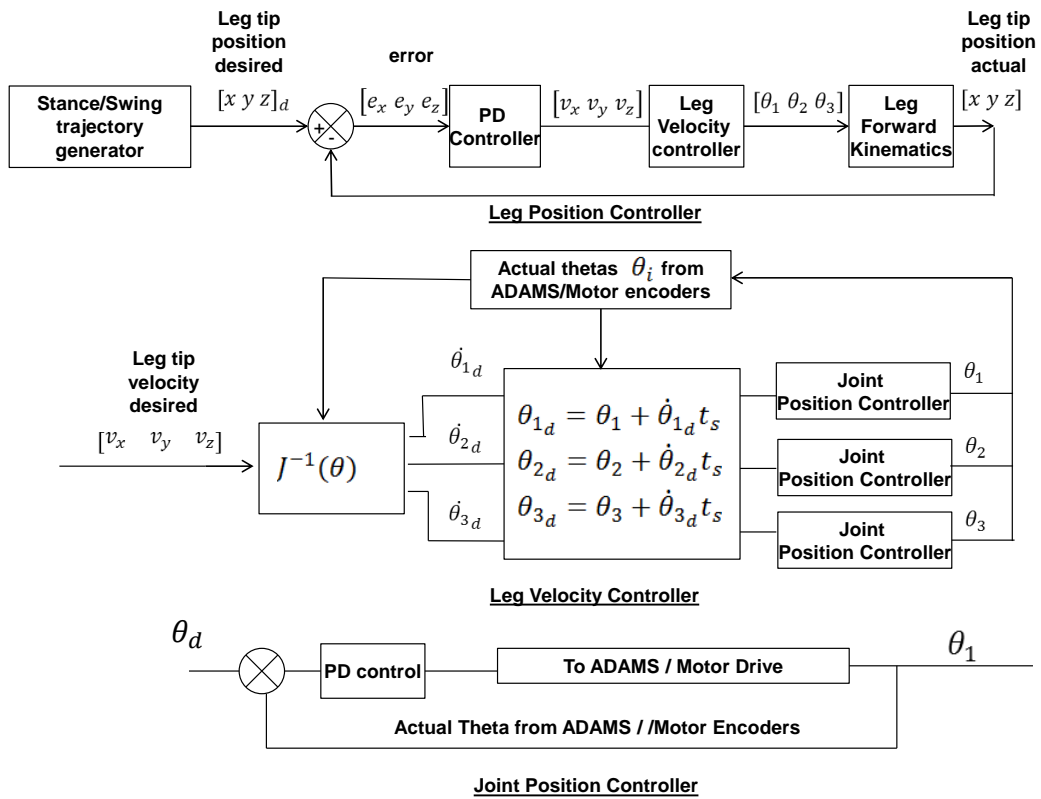
Figure 4.13: Leg Controller block diagram
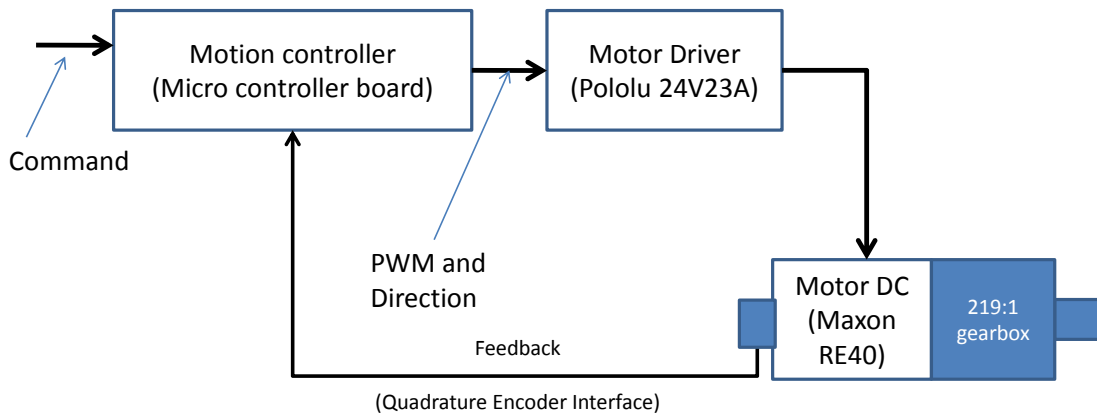
Figure 4.14: Actuator control scheme

for different configurations of the applied torque and the relative angular velocity of each actuator. The actuator control scheme is as shown in Fig. 4.14. In additionally the gearing available on the RE maxon is 219:1, this results the total torque of the order of 30N-m. Motion Controller is dsPIC30F 4011 (16-bit micro controller from MICROCHIP Inc) with QEI module (built in Quadrature Encoder Interface), the clear block diagram of complete close loop system provided.

The controller architecture for envisaged practical robot as shown in Fig. 4.15, consists of Master slave configuration, slave card for servo control of single axis, Master card for coordination of multiple axes, CAN bus for master slave communication, Host PC interface through RS232 bus, Wireless OCU (Operator Control Unit) interface through WIFI.
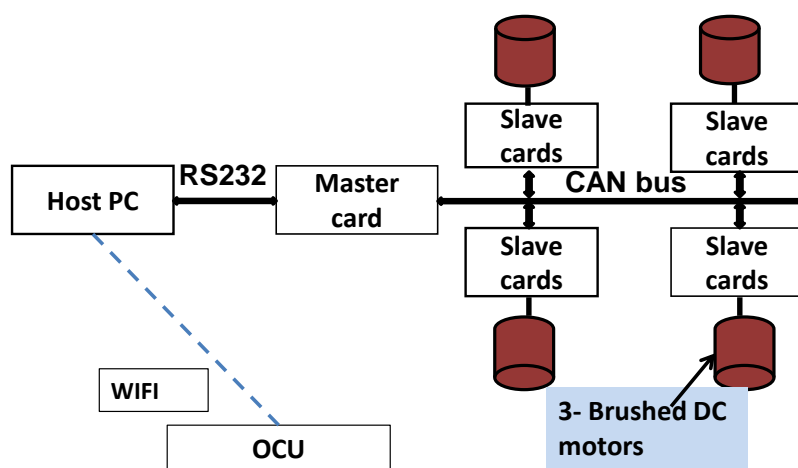
Figure 4.15: Control Architecture

4.7 Simulation

Gait planning for the even terrain is simulated for two different configurations of the robot legs. The two configurations refers to one with 2DoF leg and other with 3DoF leg. A gait refers to a walking or running pattern, the walking gaits (walk, trot) and running gait (bound, gallop) are produced by the gait planner. The gait planner algorithms are supplied through MATLAB function program. Continuous and discontinuous periodic gaits for quadruped robot have been simulated and compared. The continuous gaits are characterized by the simultaneous motion of the legs and the torso motion; whereas discontinuous gaits are characterized by the sequence motion of the legs and the torso motion. One leg is transferred with other three legs in support and halted. In discontinuous gaits the tosro is propelled with all legs in support and moving simultaneously, maintaining their footprints. Simulations were carried out on fixed torso and articulated torso quadruped robot. The analysis has been carried out on flat terrain with height obstacle.

The trajectories for the feet have been specifically defined to achieve propulsion along the X-axis (forward motion of the robot). The legs in the stance phase are given trajectory to achieve negative X- velocity to propel the body/torso forward. The leg step length of 200mm was chosen as this was

the maximum leg step length for which stable gait is achieved. The legs in the swing phase are given trajectory to achieve motion with the step length along X-axis and via point at the middle having a height of 160mm this height was chosen to enable crossing any spherical pebble like obstacle with which a terrain could be strewn with in practical situation.

In walking robot, legs in the stance used for propelling the torso along with the given direction, hence all the legs in contact ground are given identical trajectories (flat terrain) to avoid slippage. Hence in trot case the diagonal legs in stance phase are given identical motion in -ve X direction. Though the total DoF are 14 the motion of the legs is constrained by no slippage condition. Therefore the trajectories have to be defined in such a way that distance constraints between the contact points are met.

Using the control scheme described above, simulation was carried out using MSC ADAMS for multi-body dynamics simulation and MATLAB SIMULINK for control. All the quadruped robot joint motors are modeled as velocity control rotary actuators. Simulation is carried out with 3D model of the robot for step/obstacle height of 0.05m, 0.1m and 0.16m. From the simulation, it has been found that the body bends outward on the flight phase because of the free angle. This is the motion like the galloping motion of animal. Due to articulated torso the stride length has been increased and the robot speed has also been increased. On the other hand, the robot bends inward during the stance phase and it helps to accelerate the robot.

All simulations were performed using MSC ADAMS with a MATLAB/SIMULINK interface. In Fig. 4.16 the snapshots of the gait sequence for height obstacle crossing during the bounding gait are shown.

4.8   Results and Discussion

Statically stable walking quadruped robot is achieved, if the horizontal projection of its CoM lies inside the support pattern. The Static Stability Margin (SSM) was defined for a given support polygon as the smallest of the distances from the CoM projection to the edges of the support polygon [184]. SSM is the optimum stability margin for an ideal machine on horizontal, even terrain.

SSM has been computed while the robot was walking using a two-phase discontinuous gait. SSM measured over time is plotted in Fig. 4.17. The two-phase discontinuous gait used in the simulations is characterized by a sequence of leg and torso motions. The leg sequence is performed by transferring one leg at a time, while the body/torso is supported on the other three legs. The body/torso is moved forward with all four legs on the ground (body/torso motion). When the torso is in motion, at that time the SSM is not measured because all the four legs are in contact with the ground and it has maximum stability. A maximum of 80mm has been measured as the SSM during the leg motion. The complete SSM is plotted in Fig. 4.17.

Next, simulations were carried for the bounding gait for obstacle cross over during this gait. During the simulation of step climbing the reaction forces have been measured and used for the control. Fig. 4.18 shows the forces measured by the force sensors on rear legs. For the flat terrain in bounding gait the forces are normal. During the obstacle crossing, the reaction forces are increased as shown in Fig. 4.18. In simulation the ADAMS has been used for the dynamics of the quadruped robot with interface MATLAB for trajectory generation and control, the forces shown in the figure are obtained using the force probe for foot ground contact in ADAMS. Since the ADAMS has
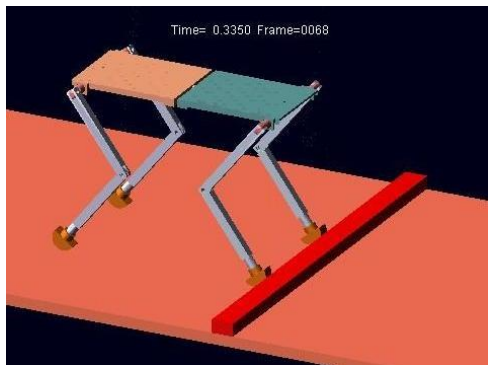
a) Start of the obstacle location and articulating torso
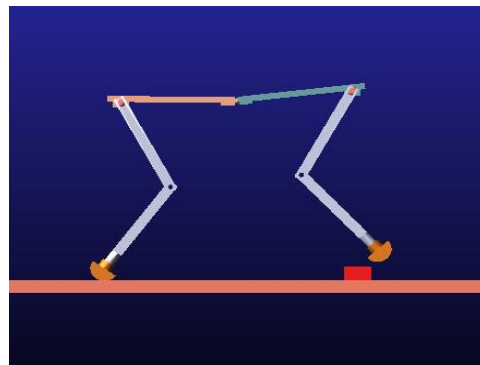
b)Articulated torso and crossing over the height obstacle
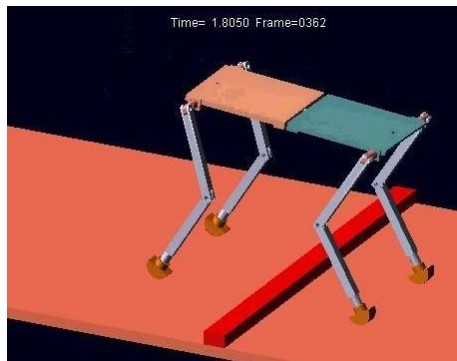
c)Normal bound after crossing
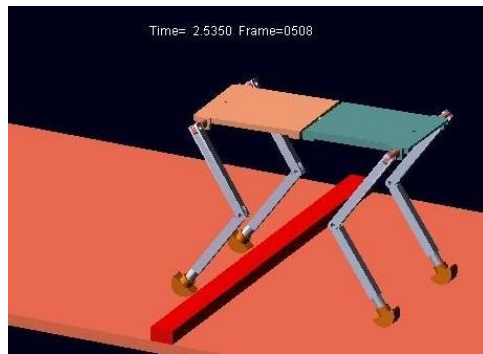
d) Start of the obstacle crossing by rear legs
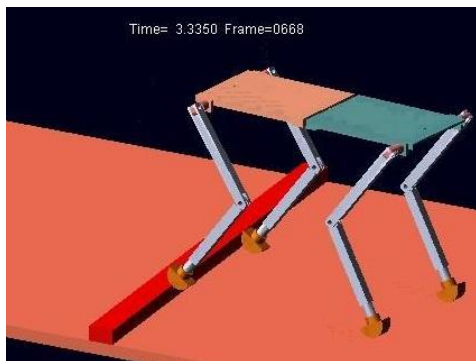
e) Cross over the height obstacle by rear legs
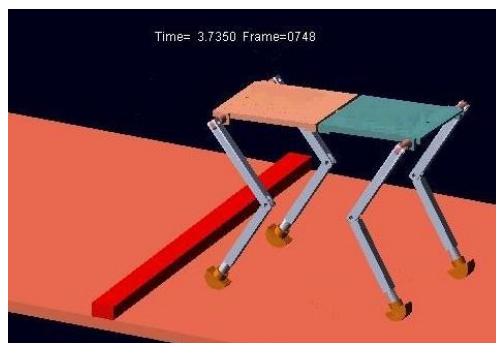
f) Normal bound after crossing the obstacle

Figure 4.16: Snap shot of simulation of height obstacle crossing of quadruped robot
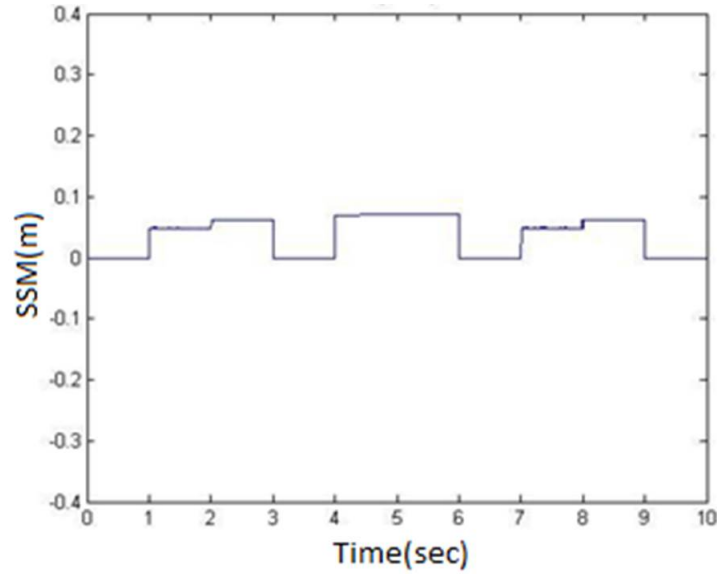
Figure 4.17: Static Stability Margin during walking gait

complete physics engine implemented, the forces include the complete dynamics of impact. Hence the force plots can show this impact forces which could be higher than the forces at static equilibrium. Whenever the contact lost the forces instantly becomes zero due to the impact dynamics. Similarly for the trot gait, the graphs can be plotted for all the 4 legs and the reaction forces can also be measured from the simulation. From this figure, it can also be found that beginning of the obstacle is detected when horizontal force F_x is more than 200N in negative direction.

Fig. 4.19 shows the forces measured by the force sensors on front legs contact. For the flat terrain in bounding gait, the forces are normal. While crossing the height obstacle, the reaction forces are found to be increased and the same has been shown in this figure.

Similarly, the variation of velocity of the front base and back base were plotted in Fig. 4.20. During the height obstacle crossing, it can be noticed that the velocity of the robot has decreased.

Variation of CoM for front base and back base were plotted in Fig. 4.21. A sudden variation can also be observed during the height obstacle crossing.

The simulation results are presented in Table 4.3. The parameters of stride length, hopping height, average speed and foot clearance were mentioned for both the articulated torso quadruped robot and fixed torso quadruped robot

Table 4.3: Comparison of Fixed Torso and Articulated Torso Quadruped Robot

Parameter	Fixed Torso Quadruped	Articulated Torso Quadruped
Stride length	0.58m	0.98m
Hopping height	0.68m	0.78m
Average Speed	1.7m/s	2.05m/s
Foot clearance	0.035m	0.16m

72
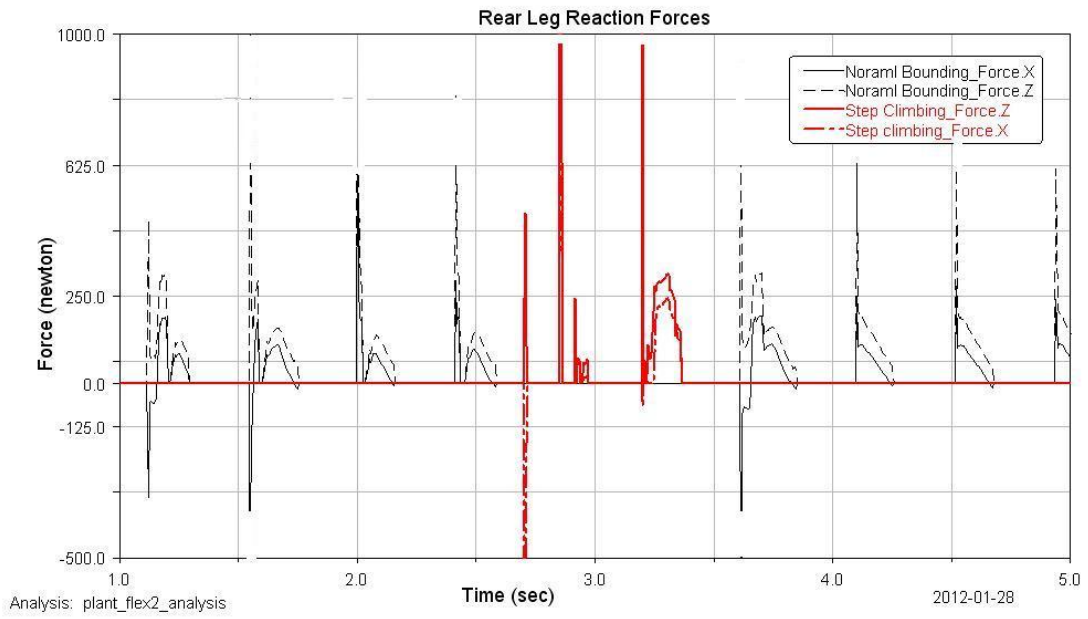
Figure 4.18: Rear Leg Reaction forces of ATQR
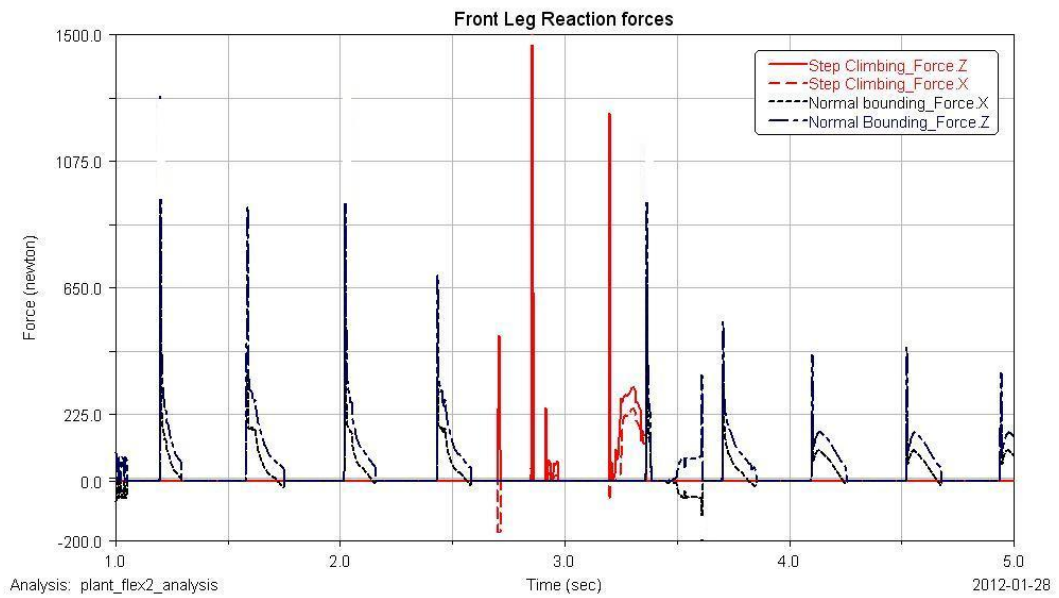
Figure 4.19: Front Leg Reaction forces of ATQR
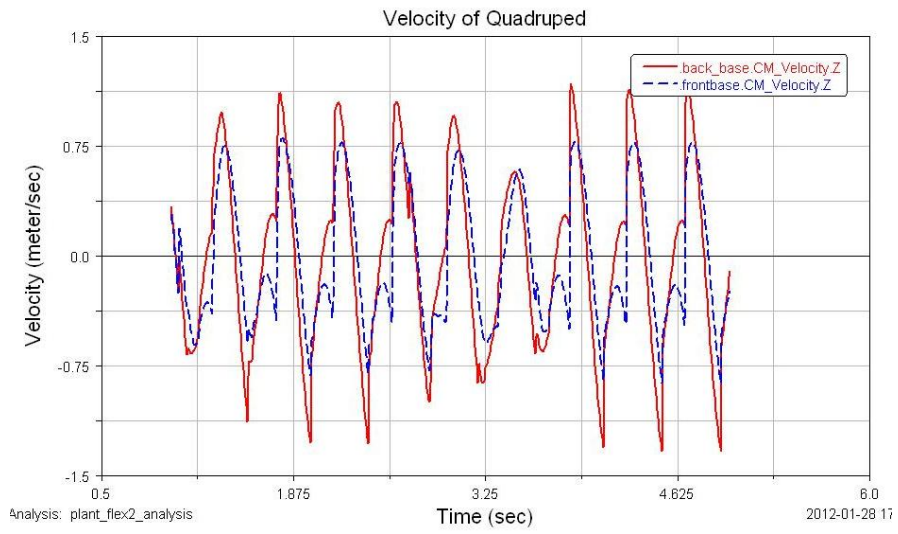
Figure 4.20: Velocity of Quadruped Robot
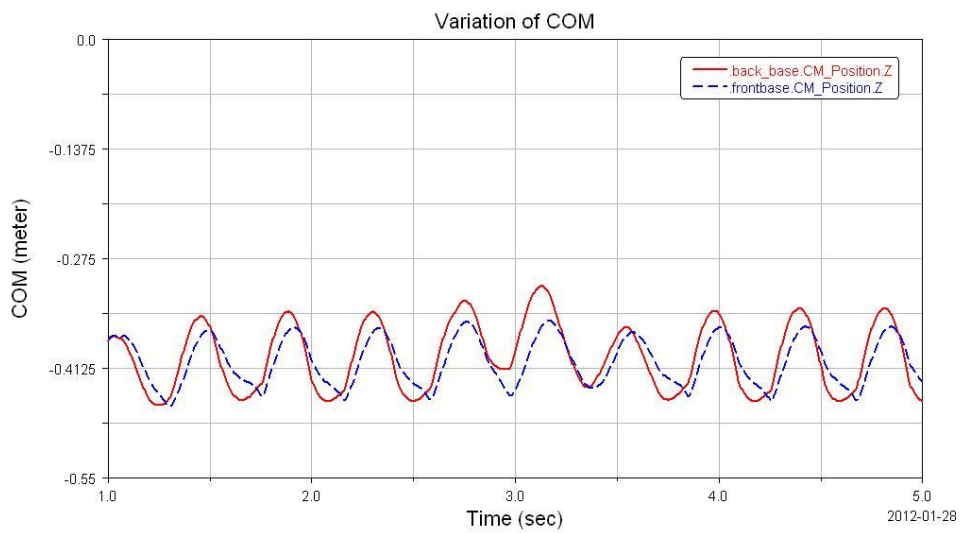
Figure 4.21: Variation of Centre of Mass

4.9 Conclusions

In this chapter, the forces acting on flat terrain with height obstacle in bounding and trot gaits have been investigated with 2DoF articulated torso quadruped robot. Simulations were carried out with articulated torso quadruped robot locomotion. This chapter also includes the effect of torso DoF on stability and energy efficiency in walking mode, trot mode and running (bounding) mode. Comparison of results with rigid torso has been carried out. The stride length, hopping height, average speed and foot clearance has increased with articulated torso quadruped compared to fixed torso quadruped robot. Hence articulated torso provides higher speed and enhanced mobility.

Chapter 5

Passive Dynamic Bounding with Symmetry Condition Control Laws

5.1 Introduction

Passive dynamic bounding gaits are periodic gaits that begin at stable or unstable initial conditions called fixed points. Such a gait when started with some initial state at the beginning of a gait cycle will end at state which is identical to the initial state (except for the horizontal distance). These gaits over a flat and level surface do not consume any additional energy for locomotion if the gait is self-stabilizing [185, 186]. This means, the Cost of Transport is theoretically zero.

Stable gaits do not require any control input and can tolerate disturbances (*i.e.*, are self-stabilizing). Unstable gaits can be stabilized by the application of appropriate control inputs. Whether a periodic gait is stable or unstable is determined by the eigenvalues of Poincare map. While self-stabilizing gaits are quite attractive to implement, the region of initial conditions (fixed points) where they exist is limited. Controllers for stabilizing gaits starting from unstable fixed points is an active area of research [187].

Passive dynamic bounding gaits with either stable or unstable fixed points, show certain symmetry properties. In this chapter, control laws for stabilizing the passive dynamic bounding gaits based on the symmetry of fixed points are introduced and studied. Implementation of control law in body-fixed touchdown angles by means of physical cross-coupling without using a controller is also discussed. With the addition of feedback of pitch angle in the control law, it is shown that the stability region is considerably increased. These control laws require that the gait does not have a double support phase.

5.2 Quadruped Robot Model for Passive Dynamic Bounding

Since bounding gait is a planar gait, the model of quadruped robot considered is planar with body and two mass-less telescopic legs with identical springs on them. The mass-less legs are connected to the robot at the hip through revolute joints. The distribution of mass in the robot body is assumed to be uniform so that the center of mass is the geometric center. Figure 5.1 shows the schematic along with notation.
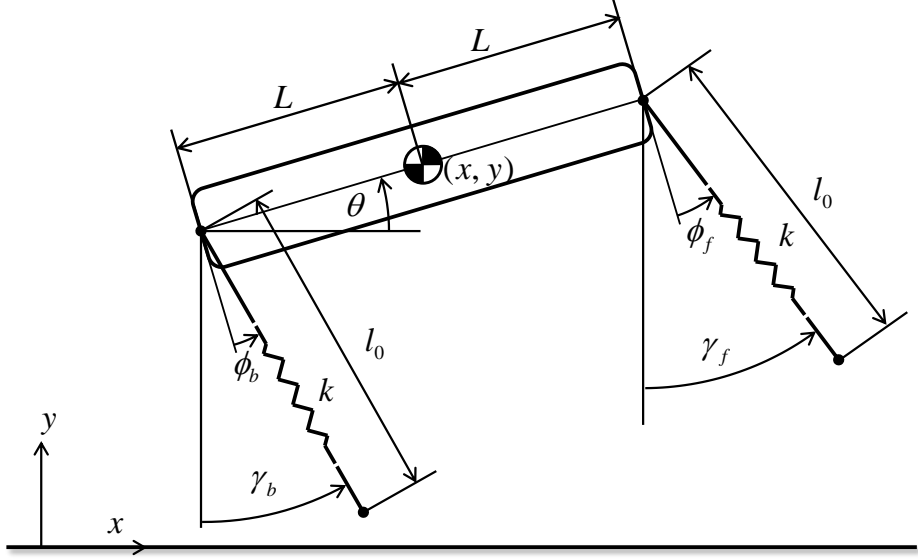
Figure 5.1: Schematic of the quadruped robot

Each gait cycle of bounding can consist of four phases: flight phase, back-leg support phase, double support phase,and front-leg support phase. In this work, we do consider gaits that do not have double support phase. Various phases of the bounding gait are shown in Fig. 5.2. In the flight phase 1 prior to the back-leg support phase, the back leg is controlled such that at the time of touching the ground it makes a back-leg touch down angle γ_b^{td} with the vertical. During back-leg support phase the back-leg spring compresses and decompresses. As soon as the length of the leg equals to the free length l_0, back support phase ends and the robot lifts off the ground at lift-off angle γ_b^{lo} to flight phase. Similarly, during the flight phase 2 prior to the front-leg support phase, the front leg is controlled such that at the time of touching the ground, it makes a front leg touchdown angle of γ_f^{td} with the vertical. Again when it lifts off the ground, it does so at a liftoff angle γ_f^{lo}. Since the legs are assumed to be massless, control action for touchdown does not influence the robot dynamics.

5.2.1 Equations of Motion

During flight phase, the equations of motions are

$$m\ddot{x} = 0, \tag{5.1}$$

$$m\ddot{y} = -mg, \tag{5.2}$$

$$I_G\ddot{\theta} = 0, \tag{5.3}$$

where x and y are the coordinates of the center of mass of the robot body, and θ is the angle made by the longitudinal axis of the body with the horizontal.
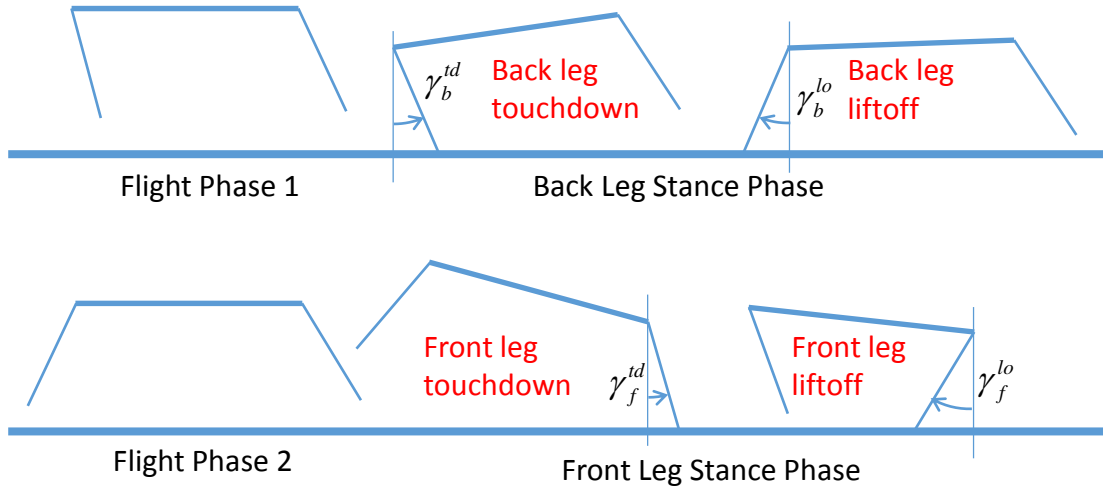
Figure 5.2: Various phases in the passive dynamic bounding gait

During back-leg or front-leg support phase, the equations of motion are

$$m\ddot{x} = F_x, \tag{5.4}$$

$$m\ddot{y} = -mg + F_y, \tag{5.5}$$

$$I_G\ddot{\theta} = r_x F_y - r_y F_x, \tag{5.6}$$

where F_x and F_y are the forces exerted by the back-leg or front-leg on the robot body at the hip joint, and r_x and r_y are the coordinates of the back or front hip joint with respect to the body center of mass. The forces F_x and F_y are calculated from the compression of the spring. If l is the length of the leg, then the spring force is given by $k(l_0 - l)$. The direction of this force is along the leg where F_x and F_y are the components of this force along x and y-axes respectively. For double support phase, forces and moments on the right hand side of the equations of motion are the sum of components of front and back leg spring forces and moments.

While the stiffness k and free length l_0 are constants, the actual length l is calculated as follows:

$$l = \sqrt{(x_{tip} - x + L\cos\theta)^2 + (y - L\sin\theta)^2}, \tag{5.7}$$

where x_{tip} is point on the ground where the tip of the back or front leg is in contact.

5.2.2 Touchdown and Liftoff Events

The transition between phases occur at the touchdown and the liftoff events. There are two touchdown events (back leg touchdown and front leg touchdown) and two liftoff events (back leg liftoff and front leg liftoff). Conditions for event detection of back and front leg touchdown events respectively are given below:

$$y - L\sin\theta - l_0\cos\gamma_b^{td} = 0, \tag{5.8}$$

$$y + L\sin\theta - l_0\cos\gamma_f^{td} = 0. \tag{5.9}$$

Similarly, the conditions for event detection of back and front leg liftoff events respectively are given below:

$$l_0 - \sqrt{(x_{btip} - x + L\cos\theta)^2 + (y - L\sin\theta)^2} = 0, \tag{5.10}$$

$$l_0 - \sqrt{(x_{ftip} - x - L\cos\theta)^2 + (y + L\sin\theta)^2} = 0, \tag{5.11}$$

where x_{btip} and x_{ftip} are the back and front tip contact points during the back and front leg support phases.

5.3 Finding Fixed Points and Stability

Legged robots are hybrid systems with discrete transformations governing transitions from one phase to another phase of motion [188, 186]. Hence, a Poincare return map is used to determine orbital stability of the trajectory. If apex height during flight phase, where $\dot{y} = 0$, is chosen as the initial condition, dimension reduction of Poincare section is possible. Further reduction is obtained by removing horizontal coordinate x of the center of mass since it increases monotonically and is not relevant to a periodic trajectory. We are left with four variables at apex height: y, θ, $\dot{x}$, and $\dot{\theta}$.

If apex event during flight phase is taken as the initial condition for a gait cycle, the final state after one gait cycle at apex event should be identical (except for the horizontal displacement x) to the initial state if the gait cycle is periodic. A Poincare return map can be defined mapping initial and final states:

$$X_{n+1} = P(X_n). \tag{5.12}$$

Equation (5.12) can be rearranged to define a function whose roots satisfy the periodicity condition.

$$X - P(X) = 0. \tag{5.13}$$

Roots of (5.13) are called the fixed points. For the given back and front touchdown angles, Newton-Raphson method can be used to search for the roots of (5.13), provided searching starts at a good initial guess. There are two different ways of finding fixed points using Newton-Raphson method. For a detailed description of these ways, refer to [186].

Stability of fixed points so found can be determined from the eigenvalues of Jacobian matrix of return map P. One of the eigenvalues is always unity, indicating the conservative nature of the system [186]. Stability of a fixed point depends on whether the remaining eigenvalues are within unit circle (stable) or outside the unit circle (unstable).

All the fixed points, stable or unstable, share two common properties: pitch angle at apex is zero, and touchdown liftoff angle symmetry. This latter condition of symmetry can be described as follows:

$$\gamma_b^{td} = -\gamma_f^{lo} \qquad \gamma_f^{td} = -\gamma_b^{lo}. \tag{5.14}$$

5.4 Symmetry Condition Control Law with Absolute Touchdown Angles

Corresponding to every fixed point $(y, \theta, \dot{x}, \dot{\theta})$, there exists at least a pair of touchdown angles which allow the gait cycle to be periodic. When a bounding gait starts from a stable fixed point, maintaining the touchdown angles corresponding to the fixed point, every gait cycle allows the gait to continue indefinitely. The same is not true with unstable fixed points because any small error in the fixed point grows rapidly till the gait fails. It is possible to stabilize unstable fixed points by using control law based on known fixed point and the error in liftoff angle [189].

Another way of stabilizing a fixed point is reported in [190], where the control law is based on touchdown angle liftoff angle symmetry condition in (5.14). The advantage of this method is that it does not require the use of known fixed point in the control law. Algorithm for the control law is as follows:

1. Start with apex initial conditions for y, θ, $\dot{x}$ and $\dot{\theta}$.

    - θ should be zero as this is the property of fixed points.
    - $\dot{\theta}$ is positive so that back leg touchdown happens first.

2. End the flight phase with some back leg touchdown angle if this is the first gait cycle or with the negative of front leg liftoff angle of the previous iteration if this is not the first gait cycle.

3. Measure and store the back leg liftoff angle after the back leg stance phase.

4. End the flight phase after the back leg stance phase with front leg touchdown angle taken as the negative of back leg liftoff angle measured in 3.

5. Measure and store the front leg liftoff angle after the front leg stance phase.

6. Go to 2.

The passive dynamic bounding is considered failed if the liftoff does not happen within a reasonable time or double support occurs. Figure 5.3 shows the stability region for back leg touchdown angles at various pitch angular velocities and forward speeds when the apex height is 0.35 m. An initial condition is considered stable if the bounding does not fail for 200 gait cycles.

5.5 Symmetry Condition Control Law with Body-Fixed Touchdown Angles

An additional property that has been observed is that the touchdown liftoff angles at fixed points show symmetry not only in terms of absolute angles measured with respect to the vertical, but also with local or relative angles measured with respect to the robot body.

$$\phi_b^{td} = -\phi_f^{lo} \qquad \phi_f^{td} = -\phi_b^{lo} \tag{5.15}$$

(a) 1 m/s forward speed   (b) 2 m/s forward speed   (c) 3 m/s forward speed   (d) 4 m/s forward speed for apex height of 0.35 m

Figure 5.3: Stability region with back leg absolute touchdown angle vs pitch angular velocity at apex

Using (5.15) in (5.14),

$$\gamma_b^{td} = -\gamma_f^{lo} \qquad\qquad \gamma_f^{td} = -\gamma_b^{lo} \qquad\qquad (5.16)$$

$$\phi_b^{td} + \theta_b^{td} = -(\phi_f^{lo} + \theta_f^{lo}) \qquad \phi_f^{td} + \theta_f^{td} = -(\phi_b^{lo} + \theta_b^{lo}) \qquad (5.17)$$

$$\theta_b^{td} = -\theta_f^{lo} \qquad\qquad \theta_f^{td} = -\theta_b^{lo} \qquad\qquad (5.18)$$

From (5.18), it is clear that symmetry condition exists even for the body pitch angle.

Instead of using touchdown angles measured with respect to absolute vertical, touchdown angles measured with respect to body can also be used for control. Body-fixed touchdown angles have several advantages compared to absolute touchdown angles as follows [191]:

1. No need to measure body pitch angle in order to maintain touchdown angle.

2. No active control is required during the flight phase in order to obtain the desired leg angle at touchdown.

Figure 5.4 shows the stability region with back leg relative touchdown angle versus pitch angular velocity at apex for various forward speeds. No stability region could be found at higher forward speeds of 3 and 4 m/s. Comparing Fig. 5.3 and Fig. 5.4, it is clear that use of absolute touchdown angles with symmetry condition control law gives larger stability region. However, the advantage of easy implementation of body fixed touchdown angles is attractive when we consider controller-less system discussed in the next section.

5.6   Inherent Stability with Physical Cross Coupling

The idea of control using symmetry condition directly as proposed in [190] is more useful if body-fixed touchdown angles are used instead of absolute touchdown angles. In addition to the advantages of body-fixed touchdown angles, there is an additional advantage of physical cross coupling (shown in Fig. 5.5) in implementing the symmetry control law. Touchdown angle once set need not be changed for a stable gait. If the back leg touchdown happens first, the front leg will be set to proper front leg touchdown angle when the back leg lifts off. During the flight phase, the legs should be locked from changing the angle by using a brake. The brake is released when the front leg touchdown happens. Similarly, when the front leg lifts off, the back leg will be in correct back leg touchdown angle.

There is a limitation introduced by the cross coupling of the legs. When both the legs are in contact with the ground, the robot body and the two legs form a four bar mechanism with the ground as a fixed link. The motion of the robot requires both the legs to rotate in the same direction about their respective contact points. This does not satisfy the symmetry condition. Hence, double support phase is not allowed when legs are physically cross coupled.

5.7   Symmetry Condition Control Law with Feedback

Stability region using symmetry condition control law with body fixed touchdown angles can be increased by adding a feedback of pitch angle at apex. The rationale for using pitch angle is as follows. Fixed points have an interesting property of zero pitch angle at apex event. There are two apex events in one gait cycle. The Pitch angle at both the apex events are zero for fixed
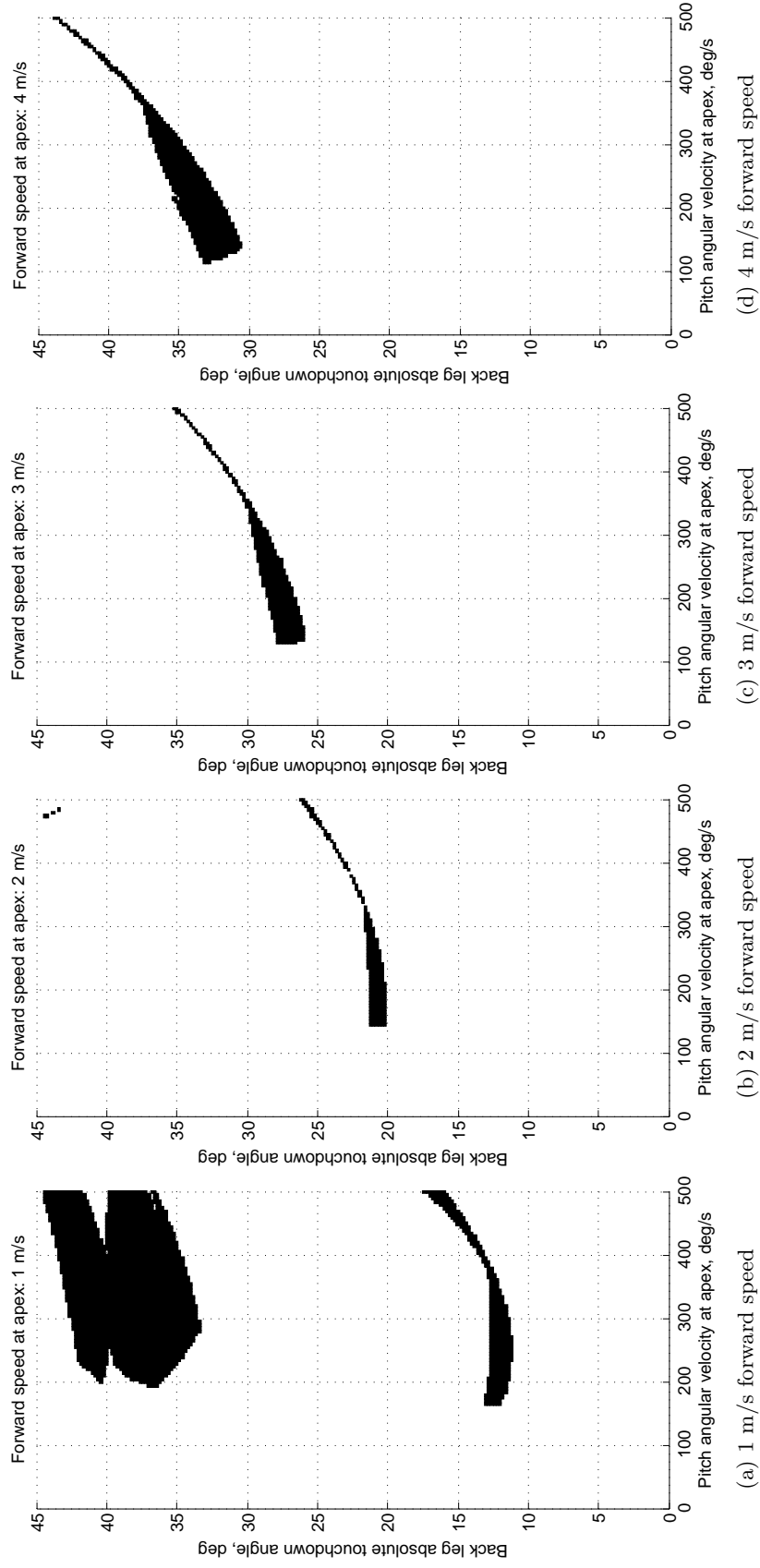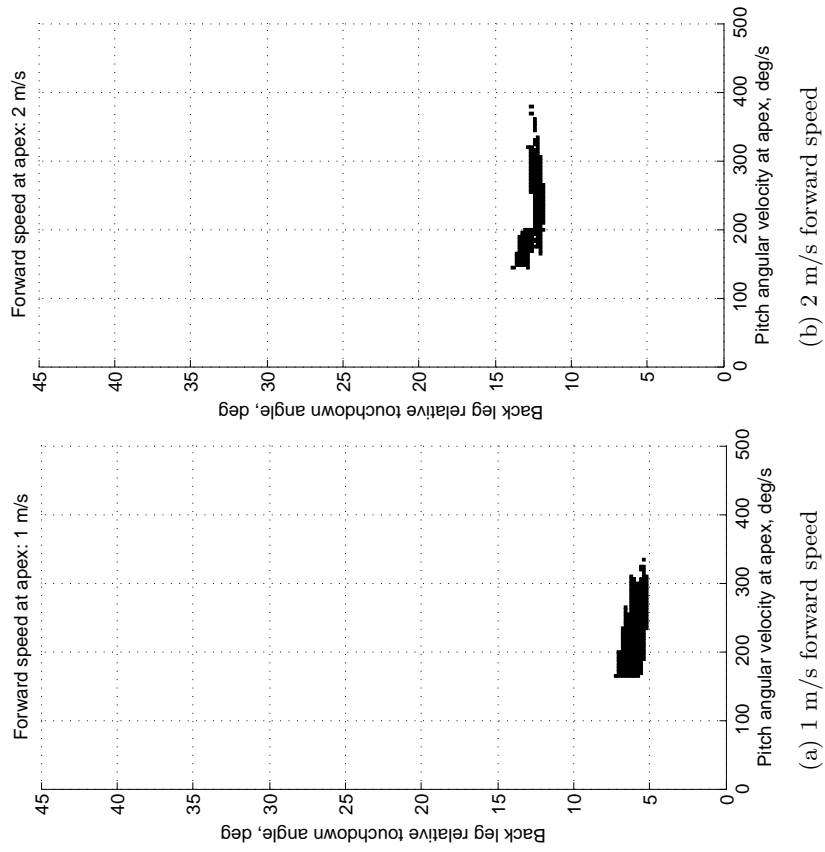
Figure 5.4: Stability region with back leg relative touchdown angle vs pitch angular velocity at apex for apex height of 0.35 m
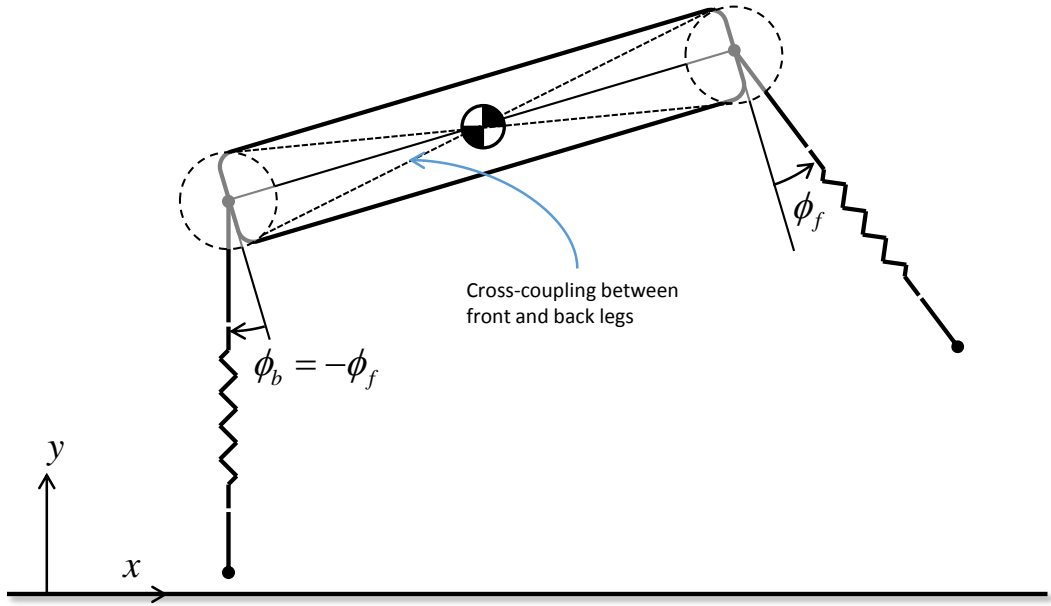
Figure 5.5: Quadruped robot with front and back leg coupled

points whether the fixed point is stable or not. If the pitch angle at apex deviates from zero, it is an indication of deviation from fixed point. This information can be used to make correction to touchdown angle so that the deviation from fixed point is prevented. The control algorithm with feedback is described as follows:

1. Start with apex initial conditions for y, θ, $\dot{x}$ and $\dot{\theta}$.

   - θ should be zero as this is the property of fixed points.
   - $\dot{\theta}$ is positive so that the back leg touchdown happens first.

2. End the flight phase with some back leg relative touchdown angle ϕ_b^{td} if this is the first gait cycle or with the negative of the front leg relative liftoff angle ϕ_f^{lo} of the previous iteration if this is not the first gait cycle.

3. Measure and store the back leg relative liftoff angle ϕ_b^{lo} after the back leg stance phase.

4. The front leg touchdown angle is calculated from

$$\phi_f^{td} = -\phi_b^{lo} - k_\theta \theta, \tag{5.19}$$

   where k_θ is a constant and θ is pitch angle at apex.

5. After the front leg stance phase, the front leg relative liftoff angle ϕ_f^{lo} is measured and stored.

6. Go to 2.

For $k_\theta = 1.7$, stability regions for various forward speeds are shown in Fig. 5.6. Although, the advantage of not needing pitch angle measurement is lost with the introduction of pitch angle

feedback, large stability regions obtained makes this control law quite useful. If physical cross-coupling is also used, only a small correction needs to be made for front leg touchdown to implement this control law.

5.8   Conclusions

Fixed points and their stability properties do not change with the addition of cross-coupling between the front and the back legs in body-fixed touchdown angles. They are found to be identical to the fixed points found using absolute touchdown angles. The main contribution of this chapter is to propose a method of automatically implementing the symmetry control law with body-fixed touchdown angles using physical cross-coupling between the front and the back legs. In so doing, we reduce the number of actuators to just one. This actuator is just a brake rather than traditional rotary actuator for rotating the legs. Although the stability region in body-fixed touchdown angle case is smallar than that of absolute touchdown angle case, it shown that the stability region can be improved using feedback of pitch angle at apex.
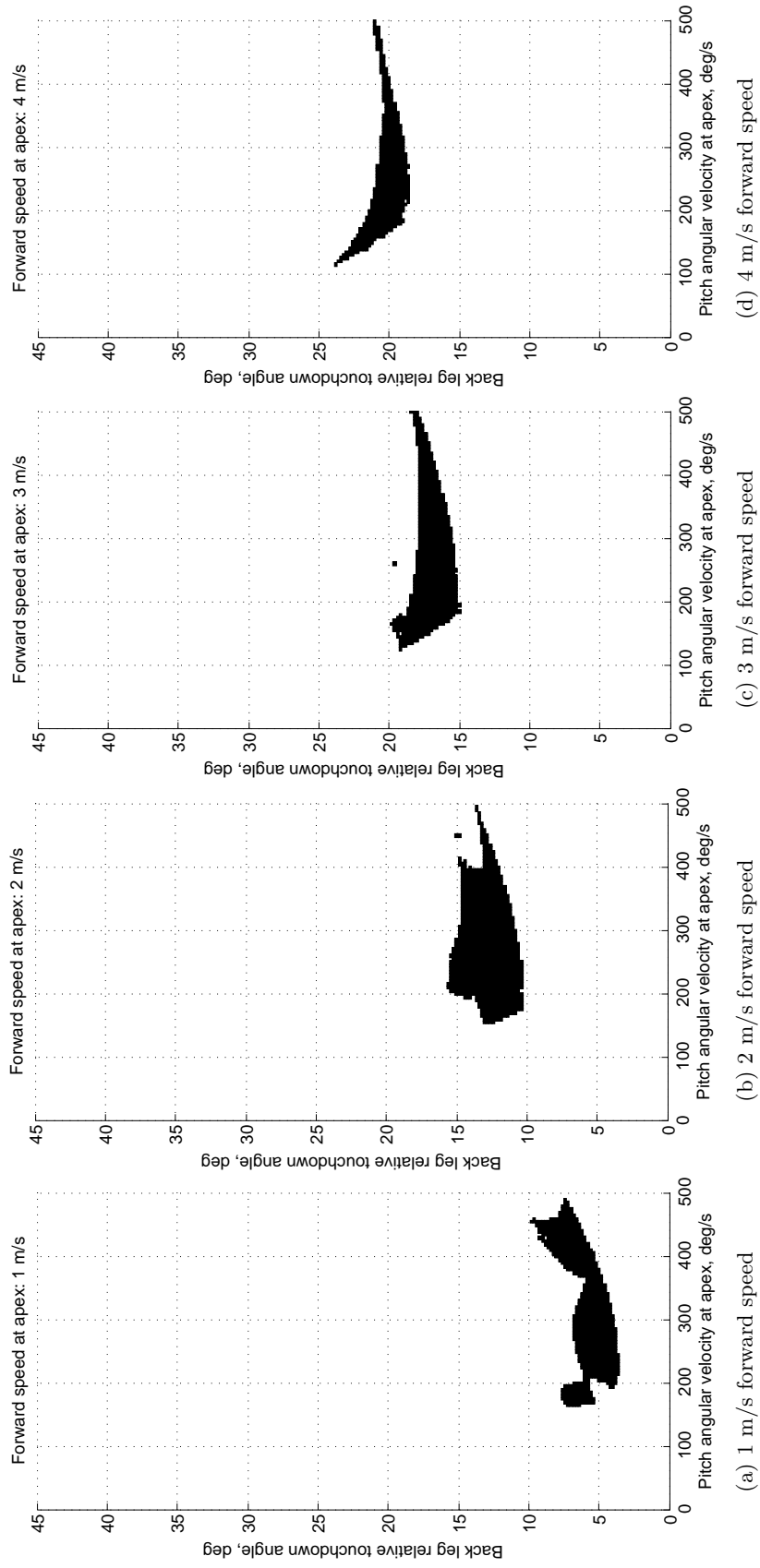
Figure 5.6: Stability region with back leg absolute touchdown angle vs pitch angular velocity at apex with pitch angle feedback

Chapter 6

Passive Dynamic Bounding with Asymmetry

6.1 Introduction

In passive dynamic bounding of quadrupeds with mass and stiffness symmetry, it has been observed that all fixed points, stable or unstable, exhibit touchdown angle symmetry condition: lift-off angle of one leg is equal to the touchdown angle of the other leg. In fact, this condition has been used in [186] to find fixed points with ease. However, what happens in the presence of mass or stiffness asymmetry has not been investigated yet with regard to stability and symmetry condition. It is important to understand the effects of asymmetry because it may be difficult to maintain symmetry in real-world applications. Zou and Schmiedeler [168] study stability with mass asymmetry for in place bounding (zero forward velocity) with legs vertical during touchdown. The focus of this chapter is on bounding with nonzero forward velocity with mass or stiffness asymmetry. Results presented in this chapter show that symmetry of lift-off and touchdown angles between front and back legs is broken when either mass or stiffness asymmetry is introduced. Further, stability is influenced by asymmetry.

6.2 Model of a Asymmetric Quadruped Robot in Bounding

Each leg of the quadruped robot has a revolute hip joint and a prismatic knee joint. The legs are free to rotate about the hip joints and resisted by linear springs along the prismatic knee joints. Since we are considering the bounding gait, two front legs and two back legs move in pairs making it a planar gait. Planar model of the quadruped robot along with nomenclature is shown in Fig. 6.1.

Each gait cycle of bounding consists of four phases: flight phase, back-leg support phase, double support phase and front-leg support phase. Double support exists only at lower speeds [186]. In flight phase, prior to back-leg support phase, the back leg is controlled such that at the time of touching the ground it makes a touch down angle γ_b^{td} with the vertical. Similarly, during the flight phase prior to front-leg support phase, the front leg is controlled such that at the time of touching the ground, it makes a touchdown angle of γ_f^{td} with the vertical. Since the legs are assumed to be massless, control action for touchdown does not influence the robot dynamics. Further, when the
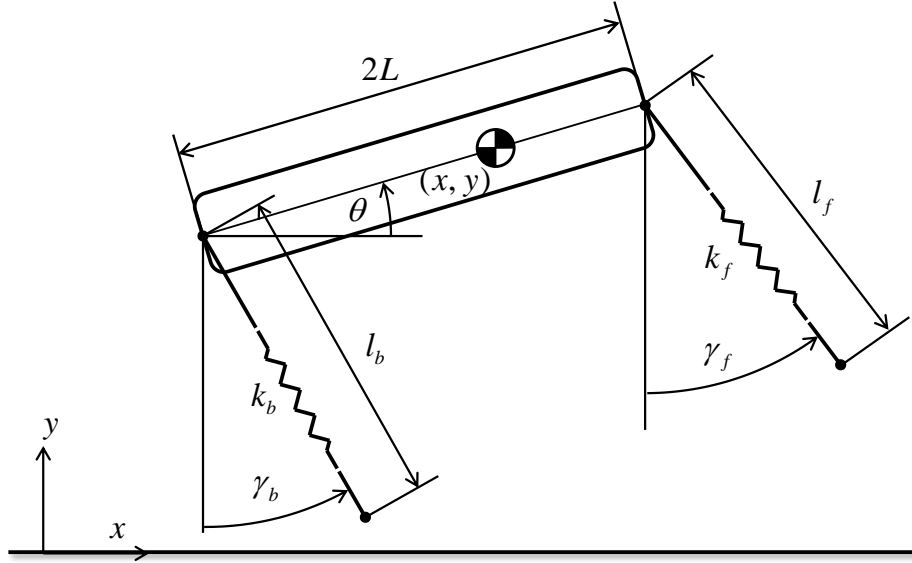
Figure 6.1: Schematic of quadruped robot

stance leg is fully extended the stance phase ends and the leg leaves the ground. The angle made by the leg at the time of leaving the ground is called the liftoff angle. For the front and back legs we can define two liftoff angles, γ_f^{lo} and γ_b^{lo} respectively. Various events in the gait cycle are detected using MATLAB event detection feature of ODE solver. The equations and motion in various phases and the event detection conditions for touchdown and liftoff are similar to equations presented in previous chapter.

6.2.1 Mass Asymmetry

Mass asymmetry can be introduced by shifting the center of mass away from the geometric center. In order to do this in a systematic way, we consider the body mass m to the be the sum of frame mass m_1, whose center of mass is at the geometric center, and payload mass m_2 that can be fixed at any location along the longitudinal axis of the body. When the payload mass is at the geometric center of the body, mass distribution in the body is symmetric. If the payload mass is moved either forward or backward with respect to the geometric center, the center of mass will no longer be at the geometric center. Although the total mass remains same, the location of center of mass as well as the centroidal moment of inertia will change. For the purpose of simulation, payload mass at either extreme end of the body is assumed to move the body center of mass to a distance of 0.1 m from the geometric center. The payload mass is calculated as

$$mx_{com} = m_1 \times 0 + m_2 \times L, \tag{6.1}$$

$$m_2 = x_{com}\frac{m}{L}, \tag{6.2}$$

where $x_{com} = 0.1$ m.

The moments of inertia of each of the masses m_1 and m_2 about their own centers of mass are

assumed to be in the same ratio as the masses:

$$I_1 = m_1 \frac{I}{m}, \tag{6.3}$$

$$I_2 = m_2 \frac{I}{m}. \tag{6.4}$$

6.2.2 Stiffness Asymmetry

Stiffness asymmetry is introduced by increasing (or decreasing) the front leg spring stiffness by some amount, and decreasing (or increasing) the back leg spring stiffness by the same amount. Therefore, stiffnesses in the back and front legs can be written as:

$$k_b = k + k_{off}, \tag{6.5}$$

$$k_f = k - k_{off}, \tag{6.6}$$

where k_{off} is the offset in stiffness.

The base parameters for simulation are adapted from [186] and are shown in Table 6.1.

Parameter	Value
Total mass, m	20.865 kg
Moment of inertia, I	1.3 kg-m
Stiffness, k	2×3520 N/m
Body half length, L	0.276 m
Free length of leg, l_0	0.323 m
Frame mass, m_1	7.5598 kg
Payload mass, m_2	13.3052 kg
Moment of inertia of frame mass, I_1	0.829 kg-m^2
Moment of inertia of payload mass, I_2	0.4710 kg-m^2
Acceleration due to gravity, g	9.81 m/s^2

Table 6.1: Parameters

6.3   Solution Procedure

There are two methods of finding fixed points reported in [186] for passive bounding of a quadruped with symmetric mass distribution and symmetric back and front leg stiffness. A brief discussion of these methods is necessary to understand the new methods being proposed in this chapter for unsymmetric cases. Both these methods rely on Newton-Raphson method in order to search for fixed points. Before we proceed to describe these methods, it is necessary to understand how the function, whose roots are fixed points, is defined. Legged robots are hybrid systems with discrete transformations governing transitions from one phase to another phase of motion [188, 186]. Hence, a Poincare return map is used to determine orbital stability of the trajectory. If apex height during flight phase, where $\dot{y} = 0$, is chosen as the initial condition, dimension reduction of Poincare section is possible. Further reduction is obtained by removing horizontal coordinate x of the center of mass since it increases monotonically and is not relevant to a periodic trajectory. We are left with four variables at apex height: y, θ, $\dot{x}$, and $\dot{\theta}$.

89

In the first method, for a given pair of back and front leg touchdown angles, the fixed points are found using Newton-Raphson method starting from an initial guess of fixed point $(y, \theta, \dot{x}, \dot{\theta})$. If the initial guess is good enough, the method converges to a fixed point corresponding to the touchdown angle pair. For all fixed points, it is found that the pitch angle θ at apex is zero. Further, symmetry condition of touchdown and lift-off angles is satisfied.

$$\gamma_b^{td} = -\gamma_f^{lo}, \text{ or } \gamma_b^{td} + \gamma_f^{lo} = 0 \tag{6.7}$$

$$\gamma_f^{td} = -\gamma_b^{lo}, \text{ or } \gamma_f^{td} + \gamma_b^{lo} = 0 \tag{6.8}$$

Although large number of fixed points can be determined with proper initial guesses, this method is not systematic and always relies on guesses.

In the second method, for a given pair of apex height and forward velocity, pitch at apex, pitch angular velocity at apex, back touchdown angle, and front touchdown angle are determined using Newton-Raphson method. In this method, symmetry condition of lift-off and touchdown angles are used to get the "output" touchdown angles from the lift-off angles corresponding to the "input" touchdown angles. Like in the first method, the fixed point that is determined after convergence depends on the initial guess. However, this is superior to the first method because we get a fixed point for particular values of apex height and forward velocity. Using this method, a continuum of fixed points can be obtained by using fixed points in the neighborhood as initial guesses. For a more elaborate detail of these methods, refer to [186].

When mass or stiffness asymmetry is introduced, fixed points can be determined using the first method through trial and error initial guesses. Two conclusions can be drawn by observing the fixed points in the presence of asymmetry:

1. pitch angle θ at apex height is not necessarily zero, and

2. touchdown-liftoff angle symmetry in (6.7) and (6.8) is broken.

Since touchdown-liftoff angle symmetry no longer holds, we cannot use the second method to find fixed points. Further, since pitch angle at apex can be nonzero, it is harder to find initial guesses that can be used in the first method.

Our method of finding fixed points is different from these two methods. Rather than using the return map in the function whose roots are fixed points, we define a new function which is quadratic in the error vector obtained from the difference between return map and another vector that is defined according to our need to make some variables as constant parameters. We first find fixed point for a particular value of apex height y and forward velocity $\dot{x}$ when there is no mass or stiffness asymmetry. Once the fixed point is obtained, asymmetry in mass or stiffness is increased in increments with initial guess of fixed point taken as the fixed point without asymmetry or that of previous increment, whichever is closer. For finding out fixed point in the absence of asymmetry, we could use the second method of [186]. However, the drawback of this method is that, the pitch angular velocity usually is not identical to the initial guess value used and sometimes far from it. For example, if we start with $(\theta, \dot{\theta}, \gamma_{td}^b, \gamma_{td}^f)$ as (0 deg, 10 deg/s, 12 deg, 11 deg) for $y = 0.35$ m and $\dot{x} = 1$ m/s, then we arrive at (0 deg, 8.96 deg/s, 12.57 deg, 11.1 deg) after convergence. For what values of $(\gamma_{td}^b, \gamma_{td}^f)$ we get the pitch angular velocity of 10 deg/s is difficult to find using this method.

In the absence of asymmetry, we propose the following function to exactly determine the fixed

point corresponding to the given height, forward velocity, pitch, and pitch angular velocity at apex:

$$f_s(\gamma_{td}^b, \gamma_{td}^f; y_i, \theta_i, \dot{x}_i, \dot{\theta}_i) = \begin{Bmatrix} (y_i - y)^2 + (\theta_i - \theta)^2 \\ (\dot{x}_i - \dot{x})^2 + (\dot{\theta}_i - \dot{\theta})^2 \end{Bmatrix} \tag{6.9}$$

where y_i, θ_i, $\dot{x}_i$, and $\dot{\theta}_i$ are the initial values at the beginning of gait cycle, and y, θ, $\dot{x}$, and $\dot{\theta}$ are the values at the end of the gait cycle and are each functions of all input arguments of f_s. Here, θ_i should always be taken as zero since it is a property of fixed points when there is no asymmetry. The choice of number of elements in the vector function f_s is not arbitrary. Since, we have only two unknowns γ_{td}^b and γ_{td}^f, Newton-Raphson method requires a two element function that yields 2×2 numerical Jacobian matrix needed to find the next estimate of γ_{td}^b and γ_{td}^f. Further, the choice of elements in f_s is also not unique. Our only requirement is that the elements are functions of unknowns, and they become zero at the fixed point. Using this method, with (0 deg, 10 deg/s, 12 deg, 11 deg) as initial condition for $y = 0.35$ m and $\dot{x} = 1$ m/s, we arrive at (0 deg, 10 deg/s, 12.65 deg, 11.01 deg) as the fixed point. Now these values of touchdown angles and the value of $\theta = 0$ deg can be used as initial guess when a small asymmetry is introduced either in mass or stiffness at $y = 0.35$ m, $\dot{x} = 1$ m/s, and $\dot{\theta} = 10$ deg/s.

When mass or stiffness asymmetry is present, we propose the following function to exactly determine the touchdown angles and the pitch angle at apex corresponding to the given height, forward velocity, and pitch angular velocity at apex:

$$f_{as}(\theta_i, \gamma_{td}^b, \gamma_{td}^f; y_i, \dot{x}_i, \dot{\theta}_i) = \begin{Bmatrix} (y_i - y)^2 \\ (\theta_i - \theta)^2 + (\dot{\theta}_i - \dot{\theta})^2 \\ (\dot{x}_i - \dot{x})^2 \end{Bmatrix} \tag{6.10}$$

For the given parameter values of y_i, $\dot{x}_i$, and $\dot{\theta}_i$, we wish to find θ_i, γ_{td}^b, and γ_{td}^f that make f_{as} zero. The reason for using a vector function f_{as} with three elements is the number of unknowns we wish to find using Newton-Raphson method. The values of θ_i, γ_{td}^b, and γ_{td}^f are used as initial guess when asymmetry in either mass or stiffness is incrementally increased further. We could use the function f_{as} even when no asymmetry is present, in which case we get $\theta_i = 0$ in the solution. However, using f_s is computationally more efficient when asymmetry is absent.

6.4 Results and Discussion

The effects of mass and stiffness asymmetries are studied independently of one another in the following subsections.

6.4.1 Effect of Mass Asymmetry

Effect of mass asymmetry on the maximum eigenvalue norm for fixed points with apex height of 0.35 m for various forward speeds is shown as a function of apex pitch angular velocity in Fig. 6.2. Maximum eigenvalue of less than one is stable. Above one, higher the value higher is the degree of instability. As magnitude of offset of center of mass from geometric center is increased, the number of fixed points decreases in all these cases. Even unstable fixed points do not exist at higher pitch angular velocity. With the increase in forward velocity, there is an increase in the number of fixed

points as the magnitude of offset is increased.
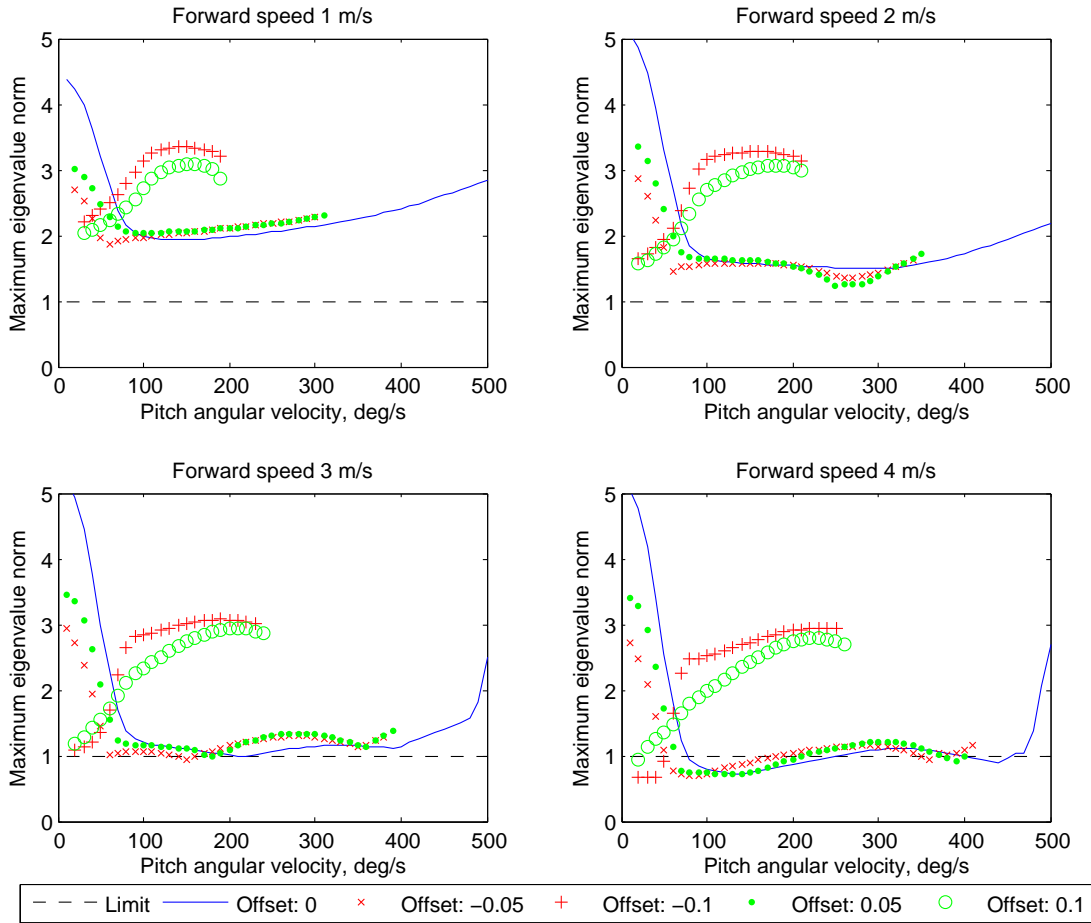
Figure 6.2: Effect of mass asymmetry on stability

Stability at very low pitch angular velocities (of about 50 deg/s) increases with the increase in the center of mass offset. This property is reversed as the pitch angular velocity is increased. At higher forward speeds, stability is further improved at lower pitch angular velocities. For forward speed of 4 m/s, some fixed points corresponding to 0.1 m offset enter into stable region at low pitch angular velocities. It can be said that, in general, mass asymmetry improves stability at low pitch angular velocities and higher forward velocities. At lower forward velocities, asymmetry does not help significantly in improving stability. Zou and Schmiedeler [168] report that, for quadruped bounding in place (zero forward velocity), asymmetry is detrimental to stability.

In order to see how much the touchdown angle - liftoff angle symmetry condition is violated as a result of introducing mass asymmetry, Fig. 6.3 is plotted with the sum of touchdown angle and liftoff angle. Ideally, when there is no mass or stiffness asymmetry, the values should be zero. This condition is shown as blue lines in Fig. 6.3. Violation is higher for larger offsets and they appear to be symmetric about the zero line.
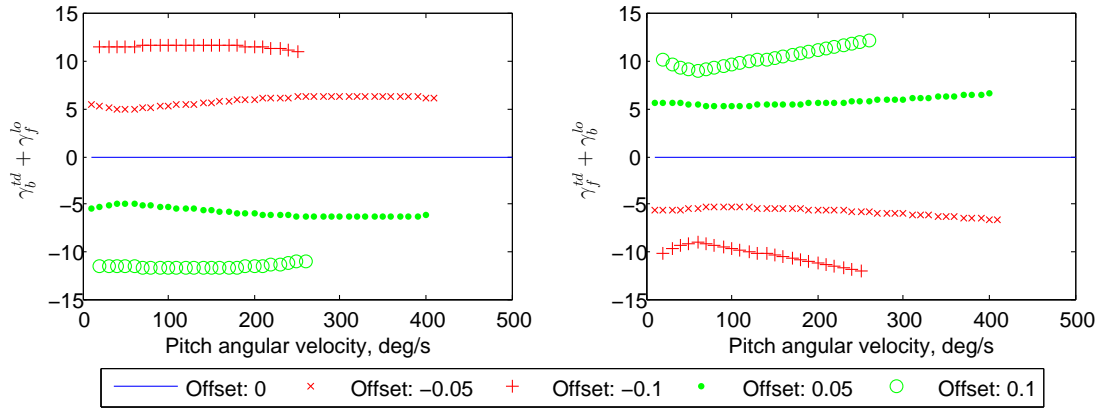
Figure 6.3: Effect of mass asymmetry on symmetry condition

6.4.2 Effect of Stiffness Asymmetry

The effect of stiffness asymmetry on the maximum eigenvalue norm for fixed points with apex height of 0.35 m for various forward speeds is shown as a function of apex pitch angular velocity in Fig. 6.4. The effect of negative offset (decreasing the back leg spring stiffness and increasing front leg spring stiffness) is marginally improved stability at lower pitch angular velocities. Increasing the offset has the opposite effect. For certain range of pitch angular velocities, fixed points do not exist at lower forward velocities and positive offsets. In general, results do not seem to favor the use of stiffness asymmetry for improving stability and positive offsets are detrimental to the existence of fixed points. Negative offsets at low pitch angular velocities are preferred if stiffness asymmetry is desired.

Violation of touchdown angle - liftoff angle symmetry condition with respect to pitch angular velocity in the presence of stiffness asymmetry is shown in Fig. 6.5. Here too, symmetry of violation about zero line can be observed. Violation is higher for larger asymmetry of stiffness.

It should be noted that the magnitude of stiffness offset required for a noticeable change in stability properties is large. The lowest offset of $\pm$ 1500 N/m is about 20 percent of the original leg stiffness.

6.5 Conclusions

Using the methods introduced in this chapter, fixed points were found in the presence of mass and stiffness asymmetry for various forward speeds and pitch angular velocities. Mass asymmetry improves stability at very low pitch angular velocities. This improvement is further enhanced as the forward speed is increased. Stiffness asymmetry improves stability for negative offsets and low pitch angular velocities. Positive offsets in the presence of stiffness asymmetry are detrimental to the existence of fixed points. With either of the mass or stiffness asymmetries, violation of touchdown-liftoff angle symmetry condition occurs and is increased with the asymmetry. As a result of this violation, control laws based on symmetry condition can become unstable in the presence of mass or stiffness asymmetry.
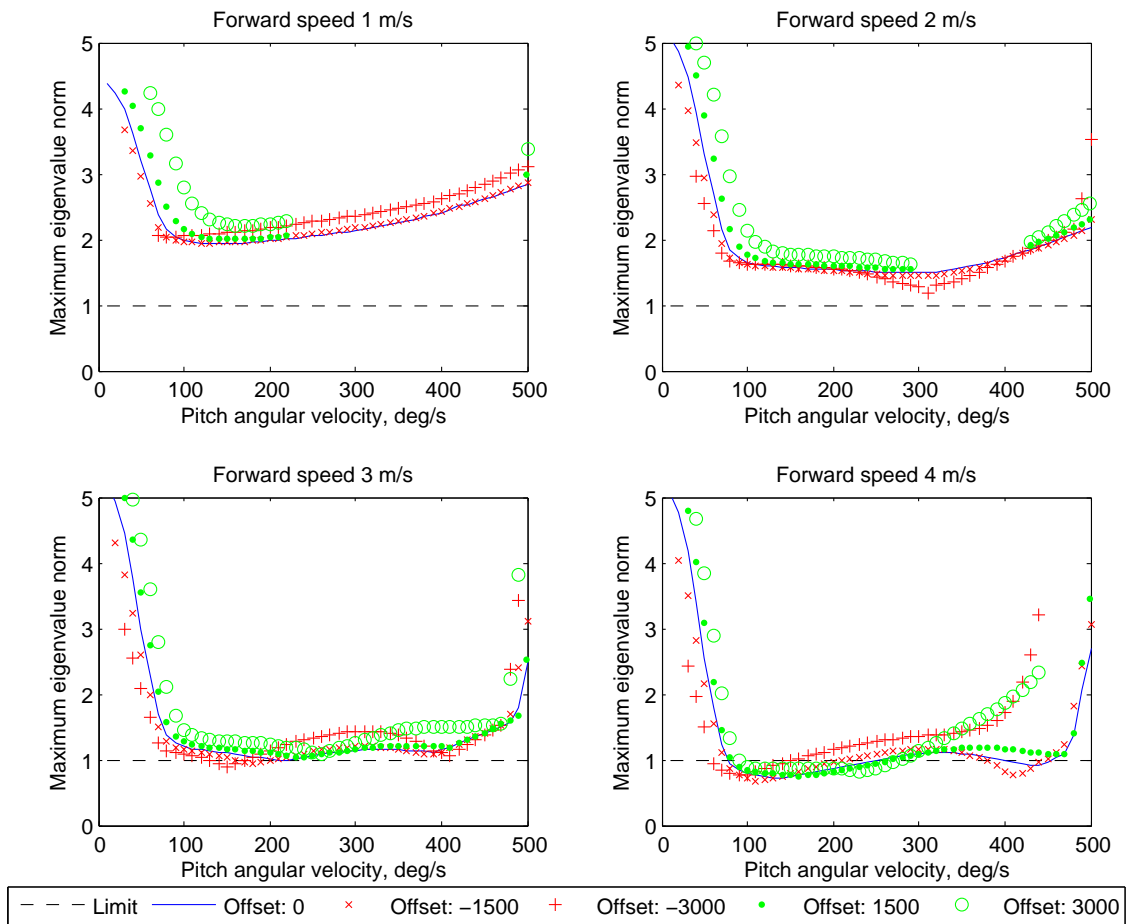
Figure 6.4: Effect of stiffness asymmetry on stability
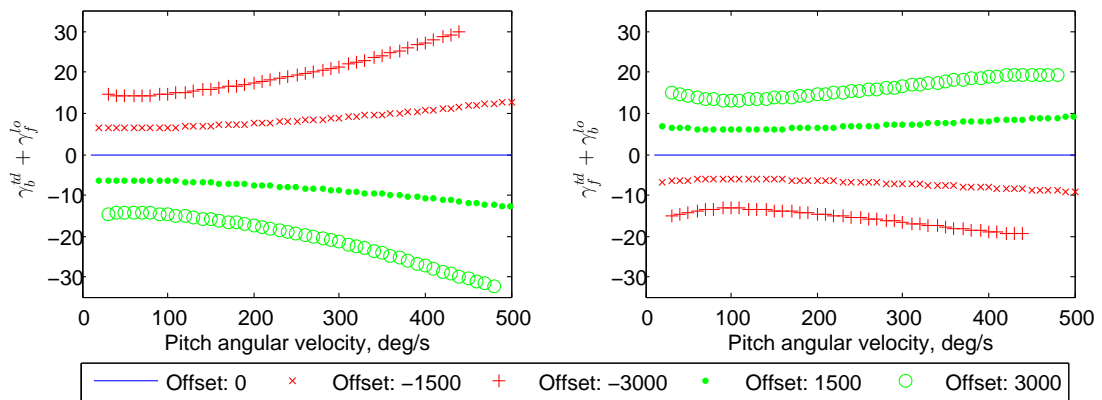
Figure 6.5: Effect of stiffness asymmetry on symmetry condition

Chapter 7

Conclusions and Recommendations for Future Work

7.1 Conclusions

- Constant height level trotting is not possible at a constant speed because of stability requirements. However, it is possible with acceleration and deceleration. A minimum norm solution gives knee actuator force when there is no mass asymmetry.

- In bounding gait (without double support phase), as the only point of contact at any point of time could be either the front leg pair or the back leg pair, only accelerating or decelerating gaits are possible due to unbalanced horizontal components of forces from the legs.

- Quadruped robot with a articulated torso has advantages such as higher possible speed, greater stride length, larger foot clearance and hopping height.

- Symmetry condition observed in passive dynamic bounding can itself be used as a control law for improving stability region. By adding feedback of pitch angle at apex, stability region can be further improved.

- Control law based on touchdown angle - liftoff angle symmetry condition can be implemented with minimal actuation using physical cross coupling between front and back legs. Such a configuration gives inherent stability with all the advantages of body-fixed touchdown angles. However, it is stable only at low forward speeds.

- The introduction of asymmetry in either mass distribution in the body or stiffness of front and back legs leads of violation of touchdown angle - liftoff angle symmetry condition observed in quadrupeds with mass and stiffness symmetry. Further, the pitch angle at the apex event can be nonzero. Control laws based on symmetry condition may fail when mass or stiffness asymmetry is present.

- The cost of transport expressions derived in Chapters 2 and 3 help us identify which of the gait and quadruped body parameters influence the energy efficiency. Hence these parameters may be appropriately chosen when designing a quadruped robot for high energy efficiency.

7.2 Recommendations for Future Work

- In this thesis, only quadruped robots with prismatic legs have been considered for deriving Cost of Transport expressions. Extension of this work to revolute knee jointed legs may not be feasible due to commplex expressions. However, numerical studies can be performed to compare the results with prismatic knee jointed legs.

- Symmetry control implemented with physical cross coupling improves stability to some extent. Control laws which can provide higher stability region, such as the feedback of pitch angle at apex discussed in chapter 5, need to be explored further.

- At present, there are no control laws for passive dynamic bounding with asymmetry. Rule based touchdown angle control can be a direction in which to explore for stabilizing control laws.

References

[1] P. G. de Santos, E. Garcia, and J. Estremera. Quadrupedal locomotion: an introduction to the control of four-legged robots. Springer, 2007.

[2] R. Siegwart, I. R. Nourbakhsh, and D. Scaramuzza. Introduction to autonomous mobile robots. MIT Press, 2011.

[3] M. H. Raibert. Legged robots that balance. MIT Press, 1986.

[4] J. Heaston, D. Hong, I. Morazzani, P. Ren, and G. Goldman. STriDER: Self-excited tripedal dynamic experimental robot. In IEEE International Conference on Robotics and Automation. IEEE, 2007 2776–2777.

[5] D. J. Todd. Walking machines: an introduction to legged robots. Chapman & Hall, 1985.

[6] Y. Ishino, T. Naruse, T. Sawano, and N. Honma. Walking robot for underwater construction. In Proceedings of International Conference on Advanced Robot. 1983 107–114.

[7] H. Lipson, J. C. Bongard, V. Zykov, and E. Malone. Evolutionary Robotics for Legged Machines: From Simulation to Physical Reality. In IAS. 2006 11–18.

[8] M. H. Raibert. Trotting, pacing and bounding by a quadruped robot. *Journal of Biomechanics* 23, (1990) 79–98.

[9] P. M. Krishna, R. P. Kumar, and S. Srivastava. Energetics of level walking trot gaits in quadruped robots. In IEEE International Conference on Robotics and Biomimetics (ROBIO). IEEE, 2012 61–65.

[10] M. Raibert, K. Blankespoor, G. Nelson, R. Playter, and the BigDog Team. Bigdog, the rough-terrain quadruped robot. In Proceedings of the 17th World Congress. 2008 10,823–10,825.

[11] S. Song and K. J. Waldron. Machines that walk: the adaptive suspension vehicle. MIT Press, 1989.

[12] R. Kurazume, A. Byong-won, K. Ohta, and T. Hasegawa. Experimental study on energy efficiency for quadruped walking vehicles. In IEEE/RSJ International Conference on Intelligent Robots and Systems (IROS 2003), volume 1. IEEE, 2003 613–618.

[13] I. I. Artobolevskiĭ. Mechanisms for the generation of plane curves. Pergamon, 1964.

[14] J. E. Shigley. The mechanics of walking vehicles. Technical Report, DTIC Document 1960.

[15] R. B. McGhee and A. A. Frank. On the stability properties of quadruped creeping gaits. *Mathematical Biosciences* 3, (1968) 331–351.

[16] H. Kimura, I. Shimoyama, and H. Miura. Dynamics in the dynamic walk of a quadruped robot. *Advanced Robotics* 4, (1989) 283–301.

[17] K. Berns. The walking machine catalogue. *http://www.fzi.de/divisions/ipt/WMC/preface/preface.html* .

[18] K. Kato and S. Hirose. Development of the quadruped walking robot, TITAN–IX–mechanical design concept and application for the humanitarian de-mining robot. *Advanced Robotics* 15, (2001) 191–204.

[19] K. Yoneda and S. Hirose. Dynamic and static fusion gait of a quadruped walking vehicle on a winding path. *Advanced Robotics* 9, (1994) 125–136.

[20] S. Hirose and K. Kato. Study on quadruped walking robot in Tokyo Institute of Technology-past, present and future. In IEEE International Conference on Robotics and Automation,ICRA, volume 1. IEEE, 2000 414–419.

[21] H. Komatsu, G. Endo, R. Hodoshima, S. Hirose, and E. F. Fukushima. Basic consideration about optimal control of a quadruped walking robot during slope walking motion. In IEEE Workshop on Advanced Robotics and its Social Impacts (ARSO). IEEE, 2013 224–230.

[22] S. Kitano, S. Hirose, G. Endo, and E. F. Fukushima. Development of lightweight sprawling-type quadruped robot TITAN-XIII and its dynamic walking. In IEEE/RSJ International Conference on Intelligent Robots and Systems (IROS). IEEE, 2013 6025–6030.

[23] P. G. De Santos, J. A. Galvez, J. Estremera, and E. Garcia. SIL04: a true walking robot for the comparative study of walking machine techniques. *Robotics and Automation Magazine, IEEE* 10, (2003) 23–32.

[24] P. Gonzalez de Santos, J. A. Cobano, E. Garcia, J. Estremera, and M. Armada. A six-legged robot-based system for humanitarian demining missions. *Mechatronics* 17, (2007) 417–430.

[25] Y. Li, B. Li, J. Ruan, and X. Rong. Research of mammal bionic quadruped robots: a review. In IEEE Conference on Robotics, Automation and Mechatronics (RAM). IEEE, 2011 166–171.

[26] K. Berns, W. Ilg, M. Deck, J. Albiez, and R. Dillmann. Mechanical construction and computer architecture of the four-legged walking machine BISAM. *IEEE/ASME Transactions on Mechatronics* 4, (1999) 32–38.

[27] H. Kimura, Y. Fukuoka, and A. H. Cohen. Adaptive dynamic walking of a quadruped robot on natural ground based on biological concepts. *The International Journal of Robotics Research* 26, (2007) 475–490.

[28] C. Maufroy, H. Kimura, and K. Takase. Integration of posture and rhythmic motion controls in quadrupedal dynamic walking using phase modulations based on leg loading/unloading. *Autonomous Robots* 28, (2010) 331–353.

[29] M. Krishna. Implementation of CPG based locomotion controller on Minimule Robot. *International Journal of Robotics and Mechatronics* 1, (2014) 37–43.

[30] I. Poulakakis, J. A. Smith, and M. Buehler. Modeling and experiments of untethered quadrupedal running with a bounding gait: The Scout II robot. *The International Journal of Robotics Research* 24, (2005) 239–256.

[31] J. Ingvast, C. Ridderström, and J. Wikander. The four legged robot system WARP1 and its capabilities. In Second Swedish Workshop on Autonomous Systems. 2002 .

[32] J. G. Nichol, S. P. Singh, K. J. Waldron, L. R. Palmer, and D. E. Orin. System design of a quadrupedal galloping machine. *The International Journal of Robotics Research* 23, (2004) 1013–1027.

[33] H. Kim, D. Won, O. Kwon, T.-J. Kim, S.-S. Kim, and S. Park. Foot trajectory generation of hydraulic quadruped robots on uneven terrain. In 17th World Congress on the International Federation of Automatic Control. 2008 3021–3026.

[34] T. J. Kim, B. So, O. Kwon, and S. Park. The energy minimization algorithm using foot rotation for hydraulic actuated quadruped walking robot with redundancy. In International Symposium on Robotics (ISR), and 6th German Conference on Robotics (ROBOTIK). VDE, 2010 1–6.

[35] C. Semini. HyQ–Design and development of a hydraulically actuated quadruped robot. *PhD Thesis, University of Genoa, Italy* .

[36] T. Boaventura, G. A. Medrano-Cerda, C. Semini, J. Buchli, and D. G. Caldwell. Stability and performance of the compliance controller of the quadruped robot hyq. In IEEE/RSJ International Conference on Intelligent Robots and Systems (IROS). IEEE, 2013 1458–1464.

[37] I. Havoutis, J. Ortiz, S. Bazeille, V. Barasuol, C. Semini, and D. G. Caldwell. Onboard perception-based trotting and crawling with the hydraulic quadruped robot (hyq). In IEEE/RSJ International Conference on Intelligent Robots and Systems (IROS). IEEE, 2013 6052–6057.

[38] K. Wait and M. Goldfarb. A Pneumatically Actuated Quadrupedal Walking Robot. *IEEE/ASME Transactions on Mechatronics* 19, (2014) 339–347.

[39] X. Wu, X. Shao, and W. Wang. Gait planning of crossing planar obstacles for a quadruped robot. In IEEE International Conference on Robotics and Biomimetics (ROBIO). IEEE, 2013 692–697.

[40] R. Playter, M. Buehler, and M. Raibert. BigDog. In Defense and Security Symposium. International Society for Optics and Photonics, 2006 62,302O–62,302O.

[41] J. Cho, J. T. Kim, S. Park, Y. Lee, and K. Kim. JINPOONG, posture control for the external force. In International Symposium on Robotics (ISR). 2013 1–2.

[42] M. Raibert. Dynamic legged robots for rough terrain. In IEEE International Conference on Humanoid Robots (Humanoids). IEEE, 2010 1–1.

[43] S. Seok, A. Wang, M. Y. Chuah, D. Otten, J. Lang, and S. Kim. Design principles for highly efficient quadrupeds and implementation on the mit cheetah robot. In IEEE International Conference on Robotics and Automation (ICRA). IEEE, 2013 3307–3312.

[44] M. Fujita. On activating human communications with pet-type robot AIBO. *Proceedings of the IEEE* 92, (2004) 1804–1813.

[45] T. Ishida. Development of a small biped entertainment robot QRIO. In International Symposium on Micro-Nanomechatronics and Human Science. IEEE, 2004 23–28.

[46] D. Gouaillier, V. Hugel, P. Blazevic, C. Kilner, J. Monceaux, P. Lafourcade, B. Marnier, J. Serre, and B. Maisonnier. Mechatronic design of NAO humanoid. In IEEE International Conference on Robotics and Automation,(ICRA). IEEE, 2009 769–774.

[47] D. F. Hoyt and C. R. Taylor. Gait and the energetics of locomotion in horses. *Journal of Nature* 292, (1981) 239–249.

[48] R. Alexander, A. Jayes, and R. Ker. Estimates of energy cost for quadrupedal running gaits. *Journal of Zoology* 190, (1980) 155–192.

[49] R. M. Alexander. The gaits of bipedal and quadrupedal animals. *The International Journal of Robotics Research* 3, (1984) 49–59.

[50] R. Alexander. Optimization and gaits in the locomotion of vertebrates. *Physiological Reviews* 69, (1989) 1199–1227.

[51] R. M. Alexander. Three uses for springs in legged locomotion. *The International Journal of Robotics Research* 9, (1990) 53–61.

[52] R. M. Alexander. Mechanics of animal movement. *Current Biology* 15, (2005) R616–R619.

[53] P. Nanua and K. Waldron. Energy comparison between trot, bound, and gallop using a simple model. *Journal of Biomechanical Engineering* 117, (1995) 466–473.

[54] R. M. Alexander. Principles of animal locomotion. Princeton University Press, 2003.

[55] R. Alexander, N. J. Dimery, and R. Ker. Elastic structures in the back and their role in galloping in some mammals. *Journal of Zoology* 207, (1985) 467–482.

[56] J. Albiez and K. Berns. Biological Inspired Walking—How Much Nature Do We Need? In Climbing and Walking Robots, 357–364. Springer, 2005.

[57] T. J. Allen, R. D. Quinn, R. J. Bachmann, and R. E. Ritzmann. Abstracted biological principles applied with reduced actuation improve mobility of legged vehicles. In IEEE/RSJ International Conference on Intelligent Robots and Systems,(IROS 2003), volume 2. IEEE, 2003 1370–1375.

[58] B. Hennion, J. Pill, and J.-C. Guinot. A biologically inspired model for quadruped locomotion. In Climbing and Walking Robots, 49–56. Springer, 2006.

[59] H. Kimura, Y. Fukuoka, and A. H. Cohen. Biologically inspired adaptive walking of a quadruped robot. *Philosophical Transactions of the Royal Society A: Mathematical, Physical and Engineering Sciences* 365, (2007) 153–170.

[60] U. Scarfogliero, C. Stefanini, and P. Dario. A bioinspired concept for high efficiency locomotion in micro robots: the jumping robot grillo. In IEEE International Conference on Robotics and Automation,ICRA. IEEE, 2006 4037–4042.

[61] C. P. Santos and V. Matos. Gait transition and modulation in a quadruped robot: A brainstem-like modulation approach. *Robotics and Autonomous Systems* 59, (2011) 620–634.

[62] M. Khoramshahi, H. Jalaly Bidgoly, S. Shafiee, A. Asaei, A. J. Ijspeert, and M. Nili Ahmadabadi. Piecewise linear spine for speed–energy efficiency trade-off in quadruped robots. *Robotics and Autonomous Systems* 61, (2013) 1350–1359.

[63] J. Kim and J. Lee. Adaptation of quadruped gaits using surface classification and gait optimization. In IEEE/RSJ International Conference on Intelligent Robots and Systems (IROS). IEEE, 2013 716–721.

[64] S. H. Park and D. P. Hong. Optimal Bio-Inspired Structure of a Quadruped by the Method of Energy Efficiency. In International Symposium on Robotics (ISR). IEEE, 2013 1–4.

[65] I. Shmue and R. Riemer. Energetically Optimal Gait Transition Velocities of a Quadruped Robot. In IEEE International Conference on Systems, Man, and Cybernetics (SMC). IEEE, 2013 2747–2752.

[66] Z. Wang, E. Dong, H. Wang, C. Liu, G. Ma, M. Xu, and J. Yang. Design and experimental study of a compliant feet quadruped robot with closed-chain mechanism legs. In IEEE International Conference on Robotics and Biomimetics (ROBIO). IEEE, 2013 722–727.

[67] G. Gabrielli and T. Von. What price speed?: specific power required for propulsion of vehicles. 1950.

[68] J. Yong, R. Smith, L. Hatano, and S. Hillmansen. What price speed-revisited. *Ingenia* 22, (2005) 46–51.

[69] S. Song, V. Vohnout, K. Waldron, and G. Kinzel. Computer-aided design of a leg for an energy efficient walking machine. *Mechanism and Machine Theory* 19, (1984) 17–24.

[70] S. Chen, X. Chen, Z. Liu, and X. Luo. Design and analysis of a bionic quadruped robot. In IEEE International Conference on Robotics and Biomimetics (ROBIO). IEEE, 2013 824–829.

[71] J. D. Ortega and C. T. Farley. Minimizing center of mass vertical movement increases metabolic cost in walking. *Journal of Applied Physiology* 99, (2005) 2099–2107.

[72] M. W. Hannan and I. D. Walker. Analysis and initial experiments for a novel elephant's trunk robot. In IEEE/RSJ International Conference on Intelligent Robots and Systems,(IROS 2000), volume 1. IEEE, 2000 330–337.

[73] M. Alamir, M. El Rafei, G. Hafidi, N. Marchand, M. Porez, and F. Boyer. Feedback design for 3d movement of an eel-like robot. In IEEE International Conference on Robotics and Automation. IEEE, 2007 256–261.

[74] C. Wright, A. Johnson, A. Peck, Z. McCord, A. Naaktgeboren, P. Gianfortoni, M. Gonzalez-Rivero, R. Hatton, and H. Choset. Design of a modular snake robot. In IEEE/RSJ International Conference on Intelligent Robots and Systems, (IROS). IEEE, 2007 2609–2614.

[75] J. Borenstein, M. Hansen, and A. Borrell. The OmniTread OT-4 serpentine robot - design and performance. *Journal of Field Robotics* 24, (2007) 601–621.

[76] B. M. Haueisen. Investigation of an Articulated Spine in a Quadruped Robotic System. Ph.D. thesis, The University of Michigan 2011.

[77] X. Wei, Y. Long, C. Wang, and S. Wang. Rotary galloping with a lock–unlock elastic spinal joint. *Proceedings of the Institution of Mechanical Engineers, Part C: Journal of Mechanical Engineering Science* 40–62.

[78] F. Iida, R. Dravid, and C. Paul. Design and control of a pendulum driven hopping robot. In Intelligent Robots and Systems, 2002. IEEE/RSJ International Conference on, volume 3. IEEE, 2002 2141–2146.

[79] S. Gracovetsky. The spinal engine. Springer-Verlag Wien-NY, 1988.

[80] Q. Zhao, K. Nakajima, H. Sumioka, H. Hauser, and R. Pfeifer. Spine dynamics as a computational resource in spine-driven quadruped locomotion. In IEEE/RSJ International Conference on Intelligent Robots and Systems (IROS). IEEE, 2013 1445–1451.

[81] A. Rosendo, S. Nakatsu, K. Narioka, and K. Hosoda. Pneupard: A biomimetic musculoskeletal approach for a feline-inspired quadruped robot. In IEEE/RSJ International Conference on Intelligent Robots and Systems, (IROS). IEEE, 2013 1452–1457.

[82] S. Nakatsu, A. Rosendo, K. Narioka, and K. Hosoda. Stable reflex-based walking of forelimbs of a bio-inspired quadruped robot-modeled cheetah. In IEEE International Conference on Robotics and Biomimetics, (ROBIO). IEEE, 2013 1813–1818.

[83] X. Zhang, H. Yu, B. Liu, and X. Gu. A bio-inspired quadruped robot with a global compliant spine. In IEEE International Conference on Robotics and Biomimetics (ROBIO),. IEEE, 2013 1312–1316.

[84] Q. Zhao, B. Ellenberger, H. Sumioka, T. Sandy, and R. Pfeifer. The effect of spine actuation and stiffness on a pneumatically-driven quadruped robot for cheetah-like locomotion. In IEEE International Conference on Robotics and Biomimetics, (ROBIO). IEEE, 2013 1807–1812.

[85] A. Paolone de Medeiros, J. Lopes dos Santos, N. Junior, and C. Lucio. Steering a quadruped robot: Simulation and experimental results. In 8th Annual IEEE on Systems Conference, (SysCon). IEEE, 2014 460–464.

[86] K. Berns, W. Ilg, M. Deck, and R. Dillmann. The mammalian-like quadrupedal walking machine BISAM. In International Workshop on Advanced Motion Control. IEEE, 1998 429–433.

[87] J. Albiez, T. Luksch, K. Berns, and R. Dillmann. An activation-based behavior control architecture for walking machines. *The International Journal of Robotics Research* 22, (2003) 203–211.

[88] K. Kim, S. Park, and Y. Lee. Development of biomimetic quadruped walking robot with 2-dof waist joint. In Control Systems and Robotics. International Society for Optics and Photonics, 2005 60,423H–60,423H.

[89] S. Park and Y. Lee. Discontinuous zigzag gait planning of a quadruped walking robot with a waist-joint. *Advanced Robotics* 21, (2007) 143–164.

[90] Q. Cao and I. Poulakakis. Quadrupedal bounding with a segmented flexible torso: passive stability and feedback control. *Bioinspiration and Biomimetics* 8, (2013) 046,007.

[91] Q. Cao and I. Poulakakis. On the Energetics of Quadrupedal Bounding With and Without Torso Compliance. In IEEE/RSJ International Conference on Intelligent Robots and Systems (IROS),. IEEE, 2014 .

[92] Q. Cao and I. Poulakakis. Passive stability and control of quadrupedal bounding with a flexible torso. In IEEE/RSJ International Conference on Intelligent Robots and Systems (IROS),. IEEE, 2013 6037–6043.

[93] Q. Cao and I. Poulakakis. Passive quadrupedal bounding with a segmented flexible torso. In IEEE/RSJ International Conference on Intelligent Robots and Systems (IROS),. IEEE, 2012 2484–2489.

[94] U. Culha and U. Saranli. Quadrupedal bounding with an actuated spinal joint. In IEEE International Conference on Robotics and Automation, (ICRA). IEEE, 2011 1392–1397.

[95] S. Pouya, M. Khodabakhsh, R. Moeckel, and A. Ijspeert. Role of spine compliance and actuation in the bounding performance of quadruped robots. In Dynamic Walking Conference, USA,(May 2012). 2012 .

[96] Q. Deng, S. Wang, W. Xu, J. Mo, and Q. Liang. Quasi passive bounding of a quadruped model with articulated spine. *Mechanism and Machine Theory* 52, (2012) 232–242.

[97] G. C. Haynes, J. Pusey, R. Knopf, and D. E. Koditschek. Dynamic bounding with a passive compliant spine. In Proceedings of Dynamic Walking Conference. 2012 .

[98] B. Satzinger and K. Byl. Control of planar bounding quadruped with passive flexible spine. In International Symposium of Adaptive Motion in Animals and Machines. 2013 129–30.

[99] K. Jeong, I. Cho, and Y. Lee. Development of autonomous eating mechanism for biomimetic robots. In ICMIT 2005: Control Systems and Robotics. International Society for Optics and Photonics, 2005 60,423G–60,423G.

[100] T. Matsuki, I. Mizuuchi, S. Kagami, M. Inaba, and H. Inoue. Motion generation and action control of a walking quadruped robot with flexible spine structure. In Proceedings of 1999 JSME Conference on Robotics and Mechatronics (ROBOMEC99), volume 2. 1999 .

[101] T. Matsuki, I. Mizuuchi, S. Kagami et al. Quadruped robot with spine structure and simulation environment. In Proceedings of the 16th Annual Conference of the Robotics Society of Japan,. 1998 18–20.

[102] I. Mizuuchi, M. Inaba, and H. Inoue. A flexible spine human-form robot-development and control of the posture of the spine. In IEEE/RSJ International Conference on Intelligent Robots and Systems,, volume 4. IEEE, 2001 2099–2104.

[103] I. Mizuuchi, R. Tajima, T. Yoshikai, D. Sato, K. Nagashima, M. Inaba, Y. Kuniyoshi, and H. Inoue. The design and control of the flexible spine of a fully tendon-driven humanoid" Kenta". In IEEE/RSJ International Conference on Intelligent Robots and Systems, volume 3. IEEE, 2002 2527–2532.

[104] I. Mizuuchi, S. Yoshida, M. Inaba, and H. Inoue. The development and control of a flexible-spine for a human-form robot. *Advanced Robotics* 17, (2003) 179–196.

[105] I. Mizuuchi, T. Yoshikai, Y. Nakanishi, and M. Inaba. A reinforceable-muscle flexible-spine humanoid" Kenji". In IEEE/RSJ International Conference on Intelligent Robots and Systems,(IROS). IEEE, 2005 4143–4148.

[106] I. Mizuuci, T. Matsuki, M. Inaba, and H. Inoue. GA-Based motion generation for quadruped robot which has soft spine structure. In Proc. 17th Annu. Conf. of the Robotics Society of Japan. 1999 199–200.

[107] M. A. Lewis. Self-organization of locomotory controllers in robots and animals. Ph.D. thesis, University of Southern California 1996.

[108] K. F. Leeser. Locomotion experiments on a planar quadruped robot with articulated spine. Ph.D. thesis, Massachusetts Institute of Technology 1996.

[109] J. M. Morrey, B. Lambrecht, A. D. Horchler, R. E. Ritzmann, and R. D. Quinn. Highly mobile and robust small quadruped robots. In IEEE/RSJ International Conference on Intelligent Robots and Systems, (IROS), volume 1. IEEE, 2003 82–87.

[110] R. Breithaupt, J. Dahnke, K. Zahedi, J. Hertzberg, and F. Pasemann. Robo-Salamander an approach for the benefit of both robotics and biology. In International Conference on Climbing and Walking Robots, (CLAWAR). 2002 55–62.

[111] A. J. Ijspeert, A. Crespi, D. Ryczko, and J.-M. Cabelguen. From swimming to walking with a salamander robot driven by a spinal cord model. *Science* 315, (2007) 1416–1420.

[112] E. Pennisi. Robot Suggests How the First Land Animals Got Walking. *Science* 315, (2007) 1352–1353.

[113] I. Poulakakis. On the passive dynamics of quadrupedal running. Ph.D. thesis, McGill University 2002.

[114] P. Chatzakos and E. Papadopoulos. A parametric study on the passive dynamics of straight-ahead level-ground quadrupedal running. In International Conference on Advanced Robotics,(ICAR). IEEE, 2009 1–6.

[115] T. McGeer. Passive dynamic walking. *The International Journal of Robotics Research* 9, (1990) 62–82.

[116] M. Garcia, A. Chatterjee, A. Ruina, and M. Coleman. The simplest walking model: stability, complexity, and scaling. *Journal of Biomechanical Engineering* 120, (1998) 281–288.

[117] A. C. Smith and M. D. Berkemeier. Passive dynamic quadrupedal walking. In IEEE International Conference on Robotics and Automation, volume 1. IEEE, 1997 34–39.

[118] R. Blickhan. The spring-mass model for running and hopping. *Journal of Biomechanics* 22, (1989) 1217–1227.

[119] R. Blickhan and R. Full. Similarity in multilegged locomotion: bouncing like a monopode. *Journal of Comparative Physiology A* 173, (1993) 509–517.

[120] R. J. Full, C. T. Farley, and J. M. Winters. Musculoskeletal dynamics in rhythmic systems: a comparative approach to legged locomotion. In Biomechanics and neural control of posture and movement, 192–205. Springer, 2000.

[121] T. A. McMahon and G. C. Cheng. The mechanics of running: how does stiffness couple with speed? *Journal of Biomechanics* 23, (1990) 65–78.

[122] A. Seyfarth, H. Geyer, M. Günther, and R. Blickhan. A movement criterion for running. *Journal of Biomechanics* 35, (2002) 649–655.

[123] W. J. Schwind and D. E. Koditschek. Approximating the stance map of a 2-DOF monoped runner. *Journal of Nonlinear Science* 10, (2000) 533–568.

[124] J. Schmitt and P. Holmes. Mechanical models for insect locomotion: dynamics and stability in the horizontal plane I. Theory. *Biological Cybernetics* 83, (2000) 501–515.

[125] T. Kubow and R. Full. The role of the mechanical system in control: a hypothesis of self–stabilization in hexapedal runners. *Philosophical Transactions of the Royal Society of London. Series B: Biological Sciences* 354, (1999) 849–861.

[126] R. Ghigliazza, R. Altendorfer, P. Holmes, and D. Koditschek. Passively stable conservative locomotion. *Journal of Applied Dynamical Systems* .

[127] R. Altendorfer, N. Moore, H. Komsuoglu, M. Buehler, H. B. Brown Jr, D. McMordie, U. Saranli, R. Full, and D. E. Koditschek. RHex: a biologically inspired hexapod runner. *Autonomous Robots* 11, (2001) 207–213.

[128] K. Murphy and M. Raibert. Trotting and bounding in a planar two-legged model. In Theory and Practice of Robots and Manipulators, 411–420. Springer, 1985.

[129] M. D. Berkemeier. Modeling the dynamics of quadrupedal running. *The International Journal of Robotics Research* 17, (1998) 971–985.

[130] H. Brown Jr and M. Raibert. Legs that deform elastically. In Proceedings of RoManSy'86: Theory and Practice of Robots and Manipulators, 436–443. Springer, 1987.

[131] R. J. Full and D. E. Koditschek. Templates and anchors: neuromechanical hypotheses of legged locomotion on land. *Journal of Experimental Biology* 202, (1999) 3325–3332.

[132] R. Holmgren. A first course in discrete dynamical systems. Springer, 1996.

[133] I. Kuznetsov and Aleksandrovich. Elements of applied bifurcation theory, volume 112. Springer, 1998.

[134] J. Guckenheimer and P. Holmes. Nonlinear oscillations, dynamical systems, and bifurcations of vector fields, volume 42. Springer Science & Business Media, 1983.

[135] H. K. Khalil and J. Grizzle. Nonlinear systems, volume 3. Prentice hall Upper Saddle River, 2002.

[136] D. E. Koditschek and M. Bühler. Analysis of a simplified hopping robot. *The International Journal of Robotics Research* 10, (1991) 587–605.

[137] C. D. Remy, K. Buffinton, and R. Siegwart. A matlab framework for efficient gait creation. In IEEE/RSJ International Conference on Intelligent Robots and Systems (IROS). IEEE, 2011 190–196.

[138] C. D. Remy, K. W. Buffinton, and R. Siegwart. Stability analysis of passive dynamic walking of quadrupeds. *The International Journal of Robotics Research* .

[139] M. Hutter, C. D. Remy, M. A. Hoepflinger, and R. Siegwart. ScarlETH: Design and control of a planar running robot. In IEEE/RSJ International Conference on Intelligent Robots and Systems (IROS). IEEE, 2011 562–567.

[140] M. Hutter, C. Holenstein, D. Fenner, C. D. Remy, M. A. Hoepflinger, and R. Siegwart. Improved Efficiency in Legged Running Using Lightweight Passive Compliant Feet. In 15th International Conference on Climbing and Walking Robot-CLAWAR 2012, EPFL-CONF-181043. 2012 .

[141] M. Hutter, C. D. Remy, M. A. Hoepflinger, and R. Siegwart. Efficient and versatile locomotion with highly compliant legs. *IEEE/ASME Transactions on Mechatronics* 18, (2013) 449–458.

[142] A. Vakakis and J. Burdick. Chaotic motions in the dynamics of a hopping robot. In IEEE International Conference on Robotics and Automation. IEEE, 1990 1464–1469.

[143] J. P. Ostrowski and J. W. Burdick. Designing feedback algorithms for controlling the periodic motions of legged robots. In IEEE International Conference on Robotics and Automation. IEEE, 1993 260–266.

[144] W. J. Schwind and D. E. Koditschek. Control of forward velocity for a simplified planar hopping robot. In IEEE International Conference on Robotics and Automation, volume 1. IEEE, 1995 691–696.

[145] R. M Closkey, J. Burdick, and A. Vakakis. On the periodic motions of simple hopping robots. In IEEE International Conference on Systems, Man and Cybernetics. IEEE, 1990 771–777.

[146] Z. Li and J. He. An energy perturbation approach to limit cycle analysis in legged locomotion systems. In IEEE Conference on Decision and Control. IEEE, 1990 1989–1994.

[147] Z. Gan and C. D. Remy. A Passive Dynamic Quadruped that Moves in a Large Variety of Gaits. In IEEE/RSJ International Conference on Intelligent Robots and Systems (IROS). IEEE, 2014 .

[148] M. D. Berkemeier. A model for quadrupedal running-in-place in the plane. In IEEE Conference on Decision and Control, volume 3. IEEE, 1996 3581–3586.

[149] M. D. Berkemeier. Approximate return maps for quadrupedal running. In IEEE International Conference on Robotics and Automation, volume 1. IEEE, 1997 805–810.

[150] C. D. Remy, M. Hutter, and R. Siegwart. Passive dynamic walking with quadrupeds-extensions towards 3d. In IEEE International Conference on Robotics and Automation (ICRA). IEEE, 2010 5231–5236.

[151] C. D. Remy, M. Hutter, M. Hoepflinger, M. Bloesch, C. Gehring, and R. Siegwart. Quadrupedal robots with stiff and compliant actuation. *International Conference on CLimbing And WAlking Robots* 60, (2012) 682–691.

[152] C. D. Remy, K. Buffinton, and R. Siegwart. Energetics of passivity–based running with high–compliance series elastic actuation. *International Journal of Mechatronics and Manufacturing Systems* 5, (2012) 120–134.

[153] I. Poulakakis, E. Papadopoulos, and M. Buehler. On the stable passive dynamics of quadrupedal running. In IEEE International Conference on Robotics and Automation, volume 1. IEEE, 2003 1368–1373.

[154] I. Poulakakis, E. Papadopoulos, and M. Buehler. On the stability of the passive dynamics of quadrupedal running with a bounding gait. *The International Journal of Robotics Research* 25, (2006) 669–687.

[155] L. R. Palmer III and D. E. Orin. Control of a 3D quadruped trot. In Climbing and Walking Robots, 165–172. Springer, 2006.

[156] D. V. Lee, E. F. Stakebake, R. M. Walter, and D. R. Carrier. Effects of mass distribution on the mechanics of level trotting in dogs. *Journal of Experimental Biology* 207, (2004) 1715–1728.

[157] M. Srinivasan. Why walk and run: energetic costs and energetic optimality in simple mechanics-based models of a bipedal animal. Ph.D. thesis, Cornell University 2006.

[158] S. Collins, A. Ruina, R. Tedrake, and M. Wisse. Efficient bipedal robots based on passive-dynamic walkers. *Science* 307, (2005) 1082–1085.

[159] U. Mettin, P. X. La Hera, L. B. Freidovich, and A. S. Shiriaev. Parallel elastic actuators as control tool for preplanned trajectories of underactuated mechanical systems. *The International Journal of Robotics Research* 29, (2010) 1186–1198.

[160] D. Haeufle, M. Taylor, S. Schmitt, and H. Geyer. A clutched parallel elastic actuator concept: towards energy efficient powered legs in prosthetics and robotics. In IEEE International Conference on Biomedical Robotics and Biomechatronics (BioRob). IEEE, 2012 1614–1619.

[161] A. Jayes and R. Alexander. Mechanics of locomotion of dogs (Canis familiaris) and sheep (Ovis aries). *Journal of Zoology* 185, (1978) 289–308.

[162] A. Shkolnik, M. Levashov, I. R. Manchester, and R. Tedrake. Bounding on rough terrain with the LittleDog robot. *The International Journal of Robotics Research* 30, (2011) 192–215.

[163] H. Kazemi, V. J. Majd, and M. M. Moghaddam. Modeling and robust backstepping control of an underactuated quadruped robot in bounding motion. *Robotica* 31, (2013) 423–439.

[164] A. Minetti, L. Ardigo, E. Reinach, and F. Saibene. The relationship between mechanical work and energy expenditure of locomotion in horses. *The Journal of Experimental Biology* 202, (1999) 2329–2338.

[165] J. Estremera and K. J. Waldron. Thrust control, stabilization and energetics of a quadruped running robot. *The International Journal of Robotics Research* 27, (2008) 1135–1151.

[166] S. Talebi, I. Poulakakis, E. Papadopoulos, and M. Buehler. Quadruped robot running with a bounding gait. In Experimental Robotics VII, 281–289. Springer, 2001.

[167] P. M. Krishna, R. P. Kumar, and S. Srivastava. Level Trot Gait in Quadruped Robots. In Proceedings of International Conference on Advances In Robotics. ACM, 2013 1–5.

[168] H. Zou and J. P. Schmiedeler. The effect of asymmetrical body-mass distribution on the stability and dynamics of quadruped bounding. *IEEE Transactions on Robotics* 22, (2006) 711–723.

[169] T. Von Karman and G. Gabrielli. What price speed? Specific power required for propulsion of vehicles. *Mechanical Engineering* 72, (1950) 775–781.

[170] J. E. Bertram and A. Gutmann. Motions of the running horse and cheetah revisited: fundamental mechanics of the transverse and rotary gallop. *Journal of The Royal Society Interface* 35, (2009) 549–559.

[171] J. Bryant, M. Bennett, J. Brust, and R. Alexander. Forces exerted on the ground by galloping dogs (Canis familiaris). *Journal of Zoology* 213, (1987) 193–203.

[172] R. M. Walter and D. R. Carrier. Ground forces applied by galloping dogs. *Journal of Experimental Biology* 210, (2007) 208–216.

[173] R. M. Walter and D. R. Carrier. Effects of fore–aft body mass distribution on acceleration in dogs. *The Journal of Experimental Biology* 214, (2011) 1763–1772.

[174] S. B. Williams, H. Tan, J. R. Usherwood, and A. M. Wilson. Pitch then power: limitations to acceleration in quadrupeds. *Biology Letters* 5, (2009) 610–613.

[175] P. E. Hudson, S. A. Corr, and A. M. Wilson. High speed galloping in the cheetah (Acinonyx jubatus) and the racing greyhound (Canis familiaris): spatio-temporal and kinetic characteristics. *The Journal of Experimental Biology* 215, (2012) 2425–2434.

[176] K. Strang and K. Steudel. Explaining the scaling of transport costs: the role of stride frequency and stride length. *Journal of Zoology* 221, (1990) 343–358.

[177] J. R. Rebula, P. D. Neuhaus, B. V. Bonnlander, M. J. Johnson, and J. E. Pratt. A controller for the littledog quadruped walking on rough terrain. In IEEE International Conference on Robotics and Automation. IEEE, 2007 1467–1473.

[178] S. H. Kwon and H. H. Yoo. Flexible Part Design of a Galloping Quadruped Robot to Save the Energy. In 15th International Congress on Sound and Vibration. 2008 958–965.

[179] L. R. Palmer III and D. E. Orin. 3D control of a high-speed quadruped trot. *Industrial Robot: An International Journal* 33, (2006) 298–302.

[180] K. Turker, I. Sharf, and M. Trentini. Step negotiation with wheel traction: a strategy for a wheel-legged robot. In IEEE International Conference on Robotics and Automation (ICRA). IEEE, 2012 1168–1174.

[181] T. Thomson, I. Sharf, and B. Beckman. Kinematic control and posture optimization of a redundantly actuated quadruped robot. In IEEE International Conference on Robotics and Automation (ICRA). IEEE, 2012 1895–1900.

[182] E. Papadopoulos and D. A. Rey. A new measure of tipover stability margin for mobile manipulators. In IEEE International Conference on Robotics and Automation (ICRA), volume 4. IEEE, 1996 3111–3116.

[183] J. J. Craig. Introduction to Robotics: Mechanics and Control, volume 3. Pearson Prentice Hall Upper Saddle River, 2005.

[184] B. Siciliano and O. Khatib. Springer handbook of robotics. Springer Science & Business Media, 2008.

[185] I. Poulakakis, E. Papadopoulos, and M. Buehler. On the stable passive dynamics of quadrupedal running. In Proceedings IEEE International Conference on Robotics and Automation, volume 1. 2003 1368–1373.

[186] I. Poulakakis, E. Papadopoulos, and M. Buehler. On the stability of the passive dynamics of quadrupedal running with a bounding gait. *International Journal of Robotics Research* 25, (2006) 669–687.

[187] Q. Cao and I. Poulakakis. Quadrupedal bounding with a segmented flexible torso: passive stability and feedback control. *Bioinspiration and Biomimetics* 8, (2013) 046,007.

[188] A. Goswami, B. Espiau, and A. Keramane. Limit cycles in a passive compass gait biped and passivity-mimicking control laws. *Autonomous Robots* 4, (1997) 273–286.

[189] X. Liu and I. Poulakakis. A Simple Controller for Quadrupedal Bounding. In Proceedings International Symposium of Adaptive Motion in Animals and Machines (AMAM). 2013 .

[190] C. Sivanand. Passive Dynamic Quadruped Robot Bounding with Front and Back Leg Coupling. Master's dissertation, Indian Institute of Technology Hyderabad, India 2014.

[191] S. Talebinejad. Compliant running and step climbing of the SCOUT II platform. Master's dissertation, McGill University, Montreal, Canada 2000.

List of Papers Based on This Thesis

Journal Papers

1. P. Murali Krishna and R. Prasanth Kumar, "Energetics of Constant Height Level Bounding in Quadruped Robots," *Robotica (in press)* (http://dx.doi.org/10.1017/S0263574714001532)

2. P. Murali Krishna and R. Prasanth Kumar, "Effect of Asymmetry in Passive Dynamic Bounding of Quadruped Robots," *under review.*

3. P. Murali Krishna, Ch. Sivanand, R. Prasanth Kumar, and S. Srivastava, "Passive Dynamic Bounding Control using Symmetry Condition Control Laws," *to be submitted.*

Conference Papers

1. P. M. Krishna, R. P. Kumar, and S. Srivastava, "Energetics of Level Walking Trot Gaits in Quadruped Robots," *in Proc. IEEE International Conference on Robotics and Biomimietics,* (2012) pp. 61-65. DOI: 10.1109/ROBIO.2012.6490944

2. P. M. Krishna, R. P. Kumar, and S. Srivastava, "Level Trot Gait in Quadruped Robots," *in Proc. International Conference on Advances in Robotics,* (2013), 1-5. DOI:10.1145/2506095.2506100

3. P. M. Krishna, R. P. Kumar, and S. Srivastava, "Dynamic Gaits and Control in Flexible Body Quadruped Robot," *in Proc. 1st International and 16th National Conference on Machines and Mechanisms,* (2013) pp. 706–713.